AN ABSTRACT OF THE THESIS OF

Anthony Hai Le for the degree of Master of Science in Bioengineering presented on December 10, 2020.

Title: Biomechanical Modeling of Isometric Muscle-Tendon Force Generation Through Tendons Coupled in Parallel and a Passive Differential Mechanism

Abstract approved: _____

Ravi Balasubramanian

There are at least fifteen types of upper extremity tendon transfer procedures for combined peripheral nerve injuries that involve re-routing a single donor muscle to multiple recipient tendons. As a result, force and movement across finger joints become coupled, resulting in limited grasping abilities. Quantification and modeling of the donor muscle's mechanical functioning after tendon transfers can contribute to understanding surgical implications and guide novel innovative solutions. Therefore, the goal of this thesis was to analysis the biomechanics of tendon transfers for combined peripheral nerve injuries, specifically the extensor carpi radialis longus-to-flexor digitorum profundus (ECRL-to-EDP) tendon transfer for high medium-ulnar nerve palsy, while leveraging the development of an implantable passive differential mechanism (PDM) to improve such surgeries. This goal was achieved by studying the chicken extensor digitorum longus muscle-tendon unit, a model that was considered analogous to the human four coupled tendon muscle-tendon unit after ECRL-to-FDP tendon transfer and developing a computational model that simulated the isometric muscle force generation through a single tendon, two tendons coupled in parallel, and a PDM. The former two tendon network configurations provided insight into the baseline mechanics of a typical muscle-tendon unit and a muscle-tendon unit where a single muscle is coupled to multiple tendons. The latter tendon network configuration highlighted the advantage of incorporating an implantable PDM into a tendon network.

Biomechanical Modeling of Isometric Muscle-Tendon Force Generation Through Tendons Coupled in Parallel and a Passive Differential Mechanism

by
Anthony Hai Le

A THESIS

submitted to

Oregon State University

in partial fulfillment of
the requirements for the
degree of

Master of Science

Presented December 10, 2020
Commencement June 2021

Master of Science thesis of Anthony Hai Le presented on December 10, 2020.

APPROVED:

Major Professor, representing Bioengineering

Head of the School of Chemical, Biological, and Environmental Engineering

Dean of the Graduate School

I understand that my thesis will become part of the permanent collection of Oregon State University libraries. My signature below authorizes release of my thesis to any reader upon request.

Anthony Hai Le, Author

ACKNOWLEDGEMENTS

I would like to express my deepest gratitude to my advisors, Drs. Ravi Balasubramanian and Jim Sweeney, for their guidance, patience, and providing the appropriate tools and resources to conduct research. I would like to also thank my committee members for their advice during my journey to PhD candidacy and eventual MS thesis when I decided to change my academic career plans this year. Special thanks to Dr. Adam Higgins for introducing me to Ravi and his project on implantable passive differential mechanism for tendon transfer surgery. I truly thought I would not be a good fit for the project but applied anyway to find that it was nevertheless a prosperous opportunity. Thank you to Dr. Bill Smart for serving as my Minor Professor and welcoming me into the robotics community even though my research had negligible relevance to robotics. Many thanks to the Robotics and Human Controls Systems Laboratory for their collaboration and support, especially Justin Casebier for his amazing work in designing and manufacturing these implants under extremely difficult design constrains.

I would like to acknowledge many researchers, veterinarians, and staff at the Oregon State University Carlson College of Veterinary Medicine including Dr. Jennifer Warnock for conducting animal surgeries and contributing her anatomical expertise to the project, Drs. Jennifer Sargent and John DenHerder for dealing with logistical and protocol matters related to the project as well as their hand in providing anesthesia and euthanization support, Dr. Duncan Russell and Kay Fischer for their expertise in histopathological analyses, Maureen Larson for her general lab and supplies management throughout the project and histology tissue sample preparation, Dr. Rob Browning for collaborating on my first journal paper at the beginning of my graduate studies, and lastly, the rest of the Laboratory Animal Resources Center/Research Animal Isolation Laboratory staff for their support in animal housing, care, and husbandry.

I would like to thank our Congressionally Directed Medical Research Programs (CDMRP) project collaborators Dr. Buddy Ranter and Prabhleen Kaur at the University of Washington and Dr. Francisco Valero-Cuevas and Suraj Chakravarthi Raji at the

University of Southern California for their outside perspectives and overall contributions to facilitate a truly interdisciplinary project.

Last, but not the least, I owe more than just gratitude to my family and friends for their support, encouragement, and all-around good times throughout my life. Shoutout to the Corvallis/Oregon State University friends for introducing me to all kinds of outdoor adventures I was not previously familiar with. Our adventures together undoubtedly got me through all the stress and depression during graduate school.

CONTRIBUTION OF AUTHORS

This thesis will be condensed and formatted into a manuscript for a publication submission to the IEEE Transactions on Biomedical Engineering with co-authors, James D. Sweeney and Ravi Balasubramanian.

TABLE OF CONTENTS

LIST OF FIGURES

LIST OF FIGURES (Continued)

LIST OF TABLES

LIST OF APPENDICES

LIST OF APPENDIX FIGURES

Chapter 1: Introduction

1.1 Motivation

Tendon transfers in the upper extremity are commonly used to restore arm and hand function after injury to a peripheral nerve caused by physical trauma or neurological disorder. In most cases, peripheral nerve injuries result in a single nerve palsy, radial, median, or ulnar nerve palsy, and in a generally localized area in the upper extremity, either proximal (upper) or distal (low) of the elbow joint. However, severe trauma to the upper extremity can result in combined peripheral nerve injuries, where multiple muscle-tendon units may be affected and require repair, leaving fewer expendable donors for tendon transfer.

There are at least 15 types of upper extremity tendon transfers that involve rerouting and directly suturing a single donor muscle to multiple recipient tendons/muscle-tendon units [1, 2]. For example, tendon transfer for high median-ulnar nerve palsy, a combined peripheral nerve injury, where the median and ulnar nerves are damaged above the elbow joint. As a result, the flexor digitorum profundus (FDP), flexor digitorum superficialis (FDS), and the intrinsic hand muscles are paralyzed leading to sensory loss and weakness or complete flexion disability in the index, middle, ring, and little fingers. The current surgical procedure for restoring finger flexion is a tendon transfers that distally detaches the single extensor carpi radialis longus (ECRL) muscle, the donor muscle innervated by the radial nerve, from its insertion and sutures it to the proximal ends of the four FDP tendons together [2, 3]. Unfortunately, this procedure has a drawback. While finger flexion is restored, this procedure couples the forces and movements of all four fingers and prevents them from individually adapting and conforming to an object's shape during grasping tasks[1, 2, 4, 5]. Therefore, our research group aims to develop novel implantable passive differential mechanisms (PDMs) that can be incorporated into the coupled tendon network following tendon transfers and enable differential actuation *in situ* between one muscle and multiple tendons. Namely, we are currently developing an implantable

PDM that takes the form of a translating, pivoting triangle created with the coupled biological tendons and strut-shaped or V-shaped artificial implants. The differential actuation of the implantable PDM refers to the additional degrees of freedom in the overall system and the transmission of forces and movements from one actuator to multiple endpoints or fingers, while allowing each endpoint or finger to find its own equilibrium. Differential mechanisms consequently allow a more even distribution of forces across multiple endpoints from a single actuator.

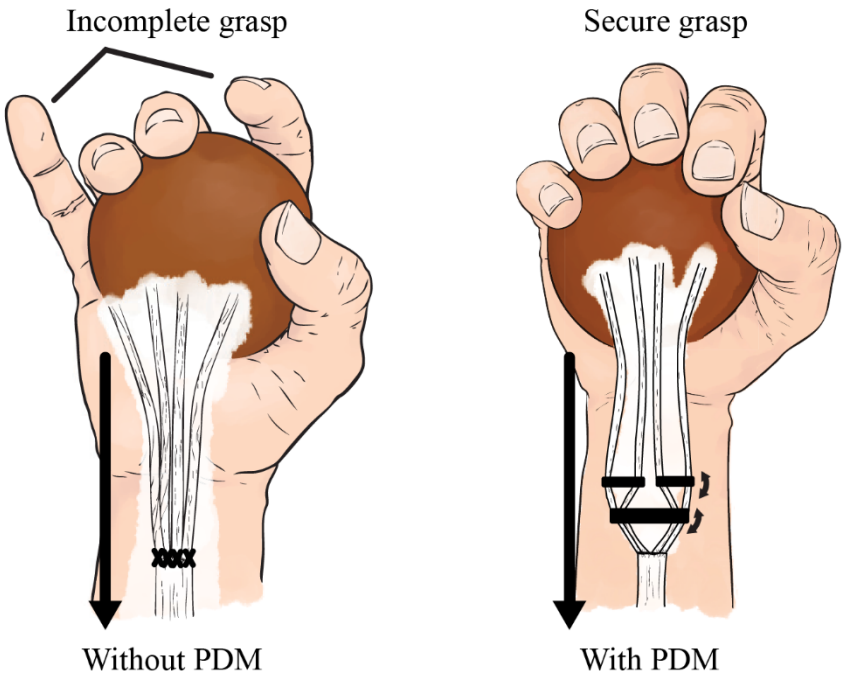

Figure 1.1.1 Illustration of limited grasping abilities following extensor carpi radialis longus-to-flexor digitorum profundus (ECRL-to-FDP) tendon transfer (left); illustration of adaptive grasping abilities following ECRL-to-FDP tendon transfer with an implantable passive differential mechanism is incorporated into the tendon network (right).

There is a gap in knowledge regarding the biomechanical analysis of tendon transfers for combined peripheral nerve injuries, particularly of tendon transfers that detach and relocate a single donor tendon of a functioning muscle-tendon unit to

multiple recipient tendons of non-functioning muscle-tendon units. These current techniques involving disproportional transfers of donor to recipient tendons, instead of a single donor tendon to a single recipient tendon to restore an individual function, result in limited, coupled function. This gap in knowledge is particularly problematic for the study of upper extremity tendon transfers because innovative improvements to current techniques and clinical outcomes can be better informed and predicted with an understanding of the biomechanical limitations in postoperative hand function; therefore, the resulting mechanics of tendon transfers for combined peripheral nerve injuries, specifically the task-based force-length or joint torque-angle relationships, must be characterized in order to advance the current standard.

1.2 Focus of the Thesis

The goal of this thesis was to analysis the biomechanics of tendon transfers for combined peripheral nerve injuries, specifically the extensor carpi radialis longus-to-flexor digitorum profundus (ECRL-to-EDP) tendon transfer for high medium-ulnar nerve palsy, while leveraging the development of an implantable PDM to improve such surgeries. This thesis aims to elucidate the mechanics responsible for postoperative limitations in hand function to better understand clinical outcomes. To accomplish this goal, both computational musculoskeletal modeling and *in vivo* animal experiments were utilized. The aims of the computational musculoskeletal modeling were (1) to model the task-based joint torque-angle relationships of a muscle-tendon unit with a single muscle attached to multiple tendons, and (2) to investigate the effects of incorporating a PDM into the same muscle-tendon unit with a single muscle attached to multiple tendons on the task-based joint torque-angle relationships. The aims of the *in vivo* animal experiments in a chicken model were (1) to provide data for building a task-based joint torque-angle relationship models of a muscle-tendon unit with a single muscle attached to multiple tendons and (2) to evaluate the task-based joint torque-angle relationships of a muscle-tendon unit with a single muscle attached to multiple tendons.

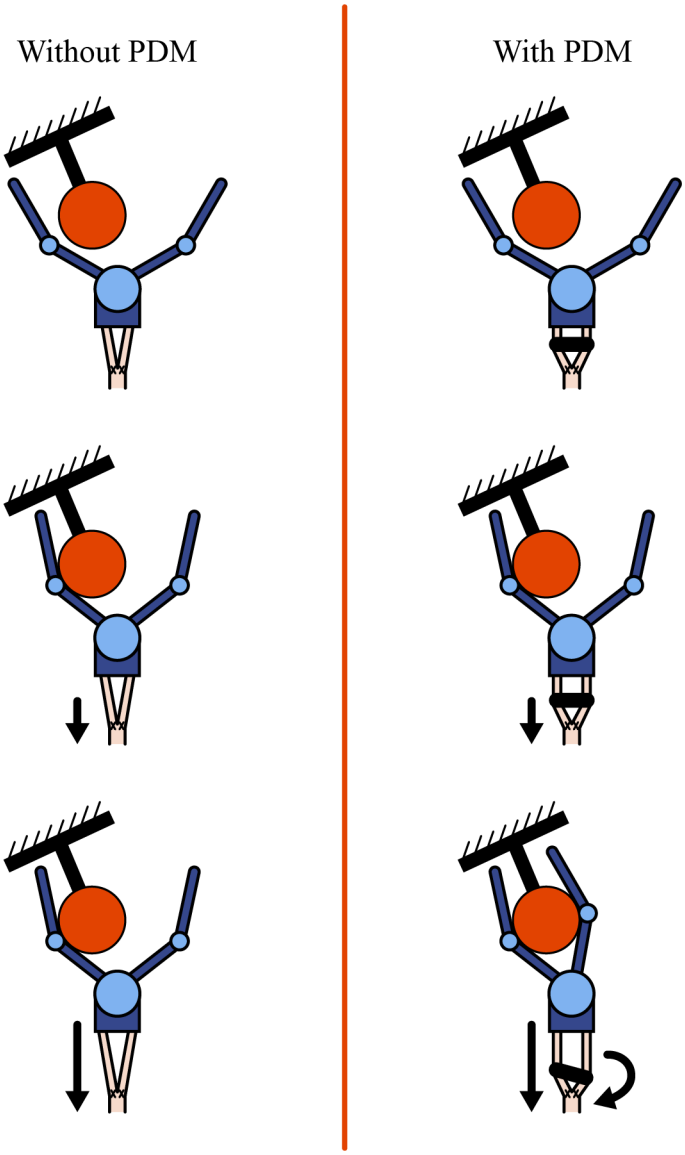

Figure 1.2.1 Simplified, two-finger robotic hand grasping animation sequence depicting the difference between grasping quality around a fixed ball without (left) and with (left) a passive differential mechanism (PDM) integrated into the tendon networking driving the fingers.

1.3 Overview

The remaining chapters of this thesis provide descriptions of the computational and experimental work that have been completed to study the biomechanics of tendon transfers for combined peripheral nerve injuries. Chapter 2 provides a general overview of the concepts and terms necessary to understand the methods, results, and conclusions of this thesis. Chapters 3 and 4 outline the main contributions of this work, both modeling and experimental aspects of the thesis. Chapter 5 concludes the thesis by summarizing the contributions and proposing future work.

Chapter 2: Background

2.1 Isometric Properties of Muscle and Tendon

A muscle-tendon unit can be modeled with the combination of three force-generating elements: contractile element (muscle), parallel elastic element (muscle/connective tissue), and series elastic element (tendon/connective tissue) [6]. This model is specifically the Hill-type model of the muscle-tendon unit. Types of muscle-tendon unit properties include isometric (constant length), concentric (shortening), eccentric (lengthening), and isotonic (constant force/load). The isometric force-length relationship is generated by maximally or near-maximally stimulating a skeletal muscle at a variety of fixed, discrete muscle-tendon lengths. This relationship illustrates the dependence of active muscle force on sarcomere strain (i.e., myofilament overlap) or muscle-tendon length at the whole organ level, where there is an optimal length for maximum isometric muscle-tendon force generation [7, 8]. If a muscle-tendon unit is fixed at a shorter or longer length away from the optimal length, isometric muscle-tendon force generation decreases (Figure 2.1.1) [9]. This isometric property characterizes the mechanical functioning and physiological operating range of a muscle-tendon unit. The term, joint torque-angle relationship, is synonymous to force-length relationship based on the moment arm of the related joint and will be used throughout the later chapters.

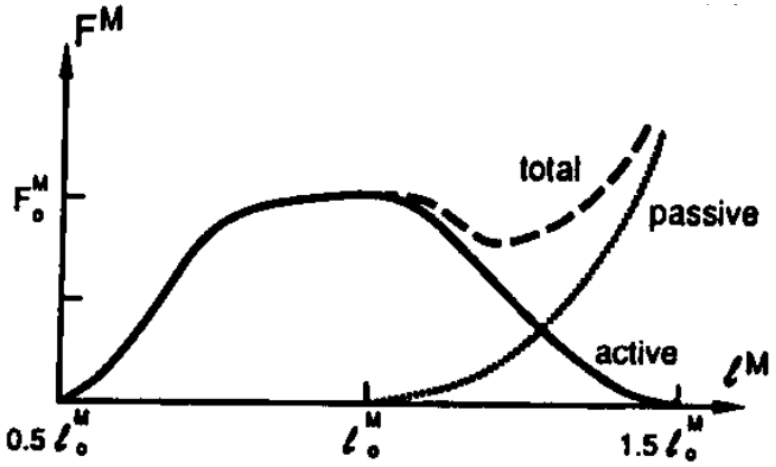

Figure 2.1.1 Isometric force-length relationship of a skeletal muscle attached to a single tendon. There are two main components of isometric muscle-tendon force generation, active and passive. Active muscle-tendon force refers to the force developed when muscle is activated. Passive muscle-tendon force refers to the passive tension of the muscle, tendon, and connective tissues. Addition of the two forces produce the total isometric force-length relationship. F^M = muscle-tendon force, l^M = muscle-tendon length, l_o^M = muscle-tendon length at which active muscle-tendon force peaks (i.e., $F^M = F_o^M$ and $l^M = l_o^M$). This figure was adapted from Zajac (1989) [9].

Passive tension is the force generated by the muscle-tendon unit in the absence of stimulation, which arises from titin and connective tissues stretching. This passive tension is characterized by the material properties or stress-strain relationships of the connective tissues and tendon. Peak active muscle-tendon force is directly proportional to physiological cross-sectional area ($PCSA$) [10-12]; $PCSA = Acos\alpha$, where A is fiber cross-sectional area and α is the pennation angle. Pennation increases $PCSA$, and thus, greater muscle force generation (Figure 2.1.2) [9]. Parallel fibers enable greater range of motion (ROM) or contraction velocities.

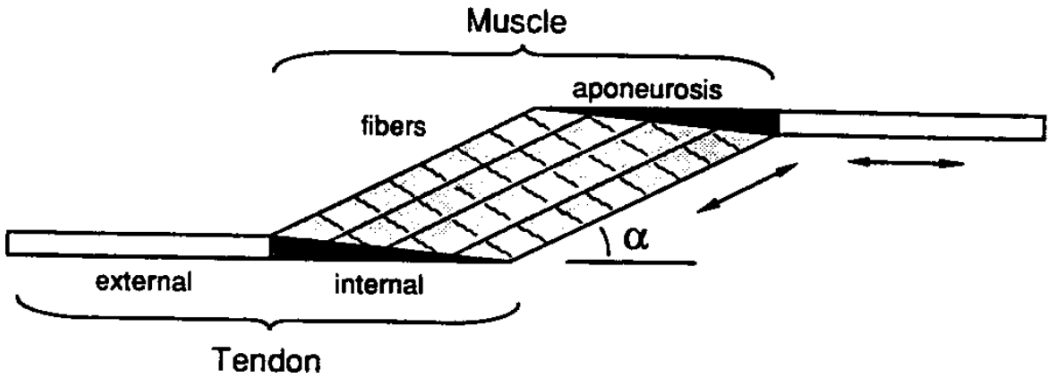

Figure 2.1.2 Illustration of a muscle-tendon unit depicting muscle fiber orientation and muscle-tendon force generation direction. This figure was adapted from Zajac (1989) [9].

A muscle-tendon unit refers to the skeletal muscle that transmits force through the tendon on bone at the origin and insertion of attachment. Joint motion and torque depend on the size of the moment arm. The moment arm depends on the muscle's line of action (i.e., attachment geometry) [13]. A larger moment arm results in greater joint torque for a given muscle force. However, a larger moment arm leads to greater change in muscle length for a given change in joint angle.

2.2 Biomechanics of Tendon Transfers

Tendon transfer is a surgical procedure that detaches the tendon of a functioning muscle-tendon unit at its insertion (donor) and subsequently relocates it to a new insertion or attachment to replace a non-functioning muscle-tendon unit (recipient). Tendon transfers are often performed to restore function and balance in the upper extremity after injury to nerves or the spinal cord caused by physical trauma or neurological disorder. The most common indication for upper extremity tendon transfers is a peripheral nerve injury that has no potential for improvement or recovery [14].

The general principles of successful tendon transfers have been identified and refined for upper extremity reconstruction following injury to the radial, median, and

ulnar nerves [1]. These principles describe how (1) the functional loss associated with the donor tendon should be minimized to maximize functional gains following tendon transfer [15], (2) the donor muscle must have normal or near normal strength [16, 17], (3) the donor muscle-tendon unit must have sufficient tendon excursion [18], (4) the direction of pull of the donor and recipient tendons should be inline [15, 16], (5) a single transfer should restore one intended function [15, 16, 19, 20], (6) the donor tendon should pass through a stable, healthy soft tissue bed for gliding with pliable, unscarred tissue and minimal adhesion [15, 16], (7) the joint controlled by the donor tendon must have supple passive ROM prior to transfer [15, 16], and (8) the donor tendon should preferably function and move in phase with the recipient tendon [15, 16, 19].

These principles apply to tendon transfer for single peripheral nerve injuries. However, there are special considerations related to combined peripheral nerve injuries, where injury to more than one of the peripheral nerves in the upper extremity occurs. In particular, the donor muscle must have normal or near normal strength, the donor muscle-tendon unit must have sufficient tendon excursion, and the donor tendon should preferably act in phase with the recipient tendon [21]. Tendon transfers rely on the redundant actions of multiple muscle-tendons in the upper extremity musculature, making some muscle-tendons expendable as donors [1, 21, 22]. An expendable muscle-tendon as a donor means that there must be another remaining muscle that can continue to adequately perform the original function of the transferred muscle-tendon unit. It does no good to restore a given function if another equally important function is lost in the process. In the case of combined peripheral nerve injuries, there are fewer available options in muscle-tendon units for transfer because of fewer tendons of shared function that are expendable are also associated with the injured tendon or muscle bellies [21].

Isometric fingertip forces during maximal voluntary contractions in specific finger postures have been explored in an effort to understand the mechanical basis underlying the coordination of finger muscles required for functional grasping and to help surgeons evaluate their options for restoring grasping [23].

Some research groups have had the opportunity to measure tendon forces of muscles just prior to being transferred using strain gauges or force transducers and transcutaneous FES [24]. Strain gauges are attached inline at the insertion end of the tendon to measure isometric forces at various muscle length imposed by stretching the muscle-tendon unit incrementally [25]. Buckle-style force transducers are attached directly to the tendon after transfer and reattachment. This method then measures isometric forces of muscle-tendon unit at various lengths imposed by manipulating the angle of the associated joint [26]. These studies are exemplars of generating task-based force-length or joint torque-angle relationships to illustrate how peak muscle force generation depends on joint angle position. Understanding this relationship provides some insight on the functional outcomes and active operating range of the transferred muscle-tendon unit and the associated joint following tendon transfer.

PCSA and fiber length-to-muscle length ratio are important for predicting peak muscle-tendon force generation and potential excursion, respectively [27]. Thus, these properties have significant influences on tendon transfer and donor muscle selection. For example, divergent architectures between synergistic muscles are seen in the radial extensors of the human wrist, the extensor carpi radialis longus (ECRL) and extensor carpi radialis brevis (ECRB). The ECRL is a muscle designed for large excursion or high velocity based on its relatively high fiber length/muscle length ratio and relatively low PCSA. The ECRB, however, is a longer muscle with shorter fibers, but has a larger PCSA compared to the ECRL, which suggest that the ECRB is preferentially designed for high force production. However, Loren et al. quantified the moment arms of both muscles acting in wrist extension to determine whether architectural differences between muscle might be compensated for by changes in wrist moment arm [28]. Lieber and colleagues measured the sarcomere length change in each muscle during wrist rotation in patients using laser diffraction intraoperatively [7]. It was found that sarcomere length change during joint rotation is a direct reflection of the fiber length/moment arm ratio [7, 29]. Interestingly, the musculoskeletal kinematics highlighted architectural differences between the muscles. The extensor moment arm of the ECRB was determined to be much greater throughout the ROM compared to the

ECRL. Therefore, the ECRL serves as a better donor muscle to replace deep finger flexors (i.e., flexor digitorum profundus, FDP) whose excursions are relatively large compared to other muscles in the forearm and hand.

To further understand functional outcomes of tendon transfers, Maas et al. has investigated the contributions of the interactions between a transferred muscle, its previous synergistic muscles, and surrounding connective tissue on joint moment. These contributions refer to epimuscular myofasical force transmissions and it is also relevant to scar tissue formation frequently observed after invasive surgeries [30]. These studies involve exploring the effects tenotomy and muscle-tendon dissections on wrist flexion moment at different wrist angles in rats using a force transducer attached to a rigidly fixed hand, where wrist rotation was only allowed [31]. It was reported that these interactions affected the mechanics of the transferred and neighboring muscles on the joint drastically [32-34].

Biomechanical simulation and modeling tools, such as OpenSim, have more recently impacted orthopaedic surgery. Computational methods present promise for simulating the conditions of tendon transfers to study surgical techniques, thereby predicting functional outcomes [9, 35]. However, subpar biological accuracy and high computational expenses have limited this approach, but progress is being made [36].

2.3 Design of Underactuated Robotic Hands

Underactuation in robotic grasping is the concept of using fewer actuators than degrees of freedom (DOF). Considering the many advantages of underactuation in anthropomorphic hands, such as reduced hardware weight, simple controls rather than having to command and coordinate several actions, and compactness, there is interest to develop mechanisms that aim at achieving underactuation between fingers. Common robotic hands do not usually consist of one single finger. Most designs have several fingers ranging between 2 and 5. The purpose of underactuation between multiple fingers is to use the power of one actuator to drive the open-close motion of all the fingers of a robotic hand collectively. The transmission mechanism used to achieve

such a property must be adaptive. In other words, when one or more fingers are blocked, the remaining finger(s) should be able to continue to move. When all the fingers are blocked, the force should be evenly distributed among the fingers and it should be possible to apply larger grasping forces while maintaining a stable grasp. Thus, incorporating underactuation between the fingers of a robotic hand reduces the complexity of the design [37-39]. The application of underactuation has been demonstrated with several prototypes. To this end, the basic element commonly used is the differential mechanism. According to the IFToMM terminology (IFToMM 1991), a differential mechanism is a 2-DOF mechanism that may resolve a single input into 2 outputs and vice versa.

2.4 Intramuscular Functional Electrical Stimulation

Skeletal muscle fibers are innervated by myelinated nerve fibers (i.e., efferent axons) that derive from α-motor neurons, whose cell bodies lie within the ventral horn of the spinal cord [40]. An α-motor neuron and the skeletal muscle fibers it innervates are known as a motor unit.

Functional electrical stimulation (FES) of skeletal muscle for motor function operate under the fundamental principle that electrical stimulation generally activates nerve rather than muscle [41]. Thus, for FES to be effective in any application, the myelinated nerve fibers must be intact from the ventral horn of the spinal cord to the neuromuscular junctions in the muscles that are to be activated [42].

Electrical current applied to the α-motor neurons can elicit action potentials. The stimulating electrodes creates a localized electric field that depolarizes the cellular membranes of nearby neurons. If the depolarization reaches a critical threshold, an influx of sodium ions across the cellular membrane produces an action potential that propagates bidirectionally away from the site of electrical stimulation [42]. Action potentials that propagate proximally in the peripheral nerve fibers are ultimately annihilated at the cell body. Action potentials that propagate distally are conducted across the neuromuscular junction via the release and binding of acetylcholine (ACh),

the neurotransmitter, to ACh receptors and into the muscle fiber through the transverse-tubule system (T-system). The T-system triggers the sarcoplasmic reticulum (SR) to release calcium ions into the proximity of the myofilaments. These calcium ions bind to the regulatory protein troponin C to permit actin-myosin interaction, initiating muscle fiber contraction and generating force. This whole process is known as excitation-contraction (EC) coupling. Muscle relaxation occurs after EC coupling where calcium ions are pumped back into the SR when electrical stimulation ceases, blocking actin-myosin interaction and inducing force relaxation [8].

The cumulative effect of repeated stimuli within a brief period is referred to as temporal summation. If a train of stimuli is delivered to a muscle via electrical stimulation, separated in time by different amounts, resulting in tetanic muscle contraction (i.e., fusion of twitch contractions) [8]. Stimuli delivered at higher frequencies results in higher force generation (less time for relaxation) while stimuli delivered at lower frequencies results in lower force generation (more time for relaxation).

There are different types of skeletal muscle fibers that can be categorized by the physiological and metabolic properties: slow oxidative (SO, Type I), fast oxidative-glycolytic (FOG, Type IIA) and fast glycolytic (FG, Type IIB) [43]. In general, Type I and Type II muscle fibers refer to slow-switch and fast-twitch fibers, respectively. These muscle fiber types (SO, FOG, and FG) correspond to slow, fast fatigue-resistant, and fast fatigable motor unit types, respectively, based on their twitch speed and fatigue resistance [44]. Slow-twitch fibers are optimized for relatively low force generation, at relatively low speeds, while fast-twitch fibers are optimized for high force generation for briefer time intervals [45]. Furthermore, the α-motor neurons innervating slow-twitch motor units tend to have slower firing rates compared to those innervating fast-twitch motor units [46].

In general, larger α-motor neurons that innervate larger (fast-twitch) motor units require less current to be activated compared to smaller α-motor neurons that innervate smaller (slow-twitch) motor units because the wider spacing between nodes of Ranvier in large α-motor neuron axons produce larger induced transmembrane voltage changes

[45, 47]. Recruitment refers the activation of a number of motor units within the skeletal muscle. Electrical stimulation tends to activate motor units in reverse recruitment order, where large motor units are activated before small ones [42, 48]. This reverse order is the opposite of the Hennemann's physiological size principle.

Muscle fatigue is the reduction in the ability to generate maximum or expected force [49, 50]. FES induces excessive neuromuscular fatigue due to multiple phenomena. First, FES tends to reverse physiological recruitment order, as mentioned previously [42, 48]. It has been postulated that reverse recruitment order may be less systematic or nonselective [51, 52]. Second, FES tends to stimulate muscle fibers so simultaneously compared to the normal, physiological, and unsynchronized recruitment process of motor units seen during voluntary muscle contractions. Additionally, increased stimulation frequencies (rate of stimuli delivery) may elicit "high-frequency fatigue" [40]. Likewise, increased stimulation pulse width or intensities (amplitude) may elicit fatigue.

The principles discussed should always be considered when designing experimental stimulation protocols for optimal force generation and minimal neuromuscular fatigue. The parameters used in designing stimulation protocols include frequency, pulse width/duration, interpulse interval (IPI), intensity (amplitude), geometric waveform shape (monophasic, biphasic, square, peaked, or sine), rest period, targeted muscle group, and pattern. Common stimulation patterns studied are constant frequency trains (CFTs), variable frequency trains (VFTs), and doublet frequency trains (DFTs) [49, 53, 54]. Simulations can also be delivered by means of constant voltage (voltage-regulated) or constant current (current-regulated). Since current-regulated stimulation create reproducible applied electric fields, percutaneous and implanted stimulation systems utilize current-regulated stimulation. On the other hand, surface (transcutaneous) stimulation systems utilize voltage-regulated stimulus because it is safer even though the stimulation may be less reproducible [40]. Selectivity depends on electrode placement; electrodes positioned close to nerves or motor points achieve better selectivity in stimulation. Also, a smaller distance between the cathode and anode minimizes "spill over" of the electric field.

Percutaneous systems make use of intramuscular electrodes that pass through the skin and are implanted into the muscles to be activated. Percutaneous electrodes can activate deep muscles and are less likely to produce pain during stimulation because they bypass the pain receptors in the skin. Furthermore, percutaneous electrodes increase the possibility for selective muscle stimulation. An electrode is inserted through the skin and implanted in the muscle using a hypodermic needle. The electrode leads exit the skin and are connected to external stimulation equipment. Extreme care must be considered in the electrode insertion site on the skin, whereby the skin must be cleaned, dressed, properly inspected, and maintained to reduce the risk of complications [55]. Percutaneous systems have served as precursors to fully implanted systems meant for long term function, hence, can provide a minimally invasive technique for investigating the feasibility of restoring functional muscle contraction before subjecting a patient or research subject to implantable system surgery [56, 57].

Intramuscular electrodes are inserted percutaneously and extend into the muscle with hypodermic needles in order to deliver the electric field directly within the muscle [58]. Consequently, no surgical procedures are required, providing a minimally invasive method for FES. Stimulation systems that use intramuscular electrodes can effectively active deeper or smaller muscles, such as the FDP muscles (i.e., deep digital flexors in the forearm) [42]. Compared to epimysial electrodes, intramuscular electrodes can provide isolated and repeatable muscle contractions since electrodes can be placed near the nerve fibers and the motor endplates (neuromuscular junction) within the muscle.

2.5 Motivation for Using a Chicken Model to Study Tendon Transfers

For the studies outlined in this thesis, the chicken was the ideal animal model due to its existing extensive use in tendon surgery research [59]. Notably, the chicken model was relatively inexpensive to purchase, grow, and care for in groups. Anatomically, the lower pelvic limbs of the chicken include distinct digits that were exceptional for evaluating kinetics and kinematics analogous to the human fingers. Moreover, the

extensor digitorum longus (EDL) tendon has a nature bifurcation that mimics tendon coupling as a result of only using sutures in the conventional ECRL-to-FDP tendon transfer in humans. The EDL tendon is also reasonably sized for designing and manufacturing implants for proof-of-concept studies. The accessibility of the EDL tendon will simplify the implantation surgery when incorporating a strut-shaped implant into the tendon network to construct a passive differential mechanism (PDM) into the EDL muscle-tendon unit.

Chapter 3: Modeling the Isometric Muscle-Tendon Force Generation Through Two Tendons Coupled in Parallel

3.1 Introduction

Numerous models exist describing the relationship between skeletal muscle properties and force generation. Models range from formulations of cross-bridge attachment and detachment rates [60] to phenomenological models of muscle force output as a function of length, activity, and velocity [9, 61]. In all these models, muscle force varies as a function of muscle length [62] and contraction velocity [63], characteristic relationships of the muscle contractile component. However, a whole muscle is not simply an amplified sarcomere generating forces by itself.

There are significant elastic elements within (in parallel) and attached (in series) to the muscle [64, 65]. Specifically, the additional component of the tendon in the skeletal muscle-tendon unit has unique properties compared to the properties of the muscle alone [9, 66, 67]. Therefore, models that account for coordination and interaction of the muscle and tendon properties together are more useful in describing normal movement. For example, a recent mammalian muscle-tendon model by Zajac [9] can be applied to any muscle-tendon actuator given appropriate scaling factors and parameter tuning.

While Zajac's generic model accomplishes its purpose and captures the essential mechanics of the muscle and tendon behind movement and function, it is not possible to simply apply that model to any muscle-tendon unit in any species since the issues of scaling and species specificity can come into play [68]. Notably, Lieber et al. [69] developed a muscle-tendon model for the frog semitendinosus (ST) based on experimental data – the phenomenological approach in muscle-tendon model development. Through this model, they were able to determine the tendon's influence in this system as they were interested in the behavior of the frog ST during normal locomotion. But like Lieber et al.'s model [69], many, if not all Hill-type isometric

models of muscle-tendon actuators, involve the construct one muscle and one tendon attached in series and are applied to humans and other species. Few studies have documented and modeled the muscle-tendon mechanics of systems where a single muscle is attached to a more complex tendon network.

The tendon transfer for high median-ulnar nerve palsy is an exemplar case of which a single muscle is attached to a more complex tendon network consisting of more than one tendon coupled in parallel. Specifically, the single donor extensor carpi radialis longus (ECRL) muscle is transferred to the four flexor digitorum longus (FDP) tendons to restore finger flexion. However, one can imagine that the single muscle actuating multiple flexor tendons can result in limited grasping abilities in the hand. Quantification of mechanical functioning after tendon transfers, where a single muscle is transferred to multiple tendons, can contribute to understanding surgical outcomes. Therefore, by following the modeling approach proposed by Zajac [9] and Lieber et al. [69], we developed a model that represents the isometric force production of muscle contraction when a pair of tendons, coupled in parallel, and attached in series with a muscle.

The objectives of this study were three-fold. One objective was to measure and characterize the isometric force generation of a single skeletal muscle through a single tendon in the chicken extensor digitorum longus (EDL) muscle-tendon unit. A second objective was to develop a Hill-type muscle-tendon model for the chicken EDL muscle-tendon actuator based on the experimental data. A third objective was to use the developed isometric force generation profile of the chicken EDL muscle to investigate the influence of a pair of tendons, coupled in parallel and attached in series, on the isometric force generation profile of the EDL muscle. In Chapter 4, the same model will be used to determine the force generation of the EDL muscle through coupled tendon network modified with a strut-shaped implant to create an implantable passive differential mechanism (PDM).

3.2 Methods

The model chosen for this study was the chicken (*Gallus gallus domesticus*) EDL muscle-tendon unit. As previously described in Chapter 2.5, this model was chosen based on its well-established use in tendon surgery research [59] and the nature bifurcation that mimics tendon coupling as a result of a single muscle transferred to multiple tendons. This coupled two-tendon model is a simplified, scaled-down version of the coupled four-tendon construct created from the ECRL-to-FDP tendon transfer in the human upper extremity.

3.2.1 Initial Experimental Data Collection for Building Phenomenological Models

Phenomenological models are scientific models that describe the empirical relationship between an independent and dependent phenomenon and are not derived from first principles. Thus, the phenomenological models of force generation for the chicken EDL muscle-tendon units in this study were based on the experimentally measured relationships between isometric EDL muscle force generation and metatarsophalangeal (MTP) joint angles

Chickens were sedated and placed in dorsal recumbency for a distal EDL tenotomy for establishing a single tendon network configuration (Figure 3.2.2A; refer to Appendix A.1 for surgical procedure details). Following the procedure and continual sedation, each chicken was moved into right recumbency and their left pelvic limb was rigidly fixed at 115° to prevent intertarsal joint rotation via a custom chicken intertarsal joint fixation unit (Figure 3.2.2A). Digit IV and digit II were splinted to prevent all interphalangeal joint rotations, except for the MTP joints, and each toe tip was affixed to a single-axis load cell (Miniature S-Beam Jr. Load Cell, LSB201, 10 lb., FUTEK Advanced Sensor Technology, Inc., Irvine, CA, USA) via a custom toe rotation unit (Figure 3.2.2B). For the model, digit IV and digit II were designated as Toe_1 and Toe_2, respectively. Intramuscular electrodes were inserted into the EDL muscle through

hypodermic needles. Functional electrical stimulation (FES) was applied to the EDL muscle via intramuscular electrodes at near-submaximal contraction stimulation parameters listed in Table 3.2.1 below.

Table 3.2.1 Intramuscular functional electrical stimulation parameters for near-submaximal tetanic muscle contraction in the chicken extensor digitorum longus muscle-tendon unit.

Parameter	Value
Current (Stimulus Amplitude)	5 mA
Stimulus Pulse Width	500 μs
Pulse Train Frequency	50 Hz
Pulse Train Duration	500 ms
Rest Period Duration	1.5 min

These FES parameters were determined in prior experiments for piloting and parameter sweeping in live chicken experiments (refer to Appendix C.1).

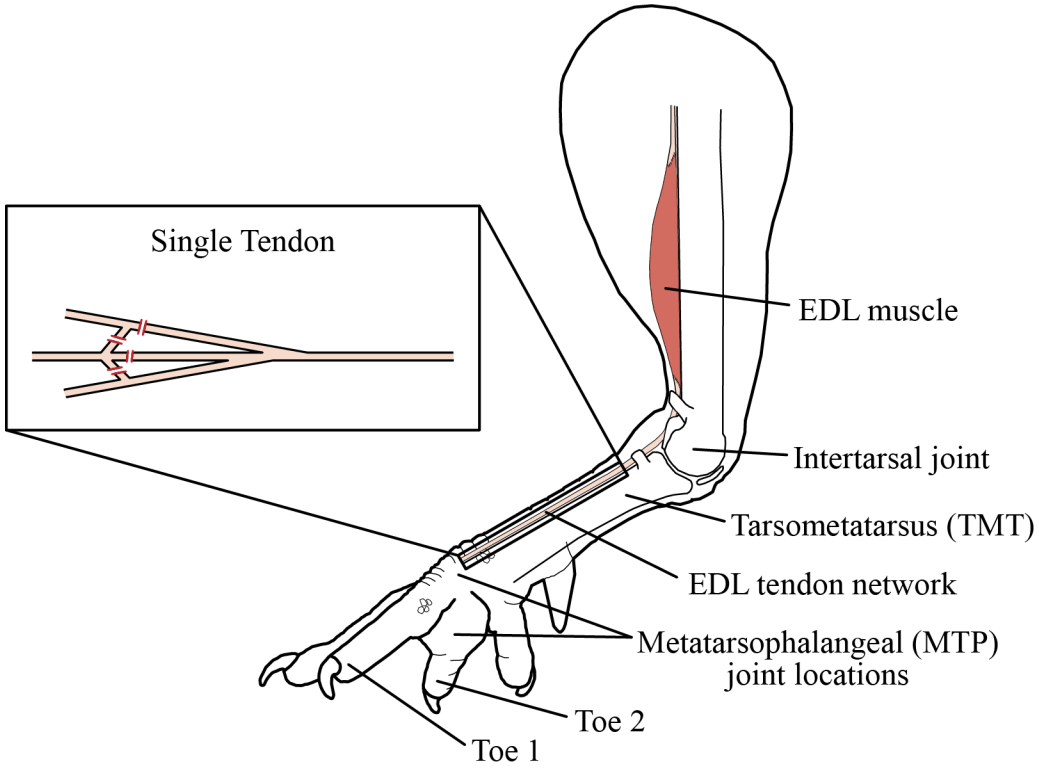

Figure 3.2.1 Single tendon network configuration established through a distal extensor digitorum longus (EDL) tenotomy to release digit II (Toe_2) and digit III, only leaving digit IV (Toe_1) intact with the EDL muscle-tendon unit.

Isometric EDL muscle force generation for toe extension was measured at each toe tip simultaneously for various combinations of Toe_1 MTP joint angles (-30°, -15°, 0°, 15°, 30°, 45°, and 60°) and Toe_2 MTP joint angles (-30°, 0°, and 60°). Extended positions were negative angles and flexed positions were positive angles. Neutral position, 0°, was defined as the toe in line with the tarsometatarsus. Toes were positioned at randomized target MTP joint angles and FES was delivered to induce tetanic contraction in the EDL muscle. Toes were return to neutral positions for a 1.5 min rest period to minizine neuromuscular fatigue. These steps were repeated twice for each Toe_1-Toe_2 MTP joint angle combination. In total, 42 stimulations were delivered to each chicken EDL muscle (21 combinations, 2 times each).

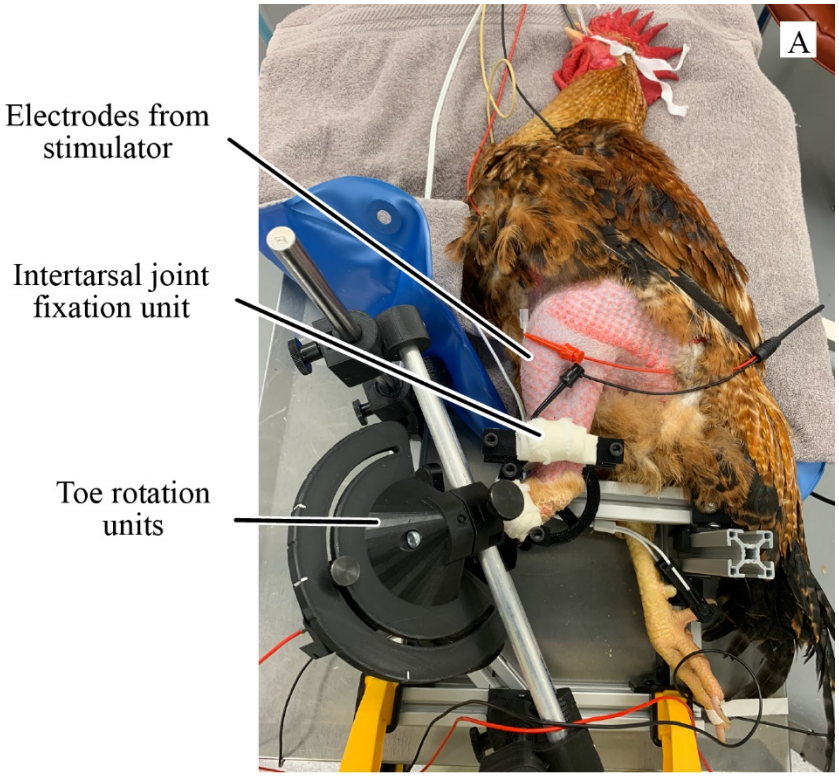

Figure 3.2.2A Chicken in right lateral recumbent position with left pelvic limb rigidly fixed to prevent intertarsal joint rotation. Fine-wire intramuscular electrodes were inserted into the extensor digitorum longus (EDL) muscle.

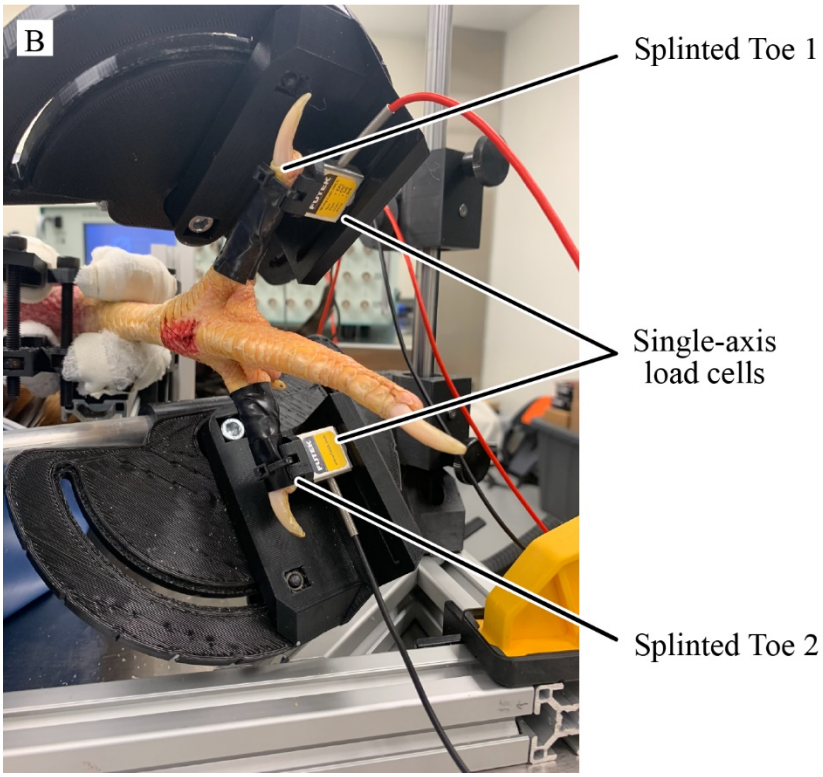

Figure 3.2.2B Each toe tip was directly attached to a load cell using a zip tie. Isometric toe tip extension forces were assessed at various metatarsophalangeal (MTP) joint angles by repositioning the load cellsin the custom-built toe rotation units.

Raw toe extension force signals from the load cells were sampled at 4 kHz frequency and filtered using a 4th-order Butterworth zero-lag filter via a custom MATLAB script (vR2020a, MathWorks Inc., Natick, MA, USA; refer to Appendix F.1). Peak active extension forces from repeated measures, defined as the difference between the baseline residual force immediately prior to stimulation and the maximum force generated during stimulation, were extracted, averaged, and converted to joint torque ($\tau = r \times F$) based on the MTP joint moment arms (r) grossly measured postmortem. The difference between the baseline force when the toes were in the neutral position and the baseline residual force when the toes were moved to targeted positions just prior to stimulation was calculated as the passive joint torque of the EDL muscle-tendon unit. The addition of passive and active MTP joint extension torques provided the total MTP joint extension torque values. However, the passive and total

MTP joint extension torque values were beyond this scope of this study and overall thesis. Nevertheless, these values are important data to be considered in future work.

Peak active extension torques were mapped to MTP joint angle combinations to generate a series of peak active extension torques for various MTP joint angle combinations – producing the active Toe_1 MTP joint torque-angle relationship curves. Since the distal EDL tenotomy only left Toe_1 and its tendon attached to the EDL muscle, it was expected that extension force would only be detected in Toe_1, and not Toe_2. Statistically significant differences between active Toe_1 MTP joint torque-angle relationship curves for each prescribed Toe_2 MTP joint angle were determined using repeated measures analysis of variance (ANOVA). Significance level was set *a priori* at $\alpha = 0.05$. Bonferroni adjusted post-hoc pairwise comparisons were performed when the repeated measures ANOVA F-test was significant. The experimental design in this study was implemented to verify that the distal EDL tenotomy completely disconnected Toe_2 from the EDL muscle. The same experimental design was used in the next study outlined in Chapter 4 to evaluate the effects of maintaining the coupled anatomy between Toe_1 and Toe_2 on the active Toe_1 MTP joint torque-angle relationship curves for each prescribed Toe_2 MTP joint angle.

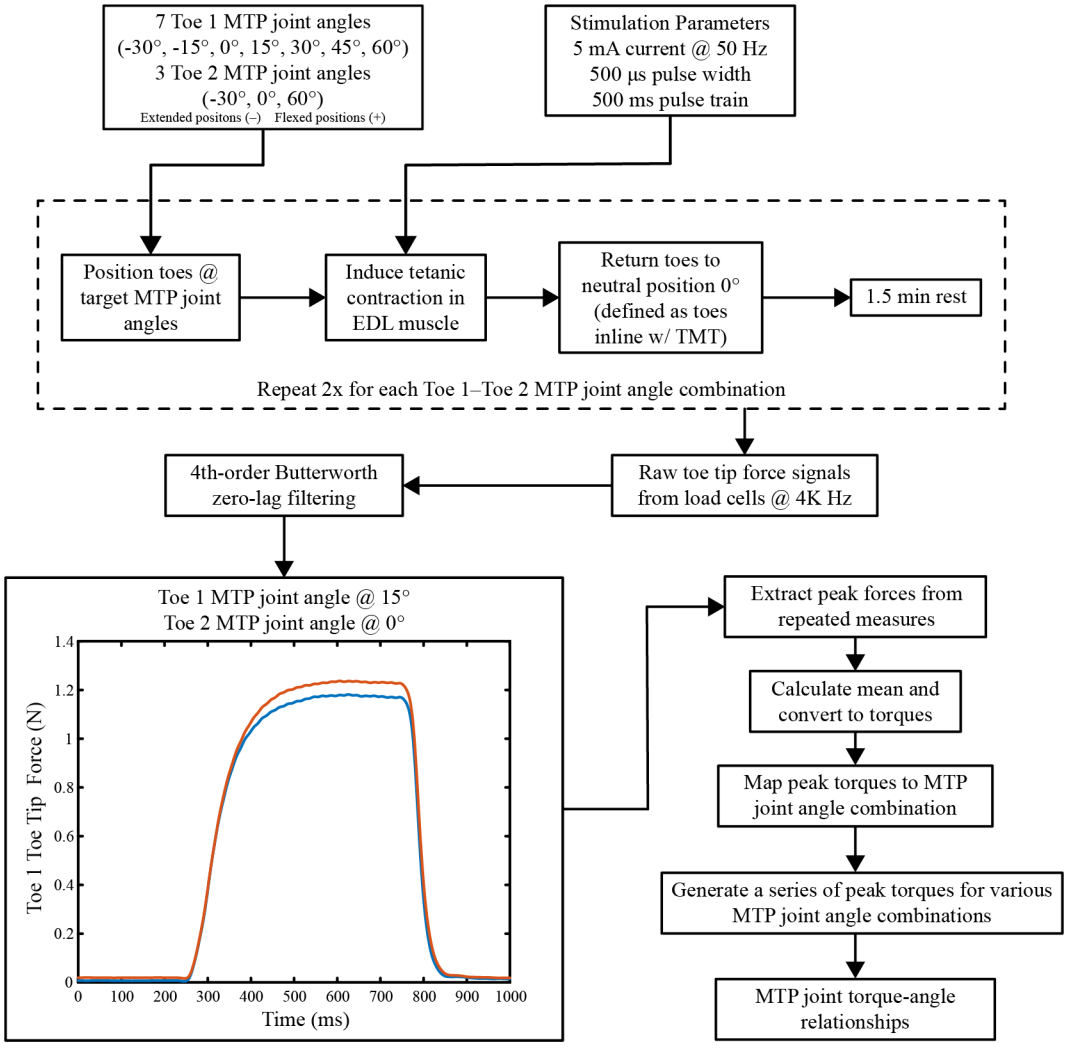

Figure 3.2.3 Experimental workflow and data processing steps for measuring and evaluating the metatarsophalangeal (MTP) joint torque-angle relationship of Toe_1 dependent of Toe_2 MTP joint angle.

3.2.2 Model Design of the Chicken Extensor Digitorum Longus Muscle-Tendon Unit with One Tendon

It was assumed that since Toe_1 tendon was only attached to the EDL muscle in series, the force generated by the EDL muscle was equal to the force experienced in Toe_1 tendon. Thus, the experimental active Toe_1 MTP joint torque-angle relationships for

each prescribed Toe_2 MTP joint angle were curve-fitted to a piecewise cubic interpolation model to ultimately formulate the active force generation relationship of the chicken EDL muscle itself. This force generation profile was used as the EDL muscle force generation input in the next steps for modeling the force generation of the chicken EDL muscle through more complex tendon networks.

3.2.3 Model Design of the Chicken Extensor Digitorum Longus Muscle-Tendon Unit with Two Tendons Coupled in Parallel

In developing the model for isometric muscle force generation through a tendon network with two tendons coupled in parallel, the muscle-tendon unit was modeled as a series of muscle fibers with a length of tendon ($Tendon_0$) subsequently attached to two more lengths of tendons ($Tendon_1$ and $Tendon_2$) coupled in parallel. Each tendon segment or element was a series elastic component. No muscle series elastic component was incorporated into the model. There were 4 attachment points or nodes in the tendon network, the first node ($Node_0$) represented the attachment point between the EDL muscle and the first length of tendon, the second node ($Node_1$) represented the bifurcation of the two tendons attached to the first length of tendon and coupled in parallel, and the third and fourth nodes ($Node_2$ and $Node_3$) each represented an endpoint or toe tip of the coupled tendons. The complete tendon network modeled in series with the muscle resembled a Y-shaped tendon network (Figure 3.2.4). The lengths of each tendon segment and the location of each node were arbitrarily determined. The overall effects of the tendon network configuration were emphasized and prioritized in this study.

The isometric muscle force generation through this coupled tendon network was evaluated as the force experienced at the endpoint nodes (toe tips), $Node_2$ and $Node_3$, using the direct stiffness method (or sometimes referred to as the nodal displacement method).

In the direct stiffness method, the tendon network was broken down into subcomponents or elements (lengths of tendon) and for each component, the

displacement values at its two ends or nodes (attachment/connection points) were the unknown variables of the problem. The mechanical properties of the underlying continuum of each subcomponent or element were represented by a stiffness matrix. It relates the nodal displacements to nodal forces via a linear transformation. Altogether, the direct stiffness method defined the tendon network as a system of force equilibrium equations established by the assembly of the global structural stiffness matrix and the force vector. To derive the systems of equations, two important conditions had to be met for the tendon network: force equilibration at each node and material response of each tendon element. The system of force-displacement equilibrium equations can be represented in terms of a matrix notation,

$$F = Ku = 0,$$

where the elemental nodal force vector, F, is equal to the product of the elemental (local) stiffness matrix, K, and the elemental nodal displacement vector, u. Here, the elemental stiffness matrix, K, can be interpreted as a linear transformation matrix, which linearly transforms the nodal displacement vector, u, onto the corresponding nodal force vector, F.

$$u = K^{-1}F$$

Therefore, the elemental stiffness matrix must be square of size n, the number of degrees of freedom in the element, symmetric ($K = K^T$), and singular (not invertible; $|K| = 0$). Furthermore, the summation of all rows and all columns must equal 0. The elemental stiffness matrix can be related to a global coordinate system by a basic coordinate transformation and given the orientation angle, θ, of the element with respect to the global coordinate system.

For the tendon network in this study (Figure 3.2.4), there were 3 tendon elements and their elemental nodal force-displacement equilibrium equations were written as:

$Tendon_0$ with $Node_0$ and $Node_1$:

$$\begin{bmatrix} f_{x0} \\ f_{y0} \\ f_{x1} \\ f_{y1} \end{bmatrix} = \begin{bmatrix} k_{11} & k_{12} & k_{13} & k_{14} \\ k_{21} & k_{22} & k_{23} & k_{24} \\ k_{31} & k_{32} & k_{33} & k_{34} \\ k_{41} & k_{42} & k_{43} & k_{44} \end{bmatrix} \begin{bmatrix} u_{x0} \\ u_{y0} \\ u_{x1} \\ u_{y1} \end{bmatrix}$$

$Tendon_1$ with $Node_1$ and $Node_2$:

$$\begin{bmatrix} f_{x1} \\ f_{y1} \\ f_{x2} \\ f_{y2} \end{bmatrix} = \begin{bmatrix} k_{11} & k_{12} & k_{13} & k_{14} \\ k_{21} & k_{22} & k_{23} & k_{24} \\ k_{31} & k_{32} & k_{33} & k_{34} \\ k_{41} & k_{42} & k_{43} & k_{44} \end{bmatrix} \begin{bmatrix} u_{x1} \\ u_{y1} \\ u_{x2} \\ u_{y2} \end{bmatrix}$$

$Tendon_2$ with $Node_1$ and $Node_3$:

$$\begin{bmatrix} f_{x1} \\ f_{y1} \\ f_{x3} \\ f_{y3} \end{bmatrix} = \begin{bmatrix} k_{11} & k_{12} & k_{13} & k_{14} \\ k_{21} & k_{22} & k_{23} & k_{24} \\ k_{31} & k_{32} & k_{33} & k_{34} \\ k_{41} & k_{42} & k_{43} & k_{44} \end{bmatrix} \begin{bmatrix} u_{x1} \\ u_{y1} \\ u_{x3} \\ u_{y3} \end{bmatrix}$$

General Stiffness Matrix:

$$K = \begin{bmatrix} k_{11} & k_{12} & k_{13} & k_{14} \\ k_{21} & k_{22} & k_{23} & k_{24} \\ k_{31} & k_{32} & k_{33} & k_{34} \\ k_{41} & k_{42} & k_{43} & k_{44} \end{bmatrix}$$

The stiffness terms, k_{ij}, were the same for a given tendon element. The transformation matrix that relates the elemental stiffness matrix, K, to the global coordinate system given the orientation angle of the element with respect to the global coordinate system was written as:

$$\begin{bmatrix} c^2 & cs & -c^2 & -cs \\ cs & s^2 & -cs & -s^2 \\ -c^2 & -cs & c^2 & cs \\ -cs & -s^2 & cs & s^2 \end{bmatrix}$$

$$c = cos\theta$$

$$s = sin\theta$$

θ: angle of the element between the local and global coordinate system

Altogether, the elemental nodal force-displacement equilibrium equations for each tendon element were then written in the global coordinate system as:

$Tendon_0$ with $Node_0$ and $Node_1$:

$$\begin{bmatrix} F_0 \\ F_1 \\ 0 \\ 0 \end{bmatrix} = \begin{bmatrix} K_0 & -K_0 & 0 & 0 \\ -K_0 & K_0 & 0 & 0 \\ 0 & 0 & 0 & 0 \\ 0 & 0 & 0 & 0 \end{bmatrix} \begin{bmatrix} U_0 \\ U_1 \\ U_2 \\ U_3 \end{bmatrix}, where\ K_0 = k_0 \begin{bmatrix} c^2 & cs \\ cs & s^2 \end{bmatrix}$$

$Tendon_1$ with $Node_1$ and $Node_2$:

$$\begin{bmatrix} 0 \\ F_1 \\ F_2 \\ 0 \end{bmatrix} = \begin{bmatrix} 0 & 0 & 0 & 0 \\ 0 & K_1 & -K_1 & 0 \\ 0 & -K_1 & K_1 & 0 \\ 0 & 0 & 0 & 0 \end{bmatrix} \begin{bmatrix} U_0 \\ U_1 \\ U_2 \\ U_3 \end{bmatrix}, where\ K_1 = k_1 \begin{bmatrix} c^2 & cs \\ cs & s^2 \end{bmatrix}$$

$Tendon_2$ with $Node_1$ and $Node_3$:

$$\begin{bmatrix} 0 \\ F_1 \\ 0 \\ F_3 \end{bmatrix} = \begin{bmatrix} 0 & 0 & 0 & 0 \\ 0 & K_2 & 0 & -K_2 \\ 0 & 0 & 0 & 0 \\ 0 & -K_2 & 0 & K_2 \end{bmatrix} \begin{bmatrix} U_0 \\ U_1 \\ U_2 \\ U_3 \end{bmatrix}, where\ K_2 = k_2 \begin{bmatrix} c^2 & cs \\ cs & s^2 \end{bmatrix}$$

The summation of the three sets of equations produced the overall global force-displacement equilibrium equations for the tendon network:

$$\begin{bmatrix} F_0 \\ F_1 \\ F_2 \\ F_3 \end{bmatrix} = \begin{bmatrix} K_0 & -K_0 & 0 & 0 \\ -K_0 & (K_0 + K_1 + K_2) & -K_1 & -K_2 \\ & 0 \quad -K_1 & K_1 & 0 \\ & 0 \quad -K_2 & 0 & K_2 \end{bmatrix} \begin{bmatrix} U_0 \\ U_1 \\ U_2 \\ U_3 \end{bmatrix}$$

$$F_0 = \begin{bmatrix} f_{x0} \\ f_{y0} \end{bmatrix},\ F_1 = \begin{bmatrix} f_{x1} \\ f_{y1} \end{bmatrix},\ F_2 = \begin{bmatrix} f_{x2} \\ f_{y2} \end{bmatrix},\ F_3 = \begin{bmatrix} f_{x3} \\ f_{y3} \end{bmatrix}$$

$$U_0 = \begin{bmatrix} u_{x0} \\ u_{y0} \end{bmatrix},\ U_1 = \begin{bmatrix} u_{x1} \\ u_{y1} \end{bmatrix},\ U_2 = \begin{bmatrix} u_{x2} \\ u_{y2} \end{bmatrix},\ U_3 = \begin{bmatrix} u_{x3} \\ u_{y3} \end{bmatrix}$$

Vectors F_n and U_n described the force and displacement at $Node_n$. Matrix K_e represented the stiffness components of $Tendon_e$.

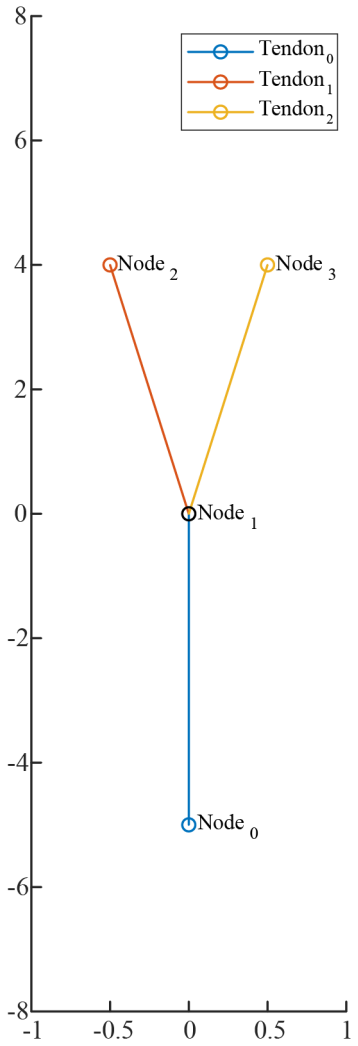

Figure 3.2.4 Model structure representing the extensor digitorum longus (EDL) tendon network of two tendons coupled in parallel. $Node_0$ represents the EDL muscle-tendon attachment point; $Node_1$ represents the natural bifurcation that occurs in the chicken EDL muscle-tendon unit; $Node_2$ and $Node_3$ represent Toe_1 and Toe_2 endpoints, respectively. The direct stiffness method was used to systematically analysis this tendon network structure built from nodes (circles) and elastic elements (solid lines).

In the initial state of the tendon network, the nodes, $Node_0$, $Node_1$, $Node_2$, and $Node_3$, were located at [0, $(-5 - L_m(i))$], [0, 0], [-0.5, $Toe_1(i)$], and [0.5, $Toe_2(j)$], respectively. The y position of $Node_0$ depended on the muscle length, $L_m(i)$, or equivocally the MTP joint angle/y position of $Toe_1(i)$. Likewise, the force acting on

$Node_0$ depended on the muscle length, $L_m(i)$. The y position of $Node_2$ depended on the MTP joint angle/y position of $Toe_1(i)$. Similarly, the y position of $Node_3$ was set to a predetermined MTP joint angle/y position of $Toe_2(j)$. The initial Euclidean lengths of tendon elements, $Tendon_0$, $Tendon_1$, and $Tendon_2$, were calculated as the vector norm of their respective nodes, their initial orientations, θ_e, were calculated as the inverse tangent function, $arctan(x)$, of their respective nodes in the global coordinate system (listed above), and their initial stiffness, k_e, of each tendon element was set to 300. Lastly, all force components, f_{xe} and f_{ye}, of each tendon element were set to 0.

The experimental setup for simulating isometric muscle force generation through this tendon network with two tendons coupled in parallel model mirrored the experimental setup used in the live animal experiment previously described in Section 3.2.1. Isometric muscle force generation was calculated at $Node_2$ (Toe_1) and $Node_3$ (Toe_2) simultaneously for a series of 100 linearly discrete Toe_1 MTP joint angles/y position ranging from 0 to 2 (i, normalized unitless lengths) in combination with each predetermined Toe_2 MTP joint angle/y position, 2, 2.25 and 4 (j, normalized unitless lengths). Extended positions were negative angles and flexed positions were positive angles. In terms of the model, extended positions translated to the node being positioned towards the negative y direction, shortening the tendon element, and flexed positions translated to the node being positioned in the positive y direction, stretching the tendon element. Accordingly, tendon element stiffness increased if the element was stretched and decreased if the element was shortened prior to simulated muscle contraction. Toe_1 MTP joint angles/y position directly related to muscle length, L_m, which determined the amount of force generated at $Node_0$. Specifically, when Toe_1 MTP joint angles/y position was placed in a more extended position, the muscle length parameter was set to a shorter length and conversely set to a longer length when Toe_1 MTP joint angles/y position was placed in a more flexed position. The muscle force-length relationship or MTP joint torque-angle relationship, developed from the experimental data collected (refer to Sections 3.2.2 and 3.2.3), governed the force acting on $Node_0$ and the subsequent resultant forces throughout the tendon network.

Table 3.2.2 Model parameter values of the extensor digitorum longus tendon network of two tendons coupled in parallel.

Parameter	Value
$L_m(i)$	$0 \leq i \leq 2$
$Node_0$	$[0, (-5 - L_m(i))]$
$Node_1$	[0, 0]
$Node_2$	[-0.5, $Toe_1(i)$]
$Node_3$	[0.5, $Toe_2(j)$],
k_0	300
k_1	300
k_2	300

3.3 Results

3.3.1 Measured Metatarsophalangeal Joint Torque-Angle Relationship of the Chicken Extensor Digitorum Longus Muscle-Tendon Unit with a Single Tendon

Repeated measures ANOVA indicated no differences in active Toe_1 MTP joint extension torque at each Toe_1 MTP joint angle across all Toe_2 MTP joint angles (Figure 3.3.1). Essentially, the active Toe_1 MTP joint torque-angle relationship curves were similar for each Toe_2 MTP joint angle. Active Toe_1 MTP joint extension torques varied as a function of Toe_1 MTP joint angle, where the maximum active Toe_1 MTP joint extension torque was measured at 15° Toe_1 MTP joint extension angle (-15°) and the minimum active Toe_1 MTP joint extension torque was measured at 30° Toe_1 MTP

joint flexion angle (Figure 3.3.1). Given there was no difference in the active Toe_1 MTP joint torque-angle relationship curves across all Toe_2 MTP joint angle, the three active Toe_1 MTP joint torque-angle relationship curves were averaged together to produce a single active Toe_1 MTP joint torque-angle relationship curve. This averaged active Toe_1 MTP joint torque-angle relationship curve was curve-fitted to a piecewise cubic interpolation model to ultimately formulate the active force generation relationship of the chicken EDL muscle itself and was used as the input isometric muscle force for succeeding models in this thesis.

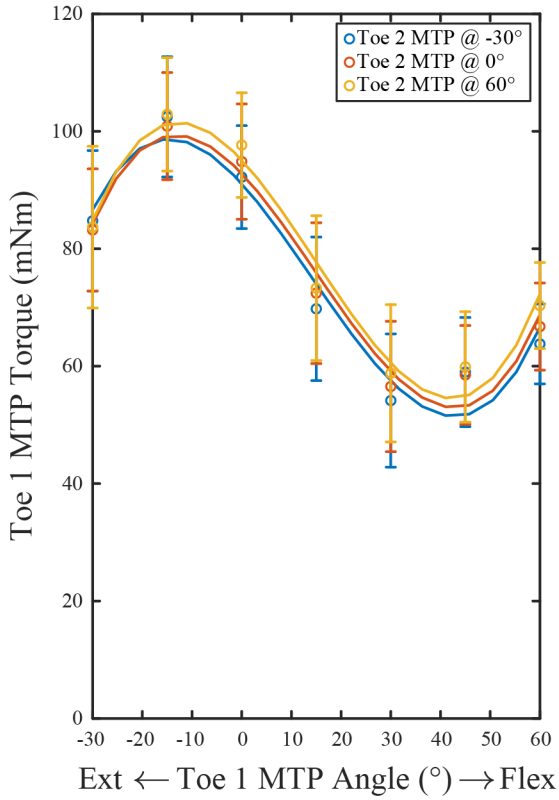

Figure 3.3.1 Measured active Toe_1 metatarsophalangeal (MTP) joint extension torque exerted by the extensor digitorum longus (EDL) muscle as a function of Toe_1 MTP joint angle for each Toe_2 MTP joint angle (-30°, 0°, and 60°) when Toe_1 and Toe_2 MTP joints were decoupled, only leaving Toe_1 MTP joint intact with the EDL muscle. Asterisk denotes significant differences ($p < 0.05$). Values are shown as mean ± SD ($n = 8$).

3.3.2 Simulated Metatarsophalangeal Joint Torque-Angle Relationship of the Chicken Extensor Digitorum Longus Muscle-Tendon Unit with Two Tendons Coupled in Parallel

As expected, this model simulating isometric force generation through a tendon network with two tendons coupled in parallel suggested that there was unbalanced distribution of forces at the endpoints, Toe_1 ($Node_2$) and Toe_2 ($Node_3$). The resultant forces experienced at Toe_1 decreased when coupled to Toe_2 overall. There was greater decrease in force experienced at Toe_1 as Toe_2 was positioned in a more flexed position/angle (at 60° compared to 0° or 30°). This effect was more apparent when Toe_1 was positioned in more extended positions/angles (-30° to 0°) and Toe_2 was completely flexed at 60°. When Toe_1 and Toe_2 were both in flexed positions, the two forces experienced at the nodes were similar. The active Toe_1 MTP joint torque-angle relationship curves maintained similar shapes for each Toe_2 joint angle (Figure 3.3.3).

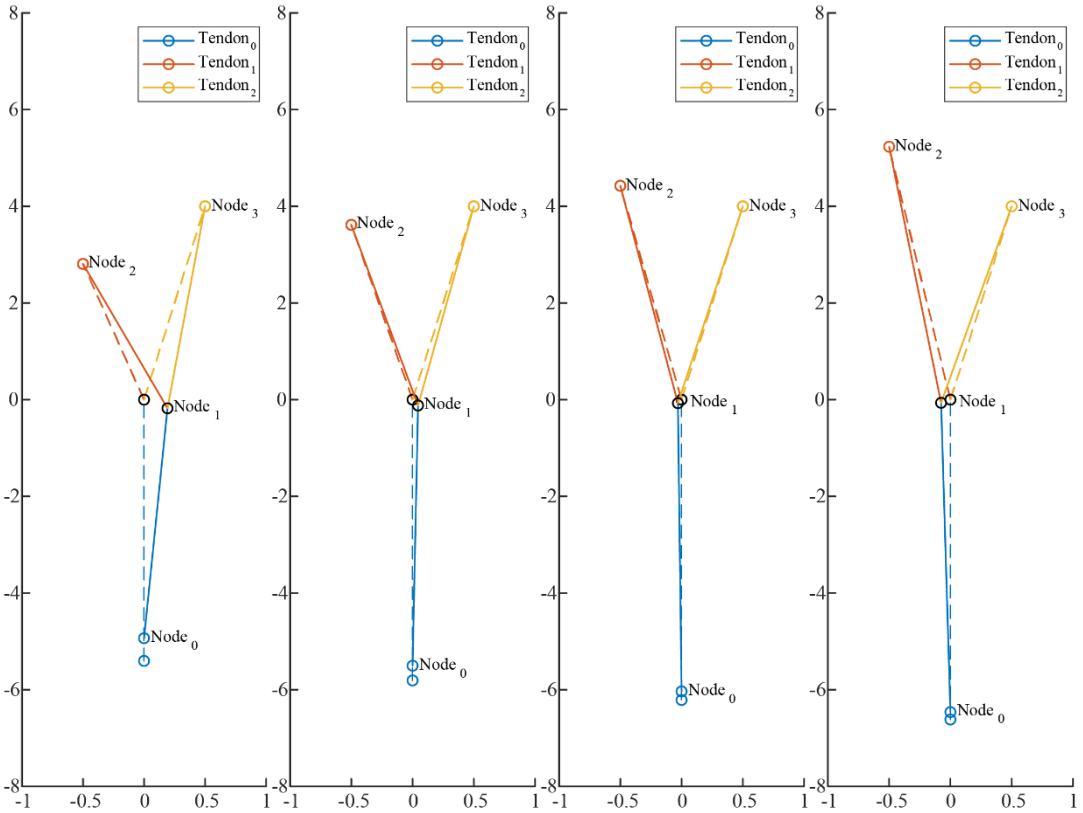

Figure 3.3.2 Simulated extensor digitorum longus (EDL) muscle-tendon force generation through the tendon network of two tendons coupled in parallel for four exemplar combinations of $Node_2$ and $Node_3$ positions out of 300 total simulated (100 $Node_2$ positions and 3 $Node_3$ positions). $Node_2$ was set at various positions while $Node_3$ was at position 4 in the series of simulations depicte. Resultant forces at $Node_2$ and $Node_3$ were analyzed via the direct stiffness method. Each simulation iteration demonstrates the initial tendon network state (dashed line and circles) and resulting tendon network state (solid lines and circles) after EDL muscle force acts on $Node_0$.

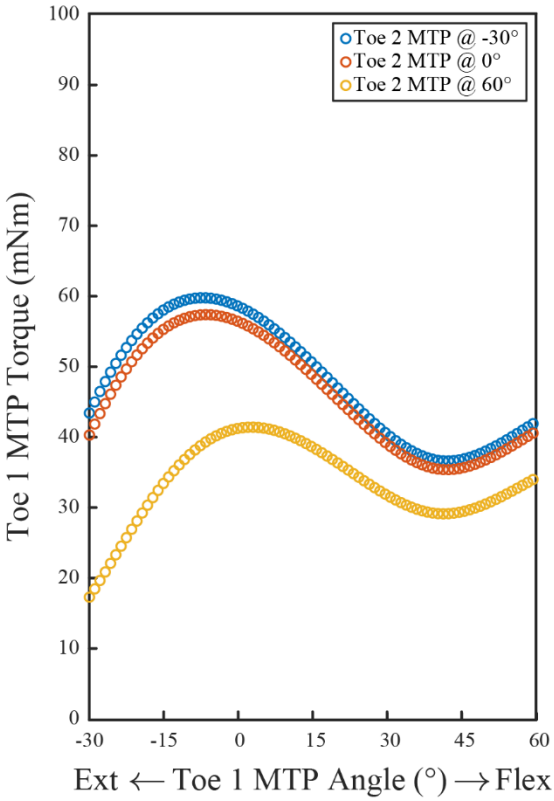

Figure 3.3.3 Simulated active Toe_1 ($Node_2$) metatarsophalangeal (MTP) joint extension torques exerted by the extensor digitorum longus (EDL) muscle as a function of Toe_1 MTP joint angles for each Toe_2 ($Node_3$) MTP joint angle (-30°, 0°, and 60°).

3.4 Discussion

In this study, the isometric force generation of the chicken EDL muscle through a single tendon was successfully measured and characterized. A method and experimental design for measuring two toe tip forces simultaneously were devised. The experimental data collected was used to create a model of isometric muscle force generation to input into a more complex tendon network model, where two tendons were coupled in parallel. Altogether, the developed isometric force generation profile of the chicken EDL muscle, the model structure of two tendons coupled in parallel, and using the direct stiffness method facilitated a systemic analysis that evaluated the behavior of isometric muscle force generation through two tendons coupled in parallel.

This study presented a unique set of experimental data and developed models based on the chicken EDL muscle-tendon unit of a live animal model that was arguably analogous to the human the resulting coupled four tendon muscle-tendon unit from ECRL-to-FDP tendon transfer. The simulated active Toe_1 ($Node_2$) MTP joint torque-angle relationship curves demonstrated that when the two tendons/toes were coupled and configured in extreme differential positions, muscle force was lost in the Toe_1 MTP joint. This phenomenon was most evident when Toe_1 was in a more extended position, while Toe_2 ($Node_3$) was in a more flexed position. In this particular combination of Toe_1-Toe_2 positions, muscle force was distributed more favorably to Toe_2 because Toe_2 was in a more advantageous positioned relative to Toe_1, creating slack in the tendon of Toe_1. Interestingly, whenever Toe_1 was in a more flexed position (≥30°), active Toe_1 MTP joint torques were similar, regardless of Toe_2's position.

The primary takeaway from the results presented in this study emphasize the disadvantage of directly suturing multiple tendons to a single muscle, creating a coupled tendon network muscle-tendon unit. Muscle forces transmitted through the tendon network will become unevenly distributed in differential configurations of the tendons/toes/fingers. The fundamental mechanics demonstrated here are inherent to the limited grasping abilities after tendon transfer for high median-ulnar nerve palsy and lead to poor interaction with objects, such as a ball, in the clinical setting.

Chapter 4: Modeling the Isometric Muscle-Tendon Force Generation Through a Passive Differential Mechanism

4.1 Introduction

Most complex engineering products, from bicycles to aircrafts, are designed using modeling and simulation. Researchers have increasing confidences in modeling and simulating approaches for design because the underlying mathematical models of materials and system dynamics have been well established over the past several decades and the available computational tools have been validated to represent analogous real-world systems. Thus, modeling and simulation of mechanical systems play a significant role in product design and engineering, especially in biomedical applications and healthcare. Modeling and simulating behaviors of biological systems, such as the mechanics of the musculoskeletal system, are just the beginning to making an impact in healthcare. However, validating these models is an important step to guarantee reliability and alignment to the analogous real-world systems.

In Chapter 3, a model of the chicken extensor digitorum longus (EDL) isometric muscle-tendon force generation was created based on quantitative data collected from live animal experiments. This model constitutes the physiological behavior and operating range of the EDL muscle force capacity at the metatarsophalangeal (MTP) joints. Then, a model describing the physical tendon network system of the chicken EDL muscle-tendon unit as elastic elements and nodes with force and displacement characteristics was defined. Together, a model simulating the isometric muscle force generation behavior of the chicken EDL muscle-tendon unit through a tendon network with tendons coupled in parallel was formulated. But before exploring the effects of a passive differential mechanism (PDM) on the chicken EDL muscle-tendon force generation and distribution, the model must be validated and scaled appropriately.

The objectives of this study were also three-fold. One objective was to measure and characterize the isometric muscle force generation of a single skeletal muscle

through two tendons coupled in parallel in the chicken EDL muscle tendon unit. A second objective was to compare the measured and simulated MTP joint torque-angle relationships of the chicken EDL muscle-tendon unit with two tendons coupled in parallel and scale the overall model to best match the measured values. A third objective was to use the appropriately scaled model to investigate the influence of a PDM on the isometric force generation profile of the EDL muscle-tendon unit with two tendons coupled in parallel.

Our research group's previous studies using biomechanical simulations in OpenSim [70] and human [71] and chicken cadavers [72] have demonstrated significant improvements in adaptability of the fingers/toes during physical interaction tasks with the differential actuation provided by an implantable PDM. Naturally, the next step is to demonstrate the differential actuation of the implantable PDM and its efficacy in a live animal model, while accounting for potential complications with foreign body responses and surrounding tissue interactions *in vivo*. The work outlined in this Chapter aimed to model and predict the isometric force generation and distribution of the chicken EDL muscle-tendon unit before conducting live animal experiments with an implantable PDM. Ultimately, this work provides a better understanding of how the implantable PDM performs in a more physiological framework – a step towards translating this technology in humans.

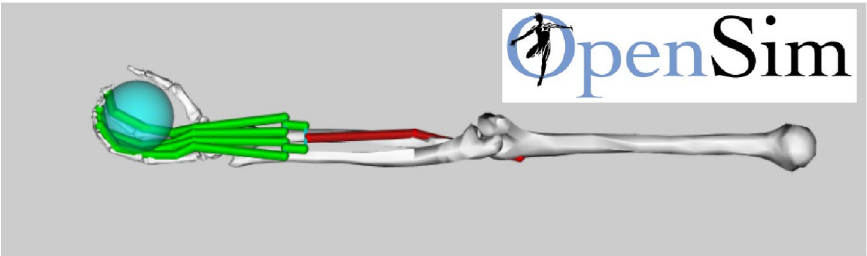

Figure 4.1.1 Hierarchical seesaw system as the passive differential mechanism (PDM) incorporated into an OpenSim model of the extensor carpi radialis longus (ECRL) muscle attached to the four flexor digitorum longus (FDP) tendons. PDM enables differential actuation between the four fingers to adaptively grasp a ball. This figure was adapted from Homayouni (2015) [70].

Figure 4.1.2 Hierarchical pulley system as the passive differential mechanism (PDM) incorporated between the single extensor carpi radialis longus (ECRL) muscle and the four flexor digitorum longus (FDP) tendons of a human upper extremity cadaver. This figure was adapted from Mardula (2015) [71].

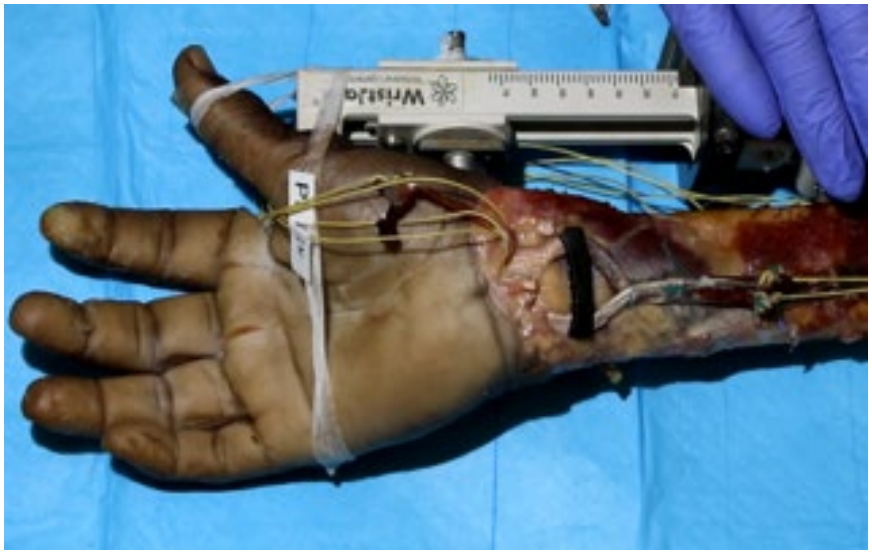

Figure 4.1.3 Single translating, pivoting triangle system, constructed from the biological tendons and an artificial strut-shaped implant, as the passive differential mechanism (PDM) incorporated between the single extensor carpi radialis longus (ECRL) muscle and two flexor digitorum longus (FDP) tendons of a human upper extremity cadaver. This image was captured during pilot human cadaver experiments conducted in collaborators with our colleagues at the University of Southern California.

4.2 Methods

4.2.1 Model Validation of the Chicken Extensor Digitorum Longus Muscle-Tendon Unit with Two Tendons Coupled in Parallel

The data used to validate the model of the chicken EDL muscle-tendon force generation through two tendons coupled in parallel was collected using the same methods described in Section 3.2.1. The same experimental was maintained to Chickens were sedated and placed in dorsal recumbency for a distal EDL tenotomy for establishing the coupled tendon network configuration (refer to Appendix A.1 for surgical procedure details). Following the procedure and continual sedation, each chicken was moved into right recumbency and their left pelvic limb was rigidly fixed at 115° to prevent intertarsal joint rotation via a custom chicken intertarsal joint fixation unit (Figure 3.2.2A). Digit IV and digit II were splinted to prevent all interphalangeal joint rotations, except for the MTP joints, and each toe tip was affixed to a single-axis load cell (Miniature S-Beam Jr. Load Cell, LSB201, 10 lb., FUTEK Advanced Sensor Technology, Inc., Irvine, CA, USA) via a custom toe rotation unit (Figure 3.2.2B). For the model, digit IV and digit II were designated as Toe_1 and Toe_2, respectively. Intramuscular electrodes were inserted into the EDL muscle through hypodermic needles. Functional electrical stimulation (FES) was applied to the EDL muscle via intramuscular electrodes at near-submaximal contraction stimulation parameters listed in Table 3.2.1 above.

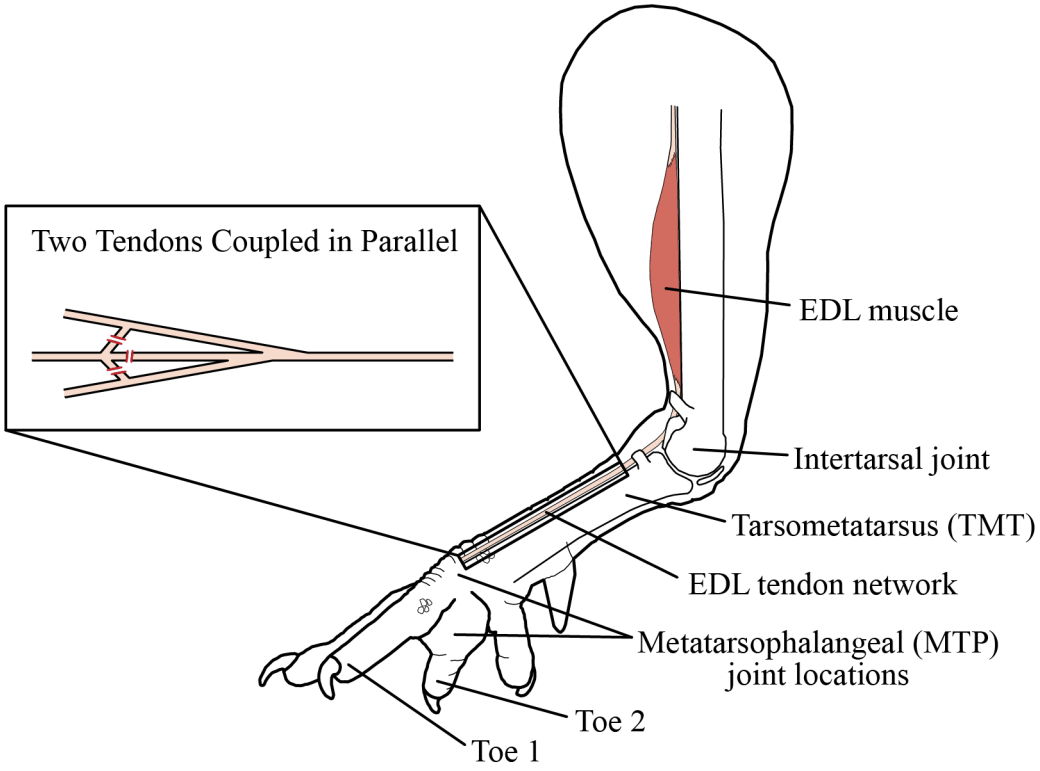

Figure 4.2.1 Coupled tendon network configuration was established from a distal extensor digitorum longus (EDL) tenotomy to release digit III, leaving digit IV (Toe_1) and digit II (Toe_2) intact with the EDL muscle-tendon unit.

Isometric EDL muscle force generation was measured at each toe tip simultaneously for various combinations of Toe_1 MTP joint angles (-30°, -15°, 0°, 15°, 30°, 45°, and 60°) and Toe_2 MTP joint angles (-30°, 0°, and 60°). Extended positions were negative angles and flexed positions were positive angles. Neutral position, 0°, was defined as the toe in line with the tarsometatarsus. Toes were positioned at randomized target MTP joint angles and FES was delivered to induce tetanic contraction in the EDL muscle. Toes were return to neutral positions for a 1.5 min rest period. These steps were repeated twice for each Toe_1-Toe_2 MTP joint angle combination. In total, 42 stimulations were delivered to each chicken EDL muscle (21 combinations, 2 times each).

Raw toe tip force signals from the load cells were sampled at 4 kHz frequency and filtered using a 4th-order Butterworth zero-lag filter via a custom MATLAB script

(vR2020a, MathWorks Inc., Natick, MA, USA; refer to Appendix F.1). Active peak forces from repeated measures, defined as the difference between the baseline residual force immediately prior to stimulation and the maximum force generated during stimulation, were extracted, averaged, and converted to joint torque ($\tau = r \times F$) based on the MTP joint moment arms (r) grossly measured postmortem. The difference between the baseline force when the toes were in the neutral position and the baseline residual force when the toes were moved to targeted position just prior to stimulation was calculated as the passive torque of the EDL muscle-tendon unit.

Active peak torques were mapped to MTP joint angle combinations to generate a series of peak torques for various MTP joint angle combinations – producing the active MTP joint torque-angle relationship curves. Statistically significant differences between Toe_1 MTP joint torque-angle relationship curves for each prescribed Toe_2 MTP joint angle were determined using repeated measures analysis of variance (ANOVA). Significance level was set *a priori* at $\alpha = 0.05$. Bonferroni adjusted post-hoc pairwise comparisons were performed when the ANOVA F-test was significant.

Experimental active MTP joint torque-angle relationship curves served as reference points for scaling the model results presented in Figure 3.3.3. Differences between the experimental and model results were minimized to match the curves magnitudes. No shape analysis on the curves were performed. Experimental data also ensured that the y positions in the model was mapped (remapped) appropriately to the MTP angles to frame the model into the analogous real-world anatomy of the chicken (i.e., MTP joint space).

4.2.2 Model Design of the Chicken Extensor Digitorum Longus Muscle-Tendon Unit with Two Tendons Integrated into a Passive Differential Mechanism

Similar to the model design and methods outlined in Section 3.2.3, the isometric muscle force generation through a PDM incorporated into the same coupled tendon network

previously described was evaluated as the force experienced at the endpoint nodes (toe tips), $Node_2$ and $Node_3$, using the direct stiffness method. In contrast, an extremely stiff elastic element representing the strut-shaped implant was added, splitting the $Tendon_1$ and $Tendon_2$ elements into two parts each ($Tendon_{1a}$, $Tendon_{1b}$ and $Tendon_{2a}$, $Tendon_{2b}$, respectively), which added two new nodes to the system, $Node_a$ and $Node_b$. Their elemental nodal force-displacement equilibrium equations were written as:

$Tendon_0$ with $Node_0$ and $Node_1$:

$$\begin{bmatrix} F_0 \\ F_1 \\ 0 \\ 0 \\ 0 \\ 0 \end{bmatrix} = \begin{bmatrix} K_0 & -K_0 & 0 & 0 & 0 & 0 \\ -K_0 & K_0 & 0 & 0 & 0 & 0 \\ 0 & 0 & 0 & 0 & 0 & 0 \\ 0 & 0 & 0 & 0 & 0 & 0 \\ 0 & 0 & 0 & 0 & 0 & 0 \\ 0 & 0 & 0 & 0 & 0 & 0 \end{bmatrix} \begin{bmatrix} U_0 \\ U_1 \\ U_a \\ U_b \\ U_2 \\ U_3 \end{bmatrix}, where\ K_0 = k_0 \begin{bmatrix} c^2 & cs \\ cs & s^2 \end{bmatrix}$$

$Tendon_{1a}$ with $Node_1$ and $Node_a$:

$$\begin{bmatrix} 0 \\ F_1 \\ F_a \\ 0 \\ 0 \\ 0 \end{bmatrix} = \begin{bmatrix} 0 & 0 & 0 & 0 & 0 & 0 \\ 0 & K_{1a} & -K_{1a} & 0 & 0 & 0 \\ 0 & -K_{1a} & K_{1a} & 0 & 0 & 0 \\ 0 & 0 & 0 & 0 & 0 & 0 \\ 0 & 0 & 0 & 0 & 0 & 0 \\ 0 & 0 & 0 & 0 & 0 & 0 \end{bmatrix} \begin{bmatrix} U_0 \\ U_1 \\ U_a \\ U_b \\ U_2 \\ U_3 \end{bmatrix}, where\ K_{1a} = k_{1a} \begin{bmatrix} c^2 & cs \\ cs & s^2 \end{bmatrix}$$

$Tendon_{2a}$ with $Node_1$ and $Node_b$:

$$\begin{bmatrix} 0 \\ F_1 \\ 0 \\ F_b \\ 0 \\ 0 \end{bmatrix} = \begin{bmatrix} 0 & 0 & 0 & 0 & 0 & 0 \\ 0 & K_{2a} & 0 & -K_{2a} & 0 & 0 \\ 0 & 0 & 0 & 0 & 0 & 0 \\ 0 & -K_{2a} & 0 & K_{2a} & 0 & 0 \\ 0 & 0 & 0 & 0 & 0 & 0 \\ 0 & 0 & 0 & 0 & 0 & 0 \end{bmatrix} \begin{bmatrix} U_0 \\ U_1 \\ U_a \\ U_b \\ U_2 \\ U_3 \end{bmatrix}, where\ K_{2a} = k_{2a} \begin{bmatrix} c^2 & cs \\ cs & s^2 \end{bmatrix}$$

$Implant$ with $Node_a$ and $Node_b$:

$$\begin{bmatrix} 0 \\ 0 \\ F_a \\ F_b \\ 0 \\ 0 \end{bmatrix} = \begin{bmatrix} 0 & 0 & 0 & 0 & 0 & 0 \\ 0 & 0 & 0 & 0 & 0 & 0 \\ 0 & 0 & K_{ab} & -K_{ab} & 0 & 0 \\ 0 & 0 & -K_{ab} & K_{ab} & 0 & 0 \\ 0 & 0 & 0 & 0 & 0 & 0 \\ 0 & 0 & 0 & 0 & 0 & 0 \end{bmatrix} \begin{bmatrix} U_0 \\ U_1 \\ U_a \\ U_b \\ U_2 \\ U_3 \end{bmatrix}, where\ K_{ab} = k_{ab} \begin{bmatrix} c^2 & cs \\ cs & s^2 \end{bmatrix}$$

$Tendon_{1b}$ with $Node_a$ and $Node_2$:

$$\begin{bmatrix} 0 \\ 0 \\ F_a \\ 0 \\ F_2 \\ 0 \end{bmatrix} = \begin{bmatrix} 0 & 0 & 0 & 0 & 0 & 0 \\ 0 & 0 & 0 & 0 & 0 & 0 \\ 0 & 0 & K_{1b} & 0 & -K_{1b} & 0 \\ 0 & 0 & 0 & 0 & 0 & 0 \\ 0 & 0 & -K_{1b} & 0 & K_{1b} & 0 \\ 0 & 0 & 0 & 0 & 0 & 0 \end{bmatrix} \begin{bmatrix} U_0 \\ U_1 \\ U_a \\ U_b \\ U_2 \\ U_3 \end{bmatrix}, where\ K_{1b} = k_{1b} \begin{bmatrix} c^2 & cs \\ cs & s^2 \end{bmatrix}$$

$Tendon_{2b}$ with $Node_b$ and $Node_3$:

$$\begin{bmatrix} 0 \\ 0 \\ 0 \\ F_b \\ 0 \\ F_3 \end{bmatrix} = \begin{bmatrix} 0 & 0 & 0 & 0 & 0 & 0 \\ 0 & 0 & 0 & 0 & 0 & 0 \\ 0 & 0 & 0 & 0 & 0 & 0 \\ 0 & 0 & 0 & K_{2b} & 0 & -K_{2b} \\ 0 & 0 & 0 & 0 & 0 & 0 \\ 0 & 0 & 0 & -K_{2b} & 0 & K_{2b} \end{bmatrix} \begin{bmatrix} U_0 \\ U_1 \\ U_a \\ U_b \\ U_2 \\ U_3 \end{bmatrix}, where\ K_{2b} = k_{2b} \begin{bmatrix} c^2 & cs \\ cs & s^2 \end{bmatrix}$$

The summation of the six sets of equations produced the overall global force-displacement equilibrium equations for the tendon network:

$$\begin{bmatrix} F_0 \\ F_1 \\ F_a \\ F_b \\ F_2 \\ F_3 \end{bmatrix} = \begin{bmatrix} K_0 & -K_0 & 0 & 0 & 0 & 0 \\ -K_0 & (K_0 + K_{1a} + K_{2a}) & -K_{1a} & -K_{2a} & 0 & 0 \\ 0 & -K_{1a} & (K_{1a} + K_{ab} + K_{1b}) & -K_{ab} & -K_{1b} & 0 \\ 0 & -K_{2a} & -K_{ab} & (K_{2a} + K_{ab} + K_{2b}) & 0 & -K_{2b} \\ 0 & 0 & -K_{1b} & 0 & K_{1b} & 0 \\ 0 & 0 & 0 & -K_{2b} & 0 & K_{2b} \end{bmatrix} \begin{bmatrix} U_0 \\ U_1 \\ U_a \\ U_b \\ U_2 \\ U_3 \end{bmatrix}$$

$$F_0 = \begin{bmatrix} f_{x0} \\ f_{y0} \end{bmatrix},\ F_1 = \begin{bmatrix} f_{x1} \\ f_{y1} \end{bmatrix},\ F_a = \begin{bmatrix} f_{xa} \\ f_{ya} \end{bmatrix},\ F_b = \begin{bmatrix} f_{xb} \\ f_{yb} \end{bmatrix}, F_2 = \begin{bmatrix} f_{x2} \\ f_{y2} \end{bmatrix},\ F_3 = \begin{bmatrix} f_{x3} \\ f_{y3} \end{bmatrix}$$

$$U_0 = \begin{bmatrix} u_{x0} \\ u_{y0} \end{bmatrix},\ U_1 = \begin{bmatrix} u_{x1} \\ u_{y1} \end{bmatrix},\ U_a = \begin{bmatrix} u_{xa} \\ u_{ya} \end{bmatrix},\ U_b = \begin{bmatrix} u_{xb} \\ u_{yb} \end{bmatrix},\ U_2 = \begin{bmatrix} u_{x2} \\ u_{y2} \end{bmatrix},\ U_3 = \begin{bmatrix} u_{x3} \\ u_{y3} \end{bmatrix}$$

Vectors F_n and U_n described the force and displacement at $Node_n$. Matrix K_e represented the stiffness components of $Tendon_e$.

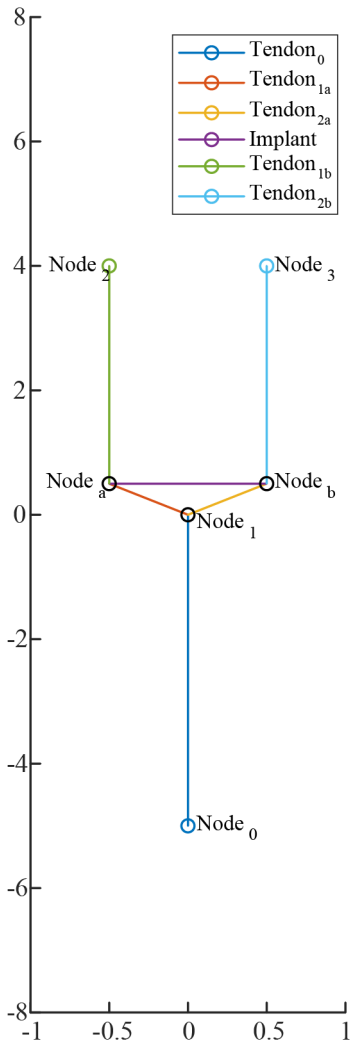

Figure 4.2.2 Model structure representing the extensor digitorum longus (EDL) tendon network of two tendons integrated into a passive differential mechanism (PDM) via a strut-shaped artificial implant. Two tendons and strut-shaped implant form a

translating, pivoting triangle mechanism. $Node_0$ represents the EDL muscle-tendon attachment point; $Node_1$ represents the natural bifurcation that occurs in the chicken EDL muscle-tendon unit; $Node_a$ and $Node_b$ represent the attachment points of the strut-shaped implant (purple horizontal line); $Node_2$ and $Node_3$ represent Toe_1 and Toe_2 endpoints, respectively. The direct stiffness method was used to systematically analysis this tendon network structure built from nodes (circles) and elastic elements (solid lines).

In the initial state of the tendon network, the nodes, $Node_0$, $Node_1$, $Node_a$, $Node_b$, $Node_2$, and $Node_3$, were located at [0, $(-5 - L_m(i))$], [0, $Bifurcation(i)$], [- 0.5, $(Implant_{height} + Implant(i))$], [0.5, $Implant_{height}$], [-0.5, $Toe_1(i)$], and [0.5, $Toe_2(j)$], respectively. The y position of $Node_0$ depended on the muscle length, $L_m(i)$, or equivocally the MTP joint angle/y position of $Toe_1(i)$. Likewise, the force acting on $Node_0$ depended on the muscle length, $L_m(i)$. The y position of $Node_1$ was based on how the $Implant$ element was positioned due to the positions of $Node_2$ and $Node_3$. The y position of $Node_a$ and $Node_b$ were related to the MTP joint angle/y position of $Toe_1(i)$ and $Toe_2(j)$, respectively. The y position of $Node_2$ depended on the MTP joint angle/y position of $Toe_1(i)$. Similarly, the y position of $Node_3$ was set to a predetermined MTP joint angle/y position of $Toe_2(j)$. The initial Euclidean lengths of tendon elements, $Tendon_0$, $Tendon_{1a}$, $Tendon_{1b}$, $Tendon_{2a}$, and $Tendon_{2b}$, were calculated as the vector norm of their respective nodes, their initial orientations, θ_e, were calculated as the inverse tangent function, $arctan(x)$, of their respective nodes in the global coordinate system (listed above), and their initial stiffness, k_e, of each tendon element was set to 300. The length and orientation of the implant element, $Implant$, was determined similarly to the tendon elements, but the initial stiffness of the implant element was arbitrarily set to a large value of 5000 to model a rigid, strut-shaped implant made of a hard plastic. Lastly, all force components, f_{xe} and f_{ye}, of each tendon element and the implant element were set to 0.

The experimental setup for simulating isometric muscle force generation through this tendon network with a PDM mirrored the experimental setup used in the

live animal experiment previously described in Section 3.2.1. Isometric muscle force generation was calculated at $Node_2$ (Toe_1) and $Node_3$ (Toe_2) simultaneously for a series of 100 linearly discrete Toe_1 MTP joint angles/y position ranging from -30°to 60°in combination with each predetermined Toe_2 MTP joint angle (-30°, 0°, and 60°). The orientation of the $Implant$ element changed relative to the positions of $Node_2$ and $Node_3$. When $Node_2$ and $Node_3$ were set at the same y position, the $Implant$ element was orientated horizontally. Extended positions were negative angles and flexed positions were positive angles. In terms of the model, extended positions translated to the node being positioned towards the negative y direction, shortening the tendon element, and flexed positions translated to the node being positioned in the positive y direction, stretching the tendon element. Accordingly, tendon element stiffness increased if the element was stretched and decreased if the element was shortened prior to simulated muscle contraction. Toe_1 MTP joint angles/y position directly related to muscle length, L_m, which determined the amount of force generated at $Node_0$. Specifically, when Toe_1 MTP joint angles/y position was placed in a more extended position, the muscle length parameter was set to a shorter length and conversely set to a longer length when Toe_1 MTP joint angles/y position was placed in a more flexed position. The muscle force-length relationship or MTP joint torque-angle relationship, developed from the experimental data collected (refer to Sections 3.2.2 and 3.2.3), governed the force acting on $Node_0$ and the subsequent resultant forces throughout the tendon network with the implant.

Table 4.2.1 Model parameter values of the extensor digitorum longus tendon network of a passive differential mechanism.

Parameter	Value
$L_m(i)$	$0 \leq i \leq 2$
$Node_0$	$[0, (-5 - L_m(i))]$
$Node_1$	$[0, Bifurcation(i)]$

$Node_a$	[- 0.5, $(Implant_{height} + Implant(i))$]
$Node_b$	[0.5, $Implant_{height}$]
$Node_2$	[-0.5, $Toe_1(i)$]
$Node_3$	[0.5, $Toe_2(j)$]
k_0	300
k_{1a}	900
k_{2a}	300
$k_{implant}$	5000
k_{1b}	900
k_{2b}	300

4.3 Results

4.3.1 Measured and Validated Metatarsophalangeal Joint Torque-Angle Relationship of the Chicken Extensor Digitorum Longus Muscle-Tendon Unit with Two Tendons Coupled in Parallel

Repeated measures ANOVA indicated differences in active Toe_1 MTP joint torque-angle relationship curves for Toe_2 MTP joint angles at -30° and 0° compared to Toe_2 MTP joint angle at 60° (Figure 4.3.1). Likewise, post-hoc pairwise comparisons found that the Toe_1 MTP joint torques at Toe_1 MTP joint angles ranging from -30° to 15° and Toe_2 MTP joint angles at -30° and 0° were greater compared to Toe_1 MTP joint torques at Toe_1 MTP joint angles ranging from -30° to 15° and Toe_2 MTP joint angles at 60° (Figure 4.3.1). There were no differences in Toe_1 MTP joint torques at Toe_1 MTP joint angles ranging from 30° to 60° across all Toe_2 MTP joint angles. Active

Toe_1 MTP joint extension torques varied as a function of Toe_1 MTP joint angle, where the maximum active Toe_1 MTP joint extension torque was measured at the neutral Toe_1 MTP joint angle (0°) and the minimum active Toe_1 MTP joint extension torque was measured at 30° Toe_1 MTP joint flexion angle (Figure 4.3.1).

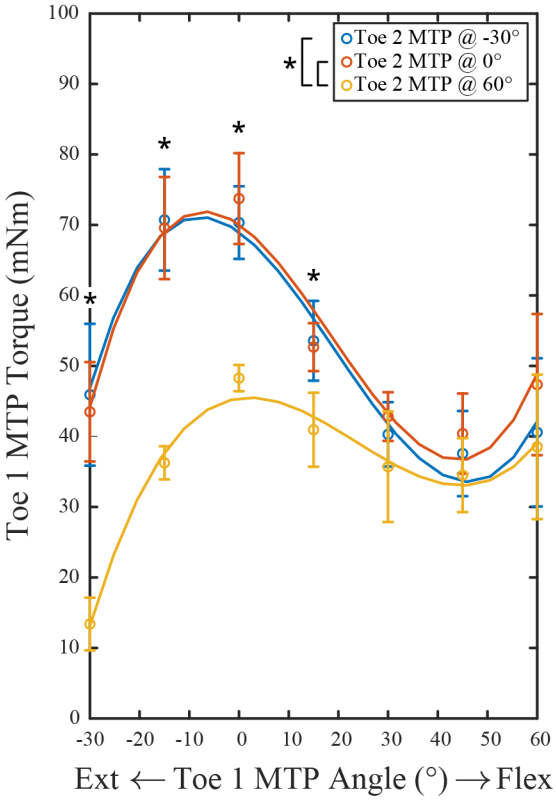

Figure 4.3.1 Measured active Toe_1 metatarsophalangeal (MTP) joint extension torque exerted by the extensor digitorum longus (EDL) muscle as a function of Toe_1 MTP joint angle for each Toe_2 MTP joint angle (-30°, 0°, 60°) when Toe_1 and Toe_2 MTP joints were coupled through tendons coupled in parallel in the EDL muscle-tendon unit. Asterisk denotes significant differences ($p < 0.05$). Values are shown as mean ± SD ($n = 7$).

Experimental data presented in Figure 4.3.1 was used to appropriately adjust and scale the model parameters to represent the *in vivo* isometric muscle force generation through two tendons coupled in parallel. The original model for simulated

active Toe_1 ($Node_2$) MTP joint torque-angle relationship curves (Figure 3.3.3) were modified in two ways: (1) the y positions of the model were remapped to MTP joint angles, specifically y positions 2, 2.25, and 4 mapped to -30°, 0°, and 60°, respectively, for Toe_2 ($Node_3$) MTP joint angles and the y position range 0 to 2 in the model were mapped to the Toe_1 MTP joint angle range -30° to 60°; (2) the input isometric muscle force generation profile was scaled by a factor of 1.2 from the original baseline formulated from curve fitting the experimental data. Ultimately, the experimental and simulated results aligned well with minimal differences and established enough confidence in the model construct for simulating isometric force generation through two tendons coupled in parallel to proceed with using the same methodology in simulating isometric force generation through two tendons integrated into a PDM.

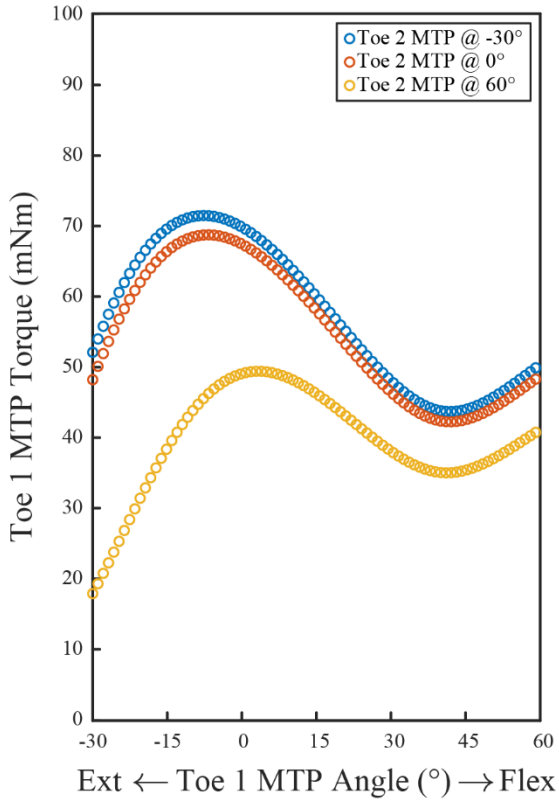

Figure 4.3.2 Adjusted, simulated active Toe_1 ($Node_2$) metatarsophalangeal (MTP) joint extension torques exerted by the extensor digitorum longus (EDL) muscle as a

function of Toe_1 MTP joint angles for each Toe_2 ($Node_3$) MTP joint angle (-30°, 0°, and 60°).

4.3.2 Simulated Metatarsophalangeal Joint Torque-Angle Relationship of the Chicken Extensor Digitorum Longus Muscle-Tendon Unit with Two Tendons Integrated into a Passive Differential Mechanism

This model simulating isometric force generation through a PDM (Figure 4.3.4) suggest that there was improved distribution of forces at the endpoints, Toe_1 ($Node_2$) and Toe_2 ($Node_3$) compared to isometric force generation through two tendons coupled in parallel (Figure 4.3.2). The overall maximum active Toe_1 MTP joint torque in the model using a PDM was less than the overall maximum active Toe_1 MTP joint torque in the model with two tendons coupled in parallel. However, the active Toe_1 MTP joint torque-angle relationship curves were similar across all Toe_2 MTP joint angles. This model also observed some discrepancies in the active Toe_1 MTP joint torque-angle relationship curves towards the flexion range of Toe_1 MTP joint (≥30°), where Toe_1 MTP joint torques were greater when Toe_2 MTP joint was position in -30° or 0° compared to 60°.

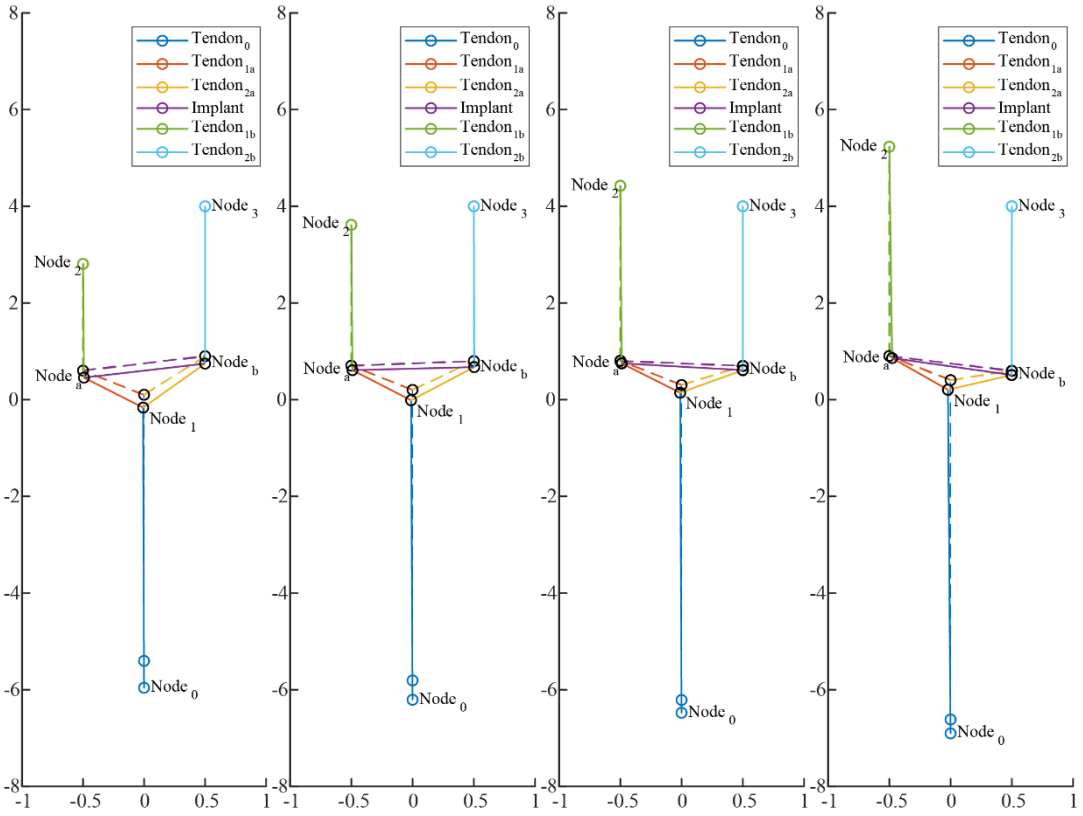

Figure 4.3.3 Simulated extensor digitorum longus (EDL) muscle-tendon force generation through the tendon network of two tendons integrated into a passive differential mechanism (PDM) via a strut-shaped artificial implant (purple horizontal line) for four exemplar combinations of $Node_2$ and $Node_3$ positions out of 300 total simulated (100 $Node_2$ positions and 3 $Node_3$ positions). $Node_2$ was set at various positions while $Node_3$ was at position 4 in the series of simulations depicted above. Resultant forces at $Node_2$ and $Node_3$ were analyzed via the direct stiffness method. Each simulation iteration demonstrates the initial tendon network state (dashed line and circles) and resulting tendon network state (solid lines and circles) after EDL muscle force acts on $Node_0$.

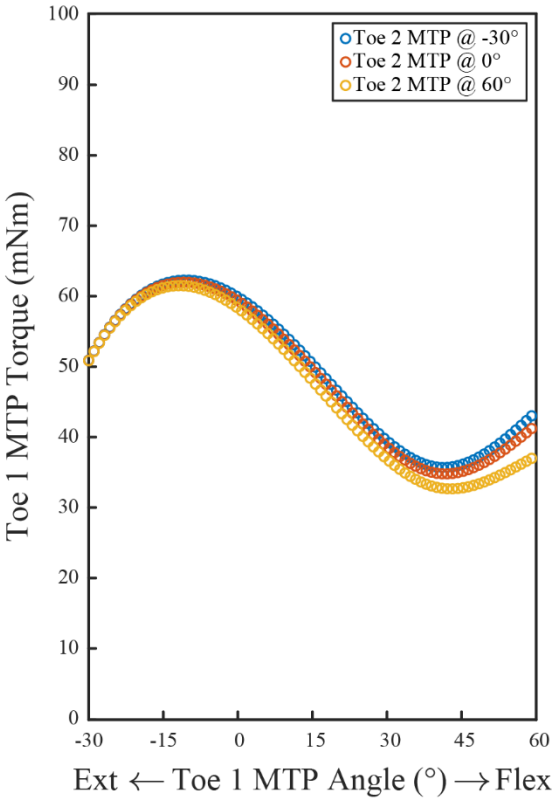

Figure 4.3.4 Simulated active Toe_1 ($Node_2$) metatarsophalangeal (MTP) joint extension torques exerted by the extensor digitorum longus (EDL) muscle as a function of Toe_1 MTP joint angles for each Toe_2 ($Node_3$) MTP joint angle (-30°, 0°, and 60°) when the tendon network model structure includes a passive differential mechanism (PDM) between two tendons coupled in parallel.

4.4 Discussion

In this study, the isometric force generation of the chicken EDL muscle through two tendons coupled in parallel was successfully measured and characterized. The same method and experimental design for measuring two toe tip forces simultaneously were implemented to maintain consistency between measuring forces through the two different tendon network configurations. The experimental data collected was used to validate and scale a model of isometric muscle force generation through two tendons coupled in parallel. Altogether, the validated model structure of two tendons coupled

in parallel and using the direct stiffness method facilitated a systemic analysis that modeled and evaluated the behavior of isometric muscle force generation through a PDM.

This study presented an approach to modeling a PDM in the chicken EDL muscle-tendon unit to observe the underlying mechanics of the system. The simulated active Toe_1 ($Node_2$) MTP joint torque-angle relationship curves demonstrated that with a PDM integrated into the tendon network muscle forces can be distributed more uniformly even when the two tendons/toes are configured in extreme differential positions.

The primary takeaway from the results presented in this study emphasize the advantage of a PDM incorporated into a coupled tendon network muscle-tendon unit. Muscle forces transmitted through the tendon network will become evenly distributed in differential configurations of the tendons/toes/fingers. The fundamental mechanics demonstrated here provide some evidence that an implantable PDM can enable adaptive grasping abilities after tendon transfer for high median-ulnar nerve palsy and lead to improved, secure interactions with objects, such as a ball, in the clinical setting.

Chapter 5: Conclusions

5.1 Summary

The goal of this thesis was to analysis the biomechanics of tendon transfer for combined peripheral nerve injuries, specifically the extensor carpi radialis longus-to-flexor digitorum profundus (ECRL-to-EDP) tendon transfer for high medium-ulnar nerve palsy, while leveraging the development of an implantable passive differential mechanism (PDM) to improve such surgeries. This goal was achieved through studying the chicken extensor digitorum longus (EDL) muscle-tendon unit, a model that was considered analogous to the human four coupled tendon muscle-tendon unit after ECRL-to-FDP tendon transfer and developing a computational model that simulated the isometric muscle force generation through a single tendon, two tendons coupled in parallel, and a passive differential mechanism. The former two tendon network configurations provided insight into the baseline mechanics of a typical muscle-tendon unit and a muscle-tendon unit where a single muscle is coupled to multiple tendons. The latter tendon network configuration highlighted the advantage of incorporating an implantable PDM into a tendon network over a coupled tendon network as a result of tendon transfer.

This thesis elucidated the mechanics responsible for postoperative limitations in hand function by both computational musculoskeletal modeling and *in vivo* animal experiments. For computational musculoskeletal modeling, a model of the mechanical functioning of a muscle-tendon unit with a single muscle attached to multiple tendons was developed (Chapter 3), and the effects of incorporating a PDM into the same muscle-tendon unit with a single muscle attached to multiple tendons were evaluated (Chapter 4). For *in vivo* animal experiments, data for building a phenomenological model of a muscle-tendon unit with a single muscle attached to multiple tendons were collected (Chapter 3), the mechanical functioning of a muscle-tendon unit with a single muscle attached to multiple tendons was observed *in vivo* (Chapter 4), and the computational musculoskeletal modeling of a muscle-tendon unit with a single muscle

attached to multiple tendons was validated to represent the *in vivo* behaviors and to establish confidence for use in subsequent, more complicated models (Chapter 4).

Altogether, this thesis demonstrated the limitations in a muscle attached to multiple tendons, which translates to limited object interaction and poor grasp – patients will need more assistance in activities of daily living. In contrast, this thesis confirms a proof-of-concept PDM to improve the muscle-tendon force distribution between multiple tendons, leading to clinical benefits including adaptive object interactions and secure grasps – patients will be more independent in activities of daily living. Lastly, this thesis also provided unique methodology for measuring isometric toe tip extension forces in a chicken model, which will be valuable for future work related to developing and validating this proof-of-concept PDM.

5.2 Future Work

This thesis confirms the proof of concept for an implantable PDM for the chicken EDL muscle-tendon unit. Combined with human cadaver and other musculoskeletal modeling studies, a fully realized implantable PDM can be designed, manufactured, and studied for optimal efficacy and safety in the human. The next step is to demonstrate the differential actuation of the implantable PDM and its efficacy in a live animal model, while accounting for potential complications with foreign body responses and surrounding tissue interactions *in vivo*. Therefore, a final study will need to be conducted where an implantable PDM is implemented in a live chicken model using the same EDL muscle-tendon unit described in this thesis. The experimental data collected from the future study can be used to confirm and validate the simulated results from this thesis. This final live animal study will ultimately prove the efficacy of an implantable PDM within physiological constrains.

Appendices

A.1 Distal Extensor Digitorum Longus Tenotomy of Digit III

The chicken will be positioned in dorsal recumbency, with the head in lateral recumbency with the endotracheal tube to prevent aspiration on the surgical table. A tourniquet will be applied just distal of the left pelvic limb intertarsal joint to minimize bleeding at the incision site. The left pelvic limb will be draped in a standard fashion with disposable sterile surgical drapes.

A 4 cm incision will be performed on the dorsal aspect of the trochlea of metatarsal III of the left pelvic limb. The connective tissues surrounding EDL tendon will be gently dissected with metzenbaum scissors and iris scissors to allow exposure and access to EDL tendon branch that extends to digit III and intertendinous connections that connect the digit III EDL tendon branch to both the digit II EDL tendon branch and the digit IV EDL tendon branch on either side.

Once exposed, the digit III EDL tendon branch and the respective intertendinous connections will be transected using a scalpel and iris scissors.

The skin will be sutured closed with 4-0 Ethilon black monofilament or another non-absorbable suture material and a swedged on reverse cutting needle point needle using simple interrupted suture pattern.

A.2 Implantation Surgery at Proximal Extensor Digitorum Longus Bifurcation

The chicken will be positioned in dorsal recumbency, with the head in lateral recumbency with the endotracheal tube to prevent aspiration on the surgical table. A tourniquet will be applied just distal of the left pelvic limb intertarsal joint to minimize bleeding at the incision site. The left pelvic limb will be draped in the standard fashion with huck towels and disposable sterile surgical drapes.

A 4 cm incision will be performed on the dorsal aspect of the lower left pelvic limb, at approximately the same level as the spur, on the tarsometatarsus. The connective tissues surrounding the extensor digitorum longus (EDL) tendon will be gently dissected with metzenbaum scissors and iris scissors to allow exposure and access to the main bifurcation of the EDL tendon, where the two branches that extend to digit II and IV. Care will be taken to minimize tissue handling and consequent trauma.

Depending on which group the chicken belongs to (Positive Control, Sham, or Implant, see Section 4.1 of the associated ACUP), surgery with minor variations will be conducted on each chicken.

Positive Control: After gentle dissection using metzenbaum scissors and iris scissors, the EDL will be exposed and a simple disk-shaped implant will be placed at the bifurcation point of the EDL tendon, unattached and "free floating." No sutures will be used to attach the implant.

Sham: Following gentle dissection similar to the previous group, the EDL tendon will be exposed and an implant will be positioned in between and attached to the two tendon branches that derive distally from the bifurcation point of the EDL tendon. The implant will be removed immediately. No sutures will be used to attach the implant.

Implant: Following gentle dissection similar to the previous groups, the EDL tendon will be exposed and an implant will be attached to and positioned in between the two tendon branches that derive distally from the bifurcation point of the EDL tendon.

The skin will be sutured closed with an apposing cruciate pattern using 4-0 Ethilon black monofilament or another non-absorbable suture material and a swedged on reverse cutting needle point needle. The surgical site will then be dressed with betadine ointment, triple antibiotic ointment, sterile gauzes, cotton cling, and sterile vetwrap.

B.1 Early Apparatus Development for Measuring Isometric Chicken Extensor Digitorum Longus Muscle-Tendon Force Generation

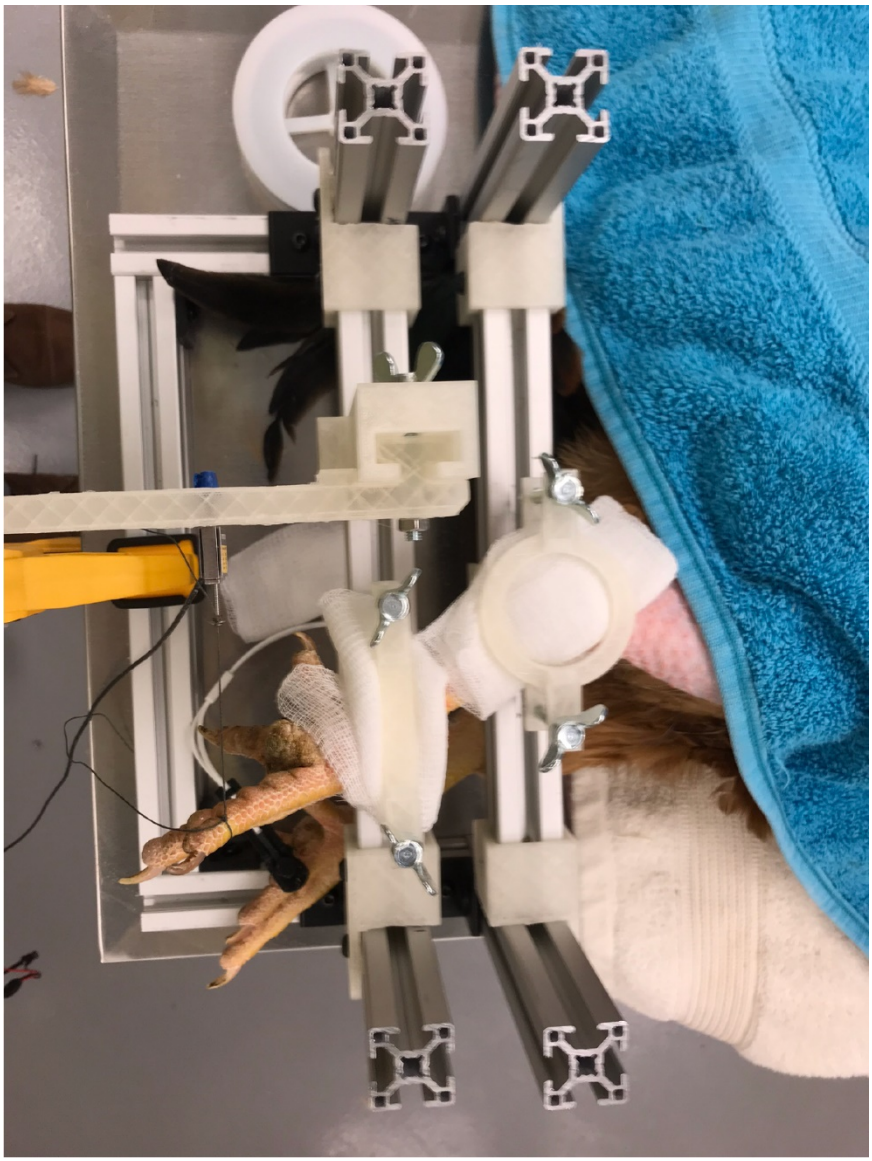

Figure B.1.1A Image of Early Chicken Experimental Setup – Side Pelvic Limb View

Figure B.1.1B Image of Early Chicken Experimental Setup – Toe View

Figure B.1.2A Image of Chicken Experimental Setup – Side Pelvic Limb View

Figure B.1.2B Image of Chicken Experimental Setup – Toe View

C.1 Functional Electrical Stimulation Parameters for Isometric Near-Submaximal Chicken Extensor Digitorum Longus Muscle Contraction

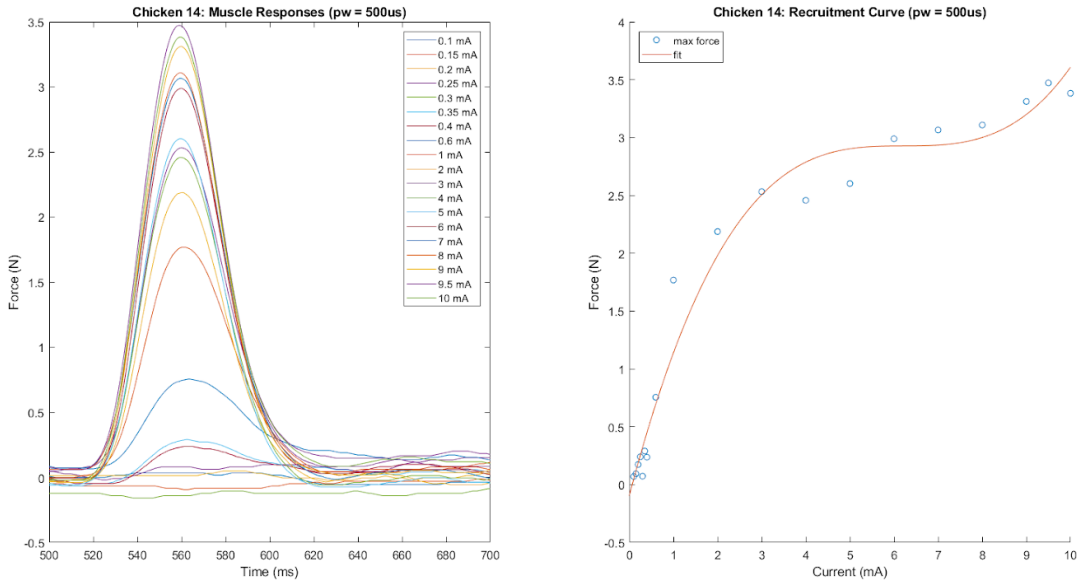

Figure C.1.1 Peak Isometric Toe Tip Force Signals and a Recruitment Curve

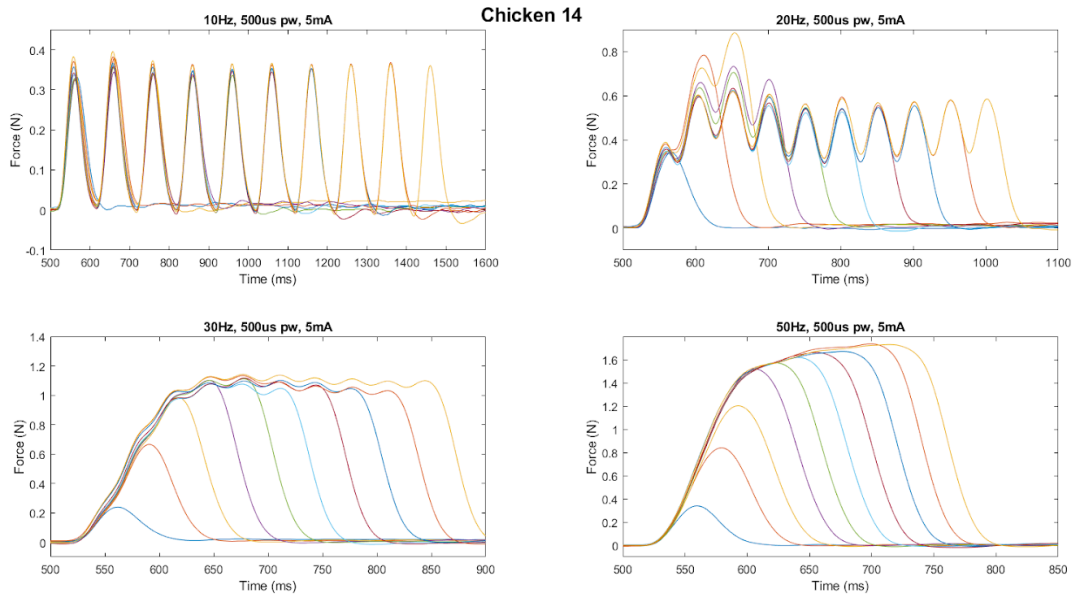

Figure C.1.2 Data from Parameter Sweep Experiments

D.1 Electrode Winding Machine for Stimulating Electrode Designing

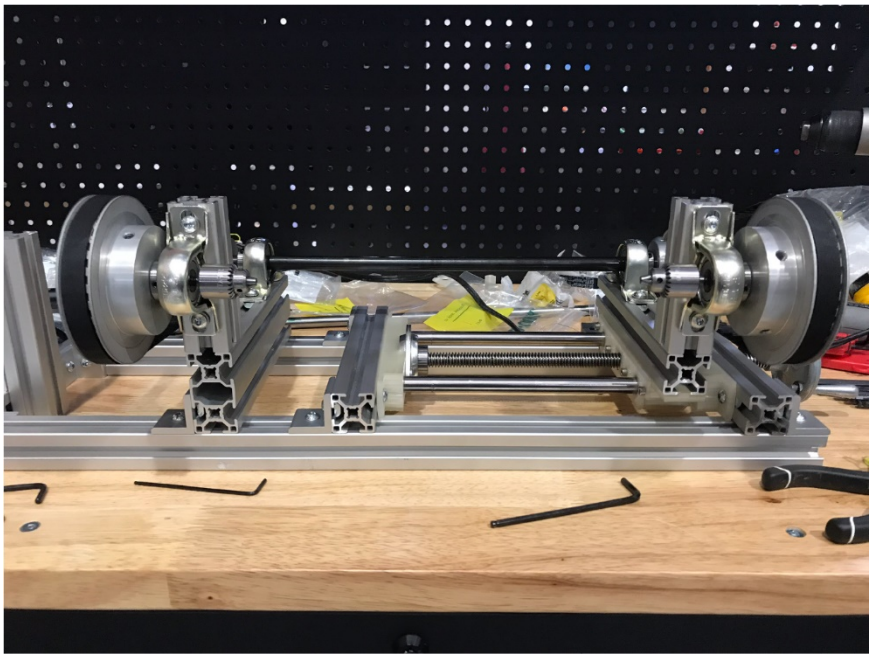

Figure D.1.1 Electrode Winding Machine for Stimulating Electrode Designing

E.1 Chicken Implantable Passive Differential Mechanism Designs

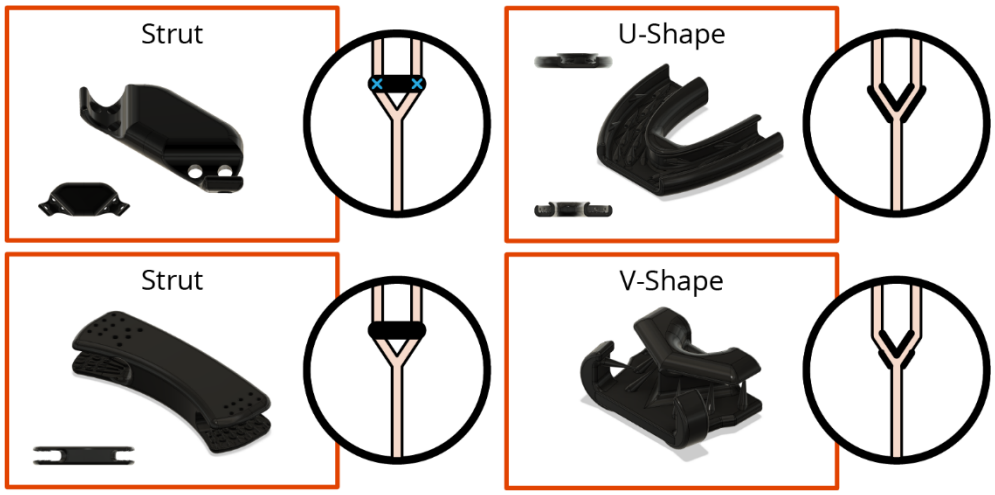

Figure E.1.1 Chicken Implantable Passive Differential Mechanism Designs

F.1 MATLAB Scripts for Data Processing Isometric Toe Tip Forces in the Chicken Model

F.1.1 Data Extraction, Filtering, and Conversion

```
% Created by: Anthony H. Le
% Last updated: 11-05-2019

%%
clear;
close all;

% load('study5_main_ttforces201908.mat');
s5_latf = load('study5_main_lat_ttforces201908.mat');
s5_medf = load('study5_main_med_ttforces201908.mat');

%%%%%%%%%%%%%%%%%%%%%%%%%%%%%%%%%%%%%%%%%%%%%%%%%%%%%%%%%%%%%%%%%%%%%%%%%%%%%%%%
%%%%%%%
NORM = 0; % want to normalize? no-0, yes-1
%%%%%%%%%%%%%%%%%%%%%%%%%%%%%%%%%%%%%%%%%%%%%%%%%%%%%%%%%%%%%%%%%%%%%%%%%%%%%%%%
%%%%%%%
F_or_M = 1; % want forces or moments vs joint angle? forces-0,
moments-1
%%%%%%%%%%%%%%%%%%%%%%%%%%%%%%%%%%%%%%%%%%%%%%%%%%%%%%%%%%%%%%%%%%%%%%%%%%%%%%%%
%%%%%%%
%% Variables, parameters, IDs, IDXs, labels
% chicken IDs
```

```
CK_IDS = {'Chicken 80: Coupled'; % 1, excluded
          'Chicken 81: Uncoupled'; % 2, excluded
          'Chicken 82: Coupled'; % 3
          'Chicken 83: Coupled'; % 4, excluded
          'Chicken 84: Uncoupled'; % 5
          'Chicken 85: Coupled'; % 6
          'Chicken 86: Coupled'; % 7, excluded
          'Chicken 87: Uncoupled'; % 8
          'Chicken 88: Uncoupled'; % 9
          'Chicken 89: Uncoupled'; % 10, excluded
          'Chicken 90: Coupled'; % 11
          'Chicken 91: Uncoupled'; % 12
          'Chicken 92: Uncoupled'; % 13
          'Chicken 93: Coupled'; % 14
          'Chicken 94: Uncoupled'}; % 15

% chicken weights
CK_WTS = [4.3; 4.63; 4.54; 4.55; 4.42; 4.81; 4.28; 4.51; 5.18; 3.99;
4.33; 4.71; 4.72; 4.45; 4.77];

% toe moment arms
lat_r = ((57.37 + 61.11) / 2) / 1000; % m
med_r = ((53.83 + 55.96) / 2) / 1000; % m

% treatment group data index
% edit to include/exclude chickens in data processing
D_IDX = [1, 3, 4, 6, 7, 11, 14]; % double
exD_IDX = [1, 4, 7];  % excluded
D_IDX = setdiff(D_IDX, exD_IDX);
S_IDX = [2, 5, 8, 9, 10, 12, 13, 15]; % single
exS_IDX = [2, 10];  % excluded
S_IDX = setdiff(S_IDX, exS_IDX);
CK_IDX = sort([D_IDX, S_IDX]);

disp(' ');
disp('Excluded the following subjects:');
disp(' ');
disp(CK_IDS([1, 4, 7]));
disp(CK_IDS([2, 10]));
disp(' ');

% create lat MTP angle mat for plotting, repeated measures
latMTP = [-30; -15; 0; 15; 30; 45; 60];
LATMTP = repmat(latMTP, [1, 2]);

% create med MTP angle mat for plotting, repeated measures
medMTP = [-30; 0; 60];

% med MTP angle IDs
MEDMTP_IDS = {'Toe 2 MTP @ 30E'; 'Toe 2 MTP @ 0N'; 'Toe 2 MTP @
60F'};

% force-length relationship IDs
```

```
if F_or_M == 1
    FLR_IDS = {'Total MTP Joint Moment-Angle Relationship'; 'Passive
MTP Joint Moment-Angle Relationship'; 'Active MTP Joint Moment-Angle
Relationship'};
else
    FLR_IDS = {'Total Toe Tip Force-MTP Joint Angle Relationship';
'Passive Toe Tip Force-MTP Joint Angle Relationship'; 'Active Toe
Tip Force-MTP Joint Angle Relationship'};
end

% variable sizes
n_CK = length(CK_IDS); % number of chickens
n_D = length(D_IDX); % number of chickens in coupled treatment group
n_S = length(S_IDX); % number of chickens in uncoupled treatment
group
n_MEDMTP = length(MEDMTP_IDS); % number of lat MTP angles
n_LATMTP = length(latMTP); % number of med MTP angles
n_STIM = 2; % number of stimuli per med-lat angle combo
n_DP = n_MEDMTP * n_LATMTP * n_STIM; % number of data points per
chicken
n_FLR = length(FLR_IDS); % number of force-length relationship types

% data point, avg, std dim index
DP_IDX = 1;
AVG_IDX = 2;
STD_IDX = 3;
SEM_IDX = 3;

% FLR dim index
TOT_IDX = 1;
PASS_IDX = 2;
ACT_IDX = 3;

% stimuli dim index
STIM_IDX = 3:4;

% med MTP angle index
M30E_IDX = 1;
M0N_IDX = 2;
M60F_IDX = 3;

%% Set x- and y-axis ranges, limits, and labels; define legends
if NORM == 1
    if F_or_M == 1
        y_lat = [-inf 1];
        y_med = [-inf 1];
        ylabel_lat = 'Normalized Digit IV MTP Moments (mNm/mNm)';
        ylabel_med = 'Normalized Digit II MTP Moments (mNm/mNm)';
    else
        y_lat = [-inf 1];
        y_med = [-inf 1];
        ylabel_lat = 'Normalized Digit IV Toe Tip Forces (N/N)';
        ylabel_med = 'Normalized Digit II Toe Tip Forces (N/N)';
```

```
    end
else
    if F_or_M == 1
        y_lat = [-1.5 2.5] .* [30 50];
        y_med = [-1.5 2.5] .* [30 50];
        ylabel_lat = 'Toe 1 MTP Moments (mNm)';
        ylabel_med = 'Toe 2 MTP Moments (mNm)';
    else
        y_lat = [-1.5 2.5];
        y_med = [-1.5 2.5];
        ylabel_lat = 'Toe 1 Toe Tip Forces (N)';
        ylabel_med = 'Toe 2 Toe Tip Forces (N)';
    end
end

x_lat = [-35 65];
xlabel_lat = 'Ext \leftarrow Toe 1 MTP Angle (deg) \rightarrow
Flex';
xlabel_med = 'Ext \leftarrow Toe 2 MTP Angle (deg) \rightarrow
Flex';

lgd1 = {'Active 1', 'Active 2', 'Passive 1', 'Passive 2'};
lgd2 = {'Total 1', 'Total 2'};
lgd3 = {'Total', 'Passive', 'Active'};
lgd4 = {'Passive', 'Active'};
lgd_grp = {'Coupled', 'Uncoupled'};
lgd_CKAVG = {'CK80 AVG', 'CK81 AVG', 'CK82 AVG', 'CK83 AVG', 'CK84
AVG', 'CK85 AVG', 'CK86 AVG', 'CK87 AVG', 'CK88 AVG', 'CK89 AVG',
'CK90 AVG', 'CK91 AVG', 'CK92 AVG', 'CK93 AVG', 'CK94 AVG'};

%% 4th-order Butterworth no-lag filter - using MATLAB function
f_s = 4000; % sampling freq
f_c = 30; % cut-off freq
T = 1 / f_s;

[b, a] = butter(2, f_c / (f_s / 2), 'low');
% freqz(b, a);

%% Organize data into cell arrays
% time = transpose(linspace(0, 1.5, 6000)); % s
time = transpose(linspace(0, 1.5, 6000)) .* 1000; % ms

CK_LATF_raw = struct2cell(s5_latf);
CK_MEDF_raw = struct2cell(s5_medf);

CK_LATF = struct2cell(s5_latf);
CK_MEDF = struct2cell(s5_medf);

CK_LATF_MIN = cell(n_CK, 1);
CK_MEDF_MIN = cell(n_CK, 1);

CK_LATF_temp = cell(n_CK, 1);
CK_MEDF_temp = cell(n_CK, 1);
```

```
%% Process data: filter, unit conversion, reshape, normalize
for i = 1:n_CK
    % filter
    if F_or_M == 1
        CK_LATF{i, 1} = filtfilt(b, a, CK_LATF{i, 1}) .* 0.0098 .*
lat_r .* 1000; % lateral toe, mNm
        CK_MEDF{i, 1} = filtfilt(b, a, CK_MEDF{i, 1}) .* 0.0098 .*
med_r .* 1000; % medial toe, mNm

%         CK_LATF{i, 1} = filtfilt(b, a, CK_LATF{i, 1}) .* 0.0098 .*
lat_r; % lateral toe, Nm
%         CK_MEDF{i, 1} = filtfilt(b, a, CK_MEDF{i, 1}) .* 0.0098 .*
med_r; % medial toe, Nm
    else
        CK_LATF{i, 1} = filtfilt(b, a, CK_LATF{i, 1}) .* 0.0098; %
lateral toe, N
        CK_MEDF{i, 1} = filtfilt(b, a, CK_MEDF{i, 1}) .* 0.0098; %
medial toe, N
    end

    % plot entire series of force waveforms, lateral and medial
%     figure();
%     subplot(2, 1, 1);
%     plot(CK_LATF{i, 1});
%     title(CK_IDS{i, 1});
%     ylabel('Lateral Toe Tip Force (N)')
%     xlim([0 length(CK_LATF{i, 1})]);
%     hold off;
%     subplot(2, 1, 2);
%     plot(CK_MEDF{i, 1});
%     ylabel('Medial Toe Tip Force (N)')
%     xlim([0 length(CK_MEDF{i, 1})]);
%     hold off;

    % lateral toe
    CK_LATF{i, 1} = reshape(CK_LATF{i, 1}, [6000, (length(CK_LATF{i,
1})/6000)]); % organize each stim into individual columns

    % medial toe
    CK_MEDF{i, 1} = reshape(CK_MEDF{i, 1}, [6000, (length(CK_MEDF{i,
1})/6000)]); % organize each stim into individual columns

    if NORM == 1 % normalization
        CK_LATF{i, 1} = (CK_LATF{i, 1} - min(min(CK_LATF{i, 1}, [],
1))) ./ (max(max(CK_LATF{i, 1}, [], 1)) - min(min(CK_LATF{i, 1}, [],
1))); % overall normalization
%         CK_LATF{i, 1} = CK_LATF{i, 1} ./ max(max(CK_LATF{i, 1},
[], 1)); % normalize to overall peak force -> magnitude
%         CK_LATF{i, 1} = CK_LATF{i, 1} ./ max(CK_LATF{i, 1}, [],
1); % normalize to peak force of each stim -> shape analysis
```

```
        CK_MEDF{i, 1} = (CK_MEDF{i, 1} - min(min(CK_MEDF{i, 1}, [],
1))) ./ (max(max(CK_MEDF{i, 1}, [], 1)) - min(min(CK_MEDF{i, 1}, [],
1))); % overall normalization
%         CK_MEDF{i, 1} = CK_MEDF{i, 1} ./ max(max(CK_MEDF{i, 1},
[], 1)); % normalize to overall peak force -> magnitude
%         CK_MEDF{i, 1} = CK_MEDF{i, 1} ./ max(CK_MEDF{i, 1}, [],
1); % normalize to peak force of each stim -> shape analysis
    end

    CK_LATF_min = repmat(mean(CK_LATF{i, 1}(1000:2000, :), 1),
[6000, 1]); % calculate mean min for samples 1000:2000, passive
force
    CK_MEDF_min = repmat(mean(CK_MEDF{i, 1}(1000:2000, :), 1),
[6000, 1]); % calculate mean min for samples 1000:2000, passive
force

%     CK_LATF_temp{i, 1} = CK_LATF{i, 1} - CK_LATF_min;
%     CK_MEDF_temp{i, 1} = CK_MEDF{i, 1} - CK_MEDF_min;
%
%     CK_LATF{i, 1} = CK_LATF{i, 1}(1001:5000, :); % crop data,
force waveforms of interest
%     CK_MEDF{i, 1} = CK_MEDF{i, 1}(1001:5000, :); % crop data,
force waveforms of interest

    CK_LATF_MIN{i, 1} = CK_LATF_min; % store baseline, passive
forces
    CK_MEDF_MIN{i, 1} = CK_MEDF_min; % store baseline, passive
forces
end
```

F.1.2 Peak Torques vs MTP Joint Angle Calculations

```
% Created by: Anthony H. Le
% Last updated: 09-18-2019

%%
toetipforces_main

if NORM == 1
    disp('Data has been normalized.');
end

s5_mtp = load('study5_main_mtpangles201908.mat'); % load med-lat MTP
angles
% med angle col 1
% lat angle col 2

%% Find peak forces, add noise to each data point
% MTP joint angles
CK_MTP = struct2cell(s5_mtp); % med-lat MTP angle combos

% repeated measures w/ med-lat MTP angle combos
% for d = 1:size(CK_MTP, 1)
```

```
%     CK_MTP{d, 1} = repelem(CK_MTP{d, 1}, 2, 1); % repeat angle
combos 2 times
% end

% initialize cell arrays
CK_LATF_TOT = cell(n_CK, 1); % total lateral forces
CK_LATF_PASS = cell(n_CK, 1); % passive lateral forces
CK_LATF_ACT = cell(n_CK, 1); % active lateral forces

CK_MEDF_TOT = cell(n_CK, 1); % total medial forces
CK_MEDF_PASS = cell(n_CK, 1); % passive medial forces
CK_MEDF_ACT = cell(n_CK, 1); % active medial forces

for j = 1:n_CK
    for jj = 1:n_DP
        % lateral toe
        if mean(CK_LATF{j, 1}(1000:2000, jj)) > mean(CK_LATF{j,
1}(3000:4000, jj)) % compression forces
            CK_LATF_TOT{j, 1}(jj, 1) = min(CK_LATF{j, 1}(2000:4500,
jj), [], 1);
            CK_LATF_PASS{j, 1}(jj, 1) = CK_LATF_MIN{j, 1}(1, jj);
            CK_LATF_ACT{j, 1}(jj, 1) = CK_LATF_TOT{j, 1}(jj, 1) -
CK_LATF_PASS{j, 1}(jj, 1);
        else
            CK_LATF_TOT{j, 1}(jj, 1) = max(CK_LATF{j, 1}(2000:4500,
jj), [], 1);
            CK_LATF_PASS{j, 1}(jj, 1) = CK_LATF_MIN{j, 1}(1, jj);
            CK_LATF_ACT{j, 1}(jj, 1) = CK_LATF_TOT{j, 1}(jj, 1) -
CK_LATF_PASS{j, 1}(jj, 1);
        end

        % medial toe
        if mean(CK_MEDF{j, 1}(1000:2000, jj)) > mean(CK_MEDF{j,
1}(3000:4000, jj)) % compression forces
            CK_MEDF_TOT{j, 1}(jj, 1) = min(CK_MEDF{j, 1}(2000:4500,
jj), [], 1);
            CK_MEDF_PASS{j, 1}(jj, 1) = CK_MEDF_MIN{j, 1}(1, jj);
            CK_MEDF_ACT{j, 1}(jj, 1) =  CK_MEDF_TOT{j, 1}(jj, 1) -
CK_MEDF_PASS{j, 1}(jj, 1);
        else
            CK_MEDF_TOT{j, 1}(jj, 1) = max(CK_MEDF{j, 1}(2000:4500,
jj), [], 1);
            CK_MEDF_PASS{j, 1}(jj, 1) = CK_MEDF_MIN{j, 1}(1, jj);
            CK_MEDF_ACT{j, 1}(jj, 1) = CK_MEDF_TOT{j, 1}(jj, 1) -
CK_MEDF_PASS{j, 1}(jj, 1);
        end
    end

    % organize forces by lat MTP angle -30 to 60
    CK_LATF_TOT{j, 1} = sortrows([CK_MTP{j, 1},
vec2mat(CK_LATF_TOT{j, 1}, 2)], [1 2]);
    CK_LATF_PASS{j, 1} = sortrows([CK_MTP{j, 1},
vec2mat(CK_LATF_PASS{j, 1}, 2)], [1 2]);
```

```
    CK_LATF_ACT{j, 1} = sortrows([CK_MTP{j, 1},
vec2mat(CK_LATF_ACT{j, 1}, 2)], [1 2]);

    CK_MEDF_TOT{j, 1} = sortrows([CK_MTP{j, 1},
vec2mat(CK_MEDF_TOT{j, 1}, 2)], [1 2]);
    CK_MEDF_PASS{j, 1} = sortrows([CK_MTP{j, 1},
vec2mat(CK_MEDF_PASS{j, 1}, 2)], [1 2]);
    CK_MEDF_ACT{j, 1} = sortrows([CK_MTP{j, 1},
vec2mat(CK_MEDF_ACT{j, 1}, 2)], [1 2]);

    % rearrange mats 2D to 3D by med MTP angle -30, 0, 60
    CK_LATF_TOT{j, 1} = permute(reshape(CK_LATF_TOT{j, 1}', [4, 7,
3]), [2, 1, 3]);
    CK_LATF_PASS{j, 1} = permute(reshape(CK_LATF_PASS{j, 1}', [4, 7,
3]), [2, 1, 3]);
    CK_LATF_ACT{j, 1} = permute(reshape(CK_LATF_ACT{j, 1}', [4, 7,
3]), [2, 1, 3]);

    CK_MEDF_TOT{j, 1} = permute(reshape(CK_MEDF_TOT{j, 1}', [4, 7,
3]), [2, 1, 3]);
    CK_MEDF_PASS{j, 1} = permute(reshape(CK_MEDF_PASS{j, 1}', [4, 7,
3]), [2, 1, 3]);
    CK_MEDF_ACT{j, 1} = permute(reshape(CK_MEDF_ACT{j, 1}', [4, 7,
3]), [2, 1, 3]);

    % clear 1st 2 col vec
%     CK_LATF_TOT{j, 1}(:, 1:2) = [];
%     CK_LATF_PASS{j, 1}(:, 1:2) = [];
%     CK_LATF_ACT{j, 1}(:, 1:2) = [];
%
%     CK_MEDF_TOT{j, 1}(:, 1:2) = [];
%     CK_MEDF_PASS{j, 1}(:, 1:2) = [];
%     CK_MEDF_ACT{j, 1}(:, 1:2) = [];

    CK_LATF{j, 1} = CK_LATF{j, 1}(1001:5000, :); % crop data
    CK_MEDF{j, 1} = CK_MEDF{j, 1}(1001:5000, :); % crop data
end
```

F.1.3 Dataframe Build

```
% Created by: Anthony H. Le
% Last updated: 09-18-2019

%% Plot peak forces vs lateral or medial MTP joint angle
% toetipforces_main
peakf_v_MTPang_main

%%
% initialize cell arrays
CK_LATF_SEMTOT = cell(n_CK, 1);
CK_LATF_SEMPASS = cell(n_CK, 1);
CK_LATF_SEMACT = cell(n_CK, 1);
```

```
CK_MEDF_SEMTOT = cell(n_CK, 1);
CK_MEDF_SEMPASS = cell(n_CK, 1);
CK_MEDF_SEMACT = cell(n_CK, 1);

CK_LATF_AVGTOT = cell(n_CK, 1);
CK_LATF_AVGPASS = cell(n_CK, 1);
CK_LATF_AVGACT = cell(n_CK, 1);

CK_MEDF_AVGTOT = cell(n_CK, 1);
CK_MEDF_AVGPASS = cell(n_CK, 1);
CK_MEDF_AVGACT = cell(n_CK, 1);

% intitialize matrices
D_LATF_SEM = zeros(n_LATMTP, n_MEDMTP, n_FLR);
D_LATF_AVG = zeros(n_LATMTP, n_MEDMTP, n_FLR);

D_MEDF_SEM = zeros(n_LATMTP, n_MEDMTP, n_FLR);
D_MEDF_AVG = zeros(n_LATMTP, n_MEDMTP, n_FLR);

S_LATF_SEM = zeros(n_LATMTP, n_MEDMTP, n_FLR);
S_LATF_AVG = zeros(n_LATMTP, n_MEDMTP, n_FLR);

S_MEDF_SEM = zeros(n_LATMTP, n_MEDMTP, n_FLR);
S_MEDF_AVG = zeros(n_LATMTP, n_MEDMTP, n_FLR);

%% Calculate std devs and averages
for k = 1:n_CK
    for kk = 1:n_MEDMTP
        % calculate std error of the mean
        CK_LATF_SEMTOT{k, 1}(:, :, kk) = std(CK_LATF_TOT{k, 1}(:,
STIM_IDX, kk), 0, 2) ./ sqrt(n_STIM);
        CK_LATF_SEMPASS{k, 1}(:, :, kk) = std(CK_LATF_PASS{k, 1}(:,
STIM_IDX, kk), 0, 2) ./ sqrt(n_STIM);
        CK_LATF_SEMACT{k, 1}(:, :, kk) = std(CK_LATF_ACT{k, 1}(:,
STIM_IDX, kk), 0, 2) ./ sqrt(n_STIM);

        CK_MEDF_SEMTOT{k, 1}(:, :, kk) = std(CK_MEDF_TOT{k, 1}(:,
STIM_IDX, kk), 0, 2) ./ sqrt(n_STIM);
        CK_MEDF_SEMPASS{k, 1}(:, :, kk) = std(CK_MEDF_PASS{k, 1}(:,
STIM_IDX, kk), 0, 2) ./ sqrt(n_STIM);
        CK_MEDF_SEMACT{k, 1}(:, :, kk) = std(CK_MEDF_ACT{k, 1}(:,
STIM_IDX, kk), 0, 2) ./ sqrt(n_STIM);

        % calculate averages
        CK_LATF_AVGTOT{k, 1}(:, :, kk) = mean(CK_LATF_TOT{k, 1}(:,
STIM_IDX, kk), 2);
        CK_LATF_AVGPASS{k, 1}(:, :, kk) = mean(CK_LATF_PASS{k, 1}(:,
STIM_IDX, kk), 2);
        CK_LATF_AVGACT{k, 1}(:, :, kk) = mean(CK_LATF_ACT{k, 1}(:,
STIM_IDX, kk), 2);

        CK_MEDF_AVGTOT{k, 1}(:, :, kk) = mean(CK_MEDF_TOT{k, 1}(:,
STIM_IDX, kk), 2);
```

```
        CK_MEDF_AVGPASS{k, 1}(:, :, kk) = mean(CK_MEDF_PASS{k, 1}(:,
STIM_IDX, kk), 2);
        CK_MEDF_AVGACT{k, 1}(:, :, kk) = mean(CK_MEDF_ACT{k, 1}(:,
STIM_IDX, kk), 2);
    end
end

%%
% STDAVG cell array, concat everything together
% cell 1st dim (within overall STDAVG cell 3rd dim): chicken
% cell 2nd dim (within overall STDAVG cell 3rd dim): data, avg, std
% mat 1st dim (within cell 2nd dim): lat MTP angle
% mat 3rd dim (within cell 2nd dim): med MTP angle
% overall STDAVG cell 3rd dim: total, passive, active
CK_LATF_SEMAVG = cell(1, 1, n_FLR);
CK_LATF_SEMAVG{TOT_IDX} = {CK_LATF_TOT{:, 1}; CK_LATF_AVGTOT{:, 1};
CK_LATF_SEMTOT{:, 1}}';
CK_LATF_SEMAVG{PASS_IDX} = {CK_LATF_PASS{:, 1}; CK_LATF_AVGPASS{:,
1}; CK_LATF_SEMPASS{:, 1}}';
CK_LATF_SEMAVG{ACT_IDX} = {CK_LATF_ACT{:, 1}; CK_LATF_AVGACT{:, 1};
CK_LATF_SEMACT{:, 1}}';

CK_MEDF_SEMAVG = cell(1, 1, n_FLR);
CK_MEDF_SEMAVG{TOT_IDX} = {CK_MEDF_TOT{:, 1}; CK_MEDF_AVGTOT{:, 1};
CK_MEDF_SEMTOT{:, 1}}';
CK_MEDF_SEMAVG{PASS_IDX} = {CK_MEDF_PASS{:, 1}; CK_MEDF_AVGPASS{:,
1}; CK_MEDF_SEMPASS{:, 1}}';
CK_MEDF_SEMAVG{ACT_IDX} = {CK_MEDF_ACT{:, 1}; CK_MEDF_AVGACT{:, 1};
CK_MEDF_SEMACT{:, 1}}';

%%
% group TPA cell arrays, concat FLR types together per group
D_LATF_TPA = cell(1, n_FLR);
D_MEDF_TPA = cell(1, n_FLR);
S_LATF_TPA = cell(1, n_FLR);
S_MEDF_TPA = cell(1, n_FLR);

% group chickens by treatment group -> eliminates a dim
% mat 3rd dim (within D/S TPA cell 2nd dim): med MTP angle
% D/S TPA cell 2nd dim: total, passive, active
for k = 1:n_FLR
    D_LATF_TPA{1, k} = cell2mat(CK_LATF_SEMAVG{k}(D_IDX, AVG_IDX));
    D_MEDF_TPA{1, k} = cell2mat(CK_MEDF_SEMAVG{k}(D_IDX, AVG_IDX));
    S_LATF_TPA{1, k} = cell2mat(CK_LATF_SEMAVG{k}(S_IDX, AVG_IDX));
    S_MEDF_TPA{1, k} = cell2mat(CK_MEDF_SEMAVG{k}(S_IDX, AVG_IDX));
end

%%
% D/S STD/AVG cell 1st dim: lat MTP angle
% D/S STD/AVG cell 2nd dim: med MTP angle
% D/S STD/AVG cell 3rd dim: total, passive, active
for k = 1:n_FLR
    for kk = 1:n_MEDMTP
        % overall std error, double
```

```
        D_LATF_SEM(:, kk, k) = std(reshape(D_LATF_TPA{1, k}(:, :,
kk), [n_LATMTP, n_D]), 0, 2) ./ sqrt(n_D);
        D_MEDF_SEM(:, kk, k) = std(reshape(D_LATF_TPA{1, k}(:, :,
kk), [n_LATMTP, n_D]), 0, 2) ./ sqrt(n_D);

        % overall std error, single
        S_LATF_SEM(:, kk, k) = std(reshape(S_LATF_TPA{1, k}(:, :,
kk), [n_LATMTP, n_S]), 0, 2) ./ sqrt(n_S);
        S_MEDF_SEM(:, kk, k) = std(reshape(S_LATF_TPA{1, k}(:, :,
kk), [n_LATMTP, n_S]), 0, 2) ./ sqrt(n_S);

        % overall averages, double
        D_LATF_AVG(:, kk, k) = mean(reshape(D_LATF_TPA{1, k}(:, :,
kk), [n_LATMTP, n_D]), 2);
        D_MEDF_AVG(:, kk, k) = mean(reshape(D_MEDF_TPA{1, k}(:, :,
kk), [n_LATMTP, n_D]), 2);

        % overall averages, single
        S_LATF_AVG(:, kk, k) = mean(reshape(S_LATF_TPA{1, k}(:, :,
kk), [n_LATMTP, n_S]), 2);
        S_MEDF_AVG(:, kk, k) = mean(reshape(S_MEDF_TPA{1, k}(:, :,
kk), [n_LATMTP, n_S]), 2);

    end
end
```

F.1.4 Data Plotting and Curve Fitting

```
% Created by: Anthony H. Le
% Last updated: 11-14-2019

%% Plot peak forces vs lateral or medial MTP joint angle
% toetipforces_main
% peakf_v_MTPang_main
peakf_v_MTPang_semavg

%%
DLF_SEM = zeros(n_LATMTP, 2, n_MEDMTP);
DMF_SEM = zeros(n_LATMTP, 2, n_MEDMTP);

SLF_SEM = zeros(n_LATMTP, 2, n_MEDMTP);
SMF_SEM = zeros(n_LATMTP, 2, n_MEDMTP);

latMTP1 = linspace(-30, 60, 20);
poly_n = [3, 3, 3];

colors = {[0, 0.4470, 0.7410], [0.8500, 0.3250, 0.0980], [0.9290,
0.6940, 0.1250]};

%% Plot overall results by groups: double and single
% for m = 1:n_MEDMTP
%     figure();
%     subplot(2, 2, 1);
```

```
%     for mm = 1:n_FLR
%         errorbar(latMTP, D_LATF_AVG(:, m, mm), D_LATF_SEM(:, m,
mm), 'o', 'color', colors{mm});
%         hold on;
%         pfit = polyfit(latMTP, D_LATF_AVG(:, m, mm), poly_n(mm));
%         f = polyval(pfit, latMTP1);
%         plot(latMTP1, f, '-', 'color', colors{mm})
%     end
%     title(['Double (n=', num2str(n_D), ')']);
%     xlabel(xlabel_lat);
%     ylabel(ylabel_lat);
%     xlim(x_lat);
%     ylim(y_lat);
%     legend(lgd3);
%     hold off;
%
%     subplot(2, 2, 3);
%     for mm = 1:n_FLR
%         errorbar(latMTP, D_MEDF_AVG(:, m, mm), D_MEDF_SEM(:, m,
mm), 'o', 'color', colors{mm});
%         hold on;
%         pfit = polyfit(latMTP, D_MEDF_AVG(:, m, mm), poly_n(mm));
%         f = polyval(pfit, latMTP1);
%         plot(latMTP1, f, '-', 'color', colors{mm})
%     end
%     xlabel(xlabel_lat);
%     ylabel(ylabel_med);
%     xlim(x_lat);
%     ylim(y_med);
%     legend(lgd3);
%     hold off;
%
%     subplot(2, 2, 2);
%     for mm = 1:n_FLR
%         errorbar(latMTP, S_LATF_AVG(:, m, mm), S_LATF_SEM(:, m,
mm), 'o', 'color', colors{mm});
%         hold on;
%         pfit = polyfit(latMTP, S_LATF_AVG(:, m, mm), poly_n(mm));
%         f = polyval(pfit, latMTP1);
%         plot(latMTP1, f, '-', 'color', colors{mm})
%     end
%     title(['Single (n=', num2str(n_S), ')']);
%     xlabel(xlabel_lat);
%     ylabel(ylabel_lat);
%     xlim(x_lat);
%     ylim(y_lat);
%     legend(lgd3);
%     hold off;
%
%     subplot(2, 2, 4);
%     for mm = 1:n_FLR
%         errorbar(latMTP, S_MEDF_AVG(:, m, mm), S_MEDF_SEM(:, m,
mm), 'o', 'color', colors{mm});
%         hold on;
%         pfit = polyfit(latMTP, S_MEDF_AVG(:, m, mm), poly_n(mm));
```

```
%         f = polyval(pfit, latMTP1);
%         plot(latMTP1, f, '-', 'color', colors{mm})
%     end
%     xlabel(xlabel_lat);
%     ylabel(ylabel_med);
%     xlim(x_lat);
%     ylim(y_med)
%     legend(lgd3);
%     hold off;
%
%     suptitle(MEDMTP_IDS{m, 1});
% end
%
% for m = 1:n_MEDMTP
%     figure();
%     subplot(1, 2, 1);
%     for mm = 1:n_FLR
%         errorbar(latMTP, D_LATF_AVG(:, m, mm), D_LATF_SEM(:, m,
mm), 'o', 'color', colors{mm});
%         hold on;
%         pfit = polyfit(latMTP, D_LATF_AVG(:, m, mm), poly_n(mm));
%         f = polyval(pfit, latMTP1);
%         plot(latMTP1, f, '-', 'color', colors{mm})
%     end
%     title(['Double (n=', num2str(n_D), ')']);
%     xlabel(xlabel_lat);
%     ylabel(ylabel_lat);
%     xlim(x_lat);
%     ylim(y_lat);
%     legend(lgd3);
%     hold off;
%
%     subplot(1, 2, 2);
%     for mm = 1:n_FLR
%         errorbar(latMTP, S_LATF_AVG(:, m, mm), S_LATF_SEM(:, m,
mm), 'o', 'color', colors{mm});
%         hold on;
%         pfit = polyfit(latMTP, S_LATF_AVG(:, m, mm), poly_n(mm));
%         f = polyval(pfit, latMTP1);
%         plot(latMTP1, f, '-', 'color', colors{mm})
%     end
%     title(['Single (n=', num2str(n_S), ')']);
%     xlabel(xlabel_lat);
%     ylabel(ylabel_lat);
%     xlim(x_lat);
%     ylim(y_lat);
%     legend(lgd3);
%     hold off;
%
%     suptitle(MEDMTP_IDS{m, 1});
% end

%% Plot overall results by medial MTP condition
% for m = 1:n_FLR
```

```
%     figure();
%     for mm = 1:n_MEDMTP
%         subplot(2, 3, mm);
%         errorbar(latMTP, D_LATF_AVG(:, mm, m), D_LATF_SEM(:, mm,
m), 'o', 'color', colors{1});
%         hold on;
%         errorbar(latMTP, S_LATF_AVG(:, mm, m), S_LATF_SEM(:, mm,
m), 'o', 'color', colors{2});
%
%         pfit1 = polyfit(latMTP, D_LATF_AVG(:, mm, m), poly_n(m));
%         f1 = polyval(pfit1, latMTP1);
%         plot(latMTP1, f1, '-', 'color', colors{1})
%
%         pfit2 = polyfit(latMTP, S_LATF_AVG(:, mm, m), poly_n(m));
%         f2 = polyval(pfit2, latMTP1);
%         plot(latMTP1, f2, '-', 'color', colors{2})
%
%         title(MEDMTP_IDS{mm, 1});
%         xlabel(xlabel_lat);
%         ylabel(ylabel_lat);
%         xlim(x_lat);
%         ylim(y_lat);
%         legend(lgd_grp);
%         hold off;
%
%         subplot(2, 3, mm+n_MEDMTP);
%         errorbar(latMTP, D_MEDF_AVG(:, mm, m), D_MEDF_SEM(:, mm,
m), 'o', 'color', colors{1});
%         hold on;
%         errorbar(latMTP, S_MEDF_AVG(:, mm, m), S_MEDF_SEM(:, mm,
m), 'o', 'color', colors{2});
%
%         pfit1 = polyfit(latMTP, D_MEDF_AVG(:, mm, m), poly_n(m));
%         f1 = polyval(pfit1, latMTP1);
%         plot(latMTP1, f1, '-', 'color', colors{1})
%
%         pfit2 = polyfit(latMTP, S_MEDF_AVG(:, mm, m), poly_n(m));
%         f2 = polyval(pfit2, latMTP1);
%         plot(latMTP1, f2, '-', 'color', colors{2})
%
%         xlabel(xlabel_lat);
%         ylabel(ylabel_med);
%         xlim(x_lat);
%         ylim(y_med);
%         legend(lgd_grp);
%         hold off;
%     end
%
%     suptitle(FLR_IDS{m, 1});
% end
%
% for m = 1:n_FLR
%     figure();
%     for mm = 1:n_MEDMTP
%         subplot(1, 3, mm);
```

```
%         errorbar(latMTP, D_LATF_AVG(:, mm, m), D_LATF_SEM(:, mm,
m), 'o', 'color', colors{1});
%         hold on;
%         errorbar(latMTP, S_LATF_AVG(:, mm, m), S_LATF_SEM(:, mm,
m), 'o', 'color', colors{2});
%
%         pfit1 = polyfit(latMTP, D_LATF_AVG(:, mm, m), poly_n(m));
%         f1 = polyval(pfit1, latMTP1);
%         plot(latMTP1, f1, '-', 'color', colors{1})
%
%         pfit2 = polyfit(latMTP, S_LATF_AVG(:, mm, m), poly_n(m));
%         f2 = polyval(pfit2, latMTP1);
%         plot(latMTP1, f2, '-', 'color', colors{2})
%
%         title(MEDMTP_IDS{mm, 1});
%         xlabel(xlabel_lat);
%         ylabel(ylabel_lat);
%         xlim(x_lat);
%         ylim(y_lat);
%         legend(lgd_grp);
%         hold off;
%     end
%
%     suptitle(FLR_IDS{m, 1});
% end
%
% %% Plot overall results by groups
% for m = 1:n_FLR
%     figure();
%     subplot(2, 2, 1);
%     for mm = 1:n_MEDMTP
%         errorbar(latMTP, D_LATF_AVG(:, mm, m), D_LATF_SEM(:, mm,
m), 'o', 'color', colors{mm});
%         hold on;
%         pfit = polyfit(latMTP, D_LATF_AVG(:, mm, m), poly_n(m));
%         f = polyval(pfit, latMTP1);
%         plot(latMTP1, f, '-', 'color', colors{mm})
%     end
%     title(['Double (n=', num2str(n_D), ')']);
%     xlabel(xlabel_lat);
%     ylabel(ylabel_lat);
%     xlim(x_lat);
%     ylim(y_lat);
%     legend(MEDMTP_IDS');
%     hold off;
%
%     subplot(2, 2, 3);
%     for mm = 1:n_MEDMTP
%         errorbar(latMTP, D_MEDF_AVG(:, mm, m), D_MEDF_SEM(:, mm,
m), 'o', 'color', colors{mm});
%         hold on;
%         pfit = polyfit(latMTP, D_MEDF_AVG(:, mm, m), poly_n(m));
%         f = polyval(pfit, latMTP1);
%         plot(latMTP1, f, '-', 'color', colors{mm})
%     end
```

```
%     xlabel(xlabel_lat);
%     ylabel(ylabel_med);
%     xlim(x_lat);
%     ylim(y_med);
%     legend(MEDMTP_IDS');
%     hold off;
%
%     subplot(2, 2, 2);
%     for mm = 1:n_MEDMTP
%         errorbar(latMTP, S_LATF_AVG(:, mm, m), S_LATF_SEM(:, mm,
m), 'o', 'color', colors{mm});
%         hold on;
%         pfit = polyfit(latMTP, S_LATF_AVG(:, mm, m), poly_n(m));
%         f = polyval(pfit, latMTP1);
%         plot(latMTP1, f, '-', 'color', colors{mm})
%     end
%     title(['Single (n=', num2str(n_S), ')']);
%     xlabel(xlabel_lat);
%     ylabel(ylabel_lat);
%     xlim(x_lat);
%     ylim(y_lat);
%     legend(MEDMTP_IDS');
%     hold off;
%
%     subplot(2, 2, 4);
%     for mm = 1:n_MEDMTP
%         errorbar(latMTP, S_MEDF_AVG(:, mm, m), S_MEDF_SEM(:, mm,
m), 'o', 'color', colors{mm});
%         hold on;
%         pfit = polyfit(latMTP, S_MEDF_AVG(:, mm, m), poly_n(m));
%         f = polyval(pfit, latMTP1);
%         plot(latMTP1, f, '-', 'color', colors{mm})
%     end
%     xlabel(xlabel_lat);
%     ylabel(ylabel_med);
%     xlim(x_lat);
%     ylim(y_med)
%     legend(MEDMTP_IDS');
%     hold off;
%
%     suptitle(FLR_IDS{m, 1});
% end

%%
for m = 1:n_FLR
    figure();
    subplot(1, 2, 1);
    for mm = 1:n_MEDMTP
        errorbar(latMTP, D_LATF_AVG(:, mm, m), D_LATF_SEM(:, mm, m),
'o', 'color', colors{mm});
        hold on;
        pfit = polyfit(latMTP, D_LATF_AVG(:, mm, m), poly_n(m));
        f = polyval(pfit, latMTP1);
        plot(latMTP1, f, '-', 'color', colors{mm})
```

```
    end
    title(['Double (n=', num2str(n_D), ')']);
    xlabel(xlabel_lat);
    ylabel(ylabel_lat);
    xlim(x_lat);
    ylim(y_lat);
    legend(MEDMTP_IDS');
    hold off;

    subplot(1, 2, 2);
    for mm = 1:n_MEDMTP
        errorbar(latMTP, S_LATF_AVG(:, mm, m), S_LATF_SEM(:, mm, m),
'o', 'color', colors{mm});
        hold on;
        pfit = polyfit(latMTP, S_LATF_AVG(:, mm, m), poly_n(m));
        f = polyval(pfit, latMTP1);
        plot(latMTP1, f, '-', 'color', colors{mm})
    end
    title(['Single (n=', num2str(n_S), ')']);
    xlabel(xlabel_lat);
    ylabel(ylabel_lat);
    xlim(x_lat);
    ylim(y_lat);
    legend(MEDMTP_IDS');
    hold off;

    suptitle(FLR_IDS{m, 1});
end

for m = 3
    figure();
    for mm = 1:n_MEDMTP
        errorbar(latMTP, S_LATF_AVG(:, mm, m), S_LATF_SEM(:, mm, m),
'o', 'color', colors{mm});
        hold on;
        pfit = polyfit(latMTP, S_LATF_AVG(:, mm, m), poly_n(m));
        f = polyval(pfit, latMTP1);
        plot(latMTP1, f, '-', 'color', colors{mm})
    end
%     title(['Single (n=', num2str(n_S), ')']);
    xlabel(xlabel_lat);
    ylabel(ylabel_lat);
    xlim([-30 60]);
    ylim([0 120]);
%     legend(MEDMTP_IDS');
    hold off;

    set(gcf, 'position', [250 100 500 750]);
end

actFit = fit(linspace(0, 2, 7)', S_LATF_AVG(:, 1, 3),
'cubicinterp');
passFit = fit(linspace(0, 2, 7)', S_LATF_AVG(:, 1, 2),
'cubicinterp');
```

```
% fit(L_M, F_CE, 'cubicinterp');

save('ChickenFits.mat', 'actFit', 'passFit');
```

F.2 MATLAB Scripts for Simulating Isometric Muscle-Tendon Force Generation Through Complex Tendon Networks

F.2.1 Model Code Simulating Isometric Muscle-Tendon Force Generation Through Two Tendons Coupled in Parallel

```
% Created by: Anthony H. Le
% Last updated: 10-29-2020

%%
close all;
clear;
clc;

% toetipforces_main
% peakf_v_MTPang_main
peakf_v_MTPang_semavg

%%
load('thelen2003_hilltype_muscle_models.mat'); % load models
load('ChickenFits.mat'); % load chicken models from experiments,
active and passive
load('F_IMPLANTS.mat');

%%
L_M = linspace(0, 2, 100)';
% B = linspace(0, 1, 100)';
P_T1 = linspace(2, 6, 100)';
D_K0 = linspace(0, 600, 100)';
D_K1 = linspace(0, 300, 100)';
D_K2 = linspace(0, 300, 100)';
MTPang = strsplit(num2str(linspace(-30, 60, 100)));

% init_FLR_CURVE = FL_CE(L_M);
init_FLR_CURVE = actFit(L_M);

F_T1 = zeros(length(L_M), 1);
F_T2 = zeros(length(L_M), 1);

THETA = zeros(length(L_M), 3);
THETA_p = zeros(length(L_M), 3);

P1 = zeros(length(L_M), 2);
```

```
P1_p = zeros(length(L_M), 2);
P2 = zeros(length(L_M), 2);
P2_p = zeros(length(L_M), 2);
P3 = zeros(length(L_M), 2);
P3_p = zeros(length(L_M), 2);
P4 = zeros(length(L_M), 2);
P4_p = zeros(length(L_M), 2);

p4_pose = [2, 2.25, 4];

F_TENDON1 = zeros(length(L_M), length(p4_pose));
F_TENDON2 = zeros(length(L_M), length(p4_pose));

for pp = 1: length(p4_pose)
    for n = 1:length(L_M)
        p1 = [0, (-5 - L_M(n))];
        p2 = [0, 0];
        p3 = [-0.5, P_T1(n)];
        p4 = [0.5, p4_pose(pp)];

        e0 = norm(p2 - p1);
        e1 = norm(p3 - p2);
        e2 = norm(p4 - p2);

        th0 = atan2d(p2(2)-p1(2), p2(1)-p1(1));
        th1 = atan2d(p3(2)-p2(2), p3(1)-p2(1));
        th2 = atan2d(p4(2)-p2(2), p4(1)-p2(1));

        k0 = 300 + D_K0(n); % tendon 0 stiffness, attached to muscle
        k1 = 300 + D_K1(n); % tendon 1 stiffness
        k2 = 300 + D_K2(n); % tendon 2 stiffness

        x1 = 0;
        y1 = 0;
        x2 = 0;
        y2 = 0;
        x3 = 0;
        y3 = 0;
        x4 = 0;
        y4 = 0;

        f1x = 0;
        f1y = -init_FLR_CURVE(n);
        f2x = 0;
        f2y = 0;
        f3x = 0;
        f3y = 0;
        f4x = 0;
        f4y = 0;

        theta = [th0, th1, th2];
        k = [k0, k1, k2];
```

```
        K = cell(3, 1);

        for i = 1:length(theta)
            c = cosd(theta(i));
            s = sind(theta(i));

            m = [c^2 c*s;
                 c*s s^2];

            M =  repmat(m, [2, 2]);

            neg = [-ones(2, 2), ones(2, 2);
                   ones(2, 2), -ones(2, 2)];

            M = M .* neg;

            K{i} = k(i) .* M;
        end

        zero = zeros(2, 2);
        row1 = 1:2;
        row2 = 3:4;
        col1 = 1:2;
        col2 = 3:4;

        glo_stiffmat = [K{1}(row1, col1) K{1}(row1, col2) zero zero;
                        K{1}(row2, col1) (K{1}(row2,
col2)+K{2}(row1, col1)+K{3}(row1, col1)) K{2}(row1, col2) K{3}(row1,
col2);
                        zero K{2}(row2, col1) K{2}(row2, col2) zero;
                        zero K{3}(row2, col1) zero K{3}(row2,
col2)];

        F = [f1x; f1y; f2x; f2y; f3x; f3y; f4x; f4y];
        X = [x1; y1; x2; y2; x3; y3; x4; y4];

        % X12 = glo_stiffmat(1:4, 1:4) \ F(1:4, :);
        X12 = pinv(glo_stiffmat(1:4, 1:4)) * F(1:4, :);

        % F34 = glo_stiffmat(5:8, 1:4) * X12;
        %
        % F(5:8, :) = F34;
        X(1:4, :) = X12(1:4);

        p1_p = p1 + X(1:2, :)';
        p2_p = p2 + X(3:4, :)';
        p3_p = p3 + X(5:6, :)';
        p4_p = p4 + X(7:8, :)';

        th0_p = atan2d(p2_p(2)-p1_p(2), p2_p(1)-p1_p(1));
        th1_p = atan2d(p3_p(2)-p2_p(2), p3_p(1)-p2_p(1));
        th2_p = atan2d(p4_p(2)-p2_p(2), p4_p(1)-p2_p(1));
```

```
        theta_p = [th0_p, th1_p, th2_p];

        K_p = cell(3, 1);

        for ii = 1:length(theta_p)
            c_p = cosd(theta_p(ii));
            s_p = sind(theta_p(ii));

            m_p = [c_p^2 c_p*s_p;
                 c_p*s_p s_p^2];

            M_p =  repmat(m_p, [2, 2]);

            neg = [ones(2, 2), -ones(2, 2);
                   -ones(2, 2), ones(2, 2)];

            M_p = M_p .* neg;

            K_p{ii} = k(ii) .* M_p;
        end

        glo_stiffmat_p = [K_p{1}(row1, col1) K_p{1}(row1, col2) zero
zero;
                          K_p{1}(row2, col1) (K_p{1}(row2,
col2)+K_p{2}(row1, col1)+K_p{3}(row1, col1)) K_p{2}(row1, col2)
K_p{3}(row1, col2);
                          zero K_p{2}(row2, col1) K_p{2}(row2, col2)
zero;
                          zero K_p{3}(row2, col1) zero K_p{3}(row2,
col2)];

        F34 = glo_stiffmat_p(5:8, 1:4) * X12;

        F(5:8, :) = F34;

        F_T1(n) = sqrt(F34(1)^2 + F34(2)^2);
        F_T2(n) = sqrt(F34(3)^2 + F34(4)^2);
        THETA(n, :) = [th0, th1, th2];
        THETA_p(n, :) = [th0_p, th1_p, th2_p];
        P1(n, :) = p1;
        P1_p(n, :) = p1_p;
        P2(n, :) = p2;
        P2_p(n, 1) = p2_p(1, 1);
        P2_p(n, 2) = -p2_p(1, 2);
        P3(n, :) = p3;
        P3_p(n, :) = p3_p;
        P4(n, :) = p4;
        P4_p(n, :) = p4_p;
    end

    F_TENDON1(:, pp) = F_T1;
```

```
    F_TENDON2(:, pp) = F_T2;
end

%%
figure();
hold on;
plot(L_M, init_FLR_CURVE, 'd');
xticks(linspace(0, 2, 8));
xticklabels([-30, -15, 0, 15, 30, 45, 60, 75]);
xlabel(xlabel_lat);
xlim([0, 1.7143]);
ylim([0, 120]);
legend('Muscle');
set(gcf, 'position', [250 100 500 750]);
hold off;

%%
y_toe1 = [-1.5 2.5] .* [30 50];
y_toe2 = [-1.5 2.5] .* [30 50];

figure();
hold on;
for pp = 1:length(p4_pose)
    plot(L_M, F_TENDON1(:, pp), 'o');
end
% xticks(linspace(0, 2, 7));
% xticklabels([-30, -15, 0, 15, 30, 45, 60]);
xlabel('MTP Angle (deg)');
ylabel('MTP Moments (mNm) [+ tension]');
ylim(y_toe1);
legend('Muscle', 'Tendon 1', 'Tendon 2');
title('Toe 1');
hold off;

% figure();
% hold on;
% for pp = 1:length(p4_pose)
%     plot(L_M, F_TENDON2(:, pp), 'o');
% end
% xticks(linspace(0, 2, 7));
% xticklabels([-30, -15, 0, 15, 30, 45, 60]);
% xlabel('MTP Angle (deg)');
% ylabel('MTP Moments (mNm) [+ tension]');
% ylim(y_toe2);
% legend('Muscle', 'Tendon 1', 'Tendon 2');
% title('Toe 2');
% hold off;

%%
for nn = 1:20:length(L_M)
    figure();
    hold on;
    plot([P1(nn, 1); P2(nn, 1)], [P1(nn, 2); P2(nn, 2)], '--o');
    plot([P2(nn, 1); P3(nn, 1)], [P2(nn, 2); P3(nn, 2)], '--o');
```

```
    plot([P2(nn, 1); P4(nn, 1)], [P2(nn, 2); P4(nn, 2)], '--o');
    plot([P1_p(nn, 1); P2_p(nn, 1)], [P1_p(nn, 2); P2_p(nn, 2)], '-
o', 'Color', [0, 0.4470, 0.7410], 'MarkerEdgeColor', [0, 0.4470,
0.7410]);
    plot([P2_p(nn, 1); P3_p(nn, 1)], [P2_p(nn, 2); P3_p(nn, 2)], '-
o', 'Color', [0.8500, 0.3250, 0.0980], 'MarkerEdgeColor', [0.8500,
0.3250, 0.0980]);
    plot([P2_p(nn, 1); P4_p(nn, 1)], [P2_p(nn, 2); P4_p(nn, 2)], '-
o', 'Color', [0.9290, 0.6940, 0.1250], 'MarkerEdgeColor', [0.9290,
0.6940, 0.1250]);
    text(P1_p(nn, 1), P1_p(nn, 2), 'Node_0');
    text(P2_p(nn, 1), P2_p(nn, 2), 'Node_1');
    text(P3_p(nn, 1), P3_p(nn, 2), 'Node_2');
    text(P4_p(nn, 1), P4_p(nn, 2), 'Node_3');
    legend('Tendon_0', 'Tendon_1', 'Tendon_2');
    xlim([-1 1]);
    ylim([-8 8]);
    set(gcf, 'position', [250 100 250 750]);
    hold off;
end

%%
for nn = 1
    figure();
    hold on;
    plot([0; 0], [-5; 0], '-o');
    plot([0; -0.5], [0; 4], '-o');
    plot([0; 0.5], [0; 4], '-o');
    text(0, -5, 'Node_0');
    text(0, 0, 'Node_1');
    text(-0.5, 4, 'Node_2');
    text(0.5, 4, 'Node_3');
    legend('Tendon_0', 'Tendon_1', 'Tendon_2');
    xlim([-1 1]);
    ylim([-8 8]);
    set(gcf, 'position', [250 100 250 750]);
    hold off;
end

%%
DLF_SEM = zeros(n_LATMTP, 2, n_MEDMTP);
DMF_SEM = zeros(n_LATMTP, 2, n_MEDMTP);

SLF_SEM = zeros(n_LATMTP, 2, n_MEDMTP);
SMF_SEM = zeros(n_LATMTP, 2, n_MEDMTP);

latMTP1 = linspace(-30, 60, 20);
poly_n = [3, 3, 3];

colors = {[0, 0.4470, 0.7410], [0.8500, 0.3250, 0.0980], [0.9290,
0.6940, 0.1250]};

%%
```

```
% for m = 3
%     figure();
%     subplot(1, 3, 1);
%     for mm = 1:n_MEDMTP
%         errorbar(latMTP, D_LATF_AVG(:, mm, m), D_LATF_SEM(:, mm,
m), 'o', 'color', colors{mm});
%         hold on;
%         pfit = polyfit(latMTP, D_LATF_AVG(:, mm, m), poly_n(m));
%         f = polyval(pfit, latMTP1);
%         plot(latMTP1, f, '-', 'color', colors{mm})
%     end
%     title('Experimental: Without Implant');
%     xlabel(xlabel_lat);
%     ylabel(ylabel_lat);
%     xlim([-30, 60]);
%     ylim([0, 100]);
%     hold off;
%
%     subplot(1, 3, 2);
%     hold on;
%     for pp = 1:length(p4_pose)
%         plot(L_M, F_TENDON1(:, pp), 'o');
%     end
%     xticks(linspace(0, 2, 8));
%     xticklabels([-30, -15, 0, 15, 30, 45, 60, 75]);
%     xlabel(xlabel_lat);
%     ylabel(ylabel_lat);
%     xlim([0, 1.7143]);
%     ylim([0, 100]);
%     legend(MEDMTP_IDS');
%     title('Model: Without Implant');
%     hold off;
%
%     subplot(1, 3, 3);
%     hold on;
%     for pp = 1:length(p4_pose)
%         plot(L_M, F_IMPLANT1(:, pp), 'o');
%     end
%     xticks(linspace(0, 2, 8));
%     xticklabels([-30, -15, 0, 15, 30, 45, 60, 75]);
%     xlabel(xlabel_lat);
%     ylabel(ylabel_lat);
%     xlim([0, 1.7143]);
%     ylim([0, 100]);
%     legend(MEDMTP_IDS');
%     title('Model: With Implant');
%     hold off;
%
%     suptitle(FLR_IDS{m, 1});
% end
```

F.2.2 Model Code Simulating Isometric Muscle-Tendon Force Generation Through a Passive Differential Mechanism

```
% Created by: Anthony H. Le
% Last updated: 10-21-2020

%%
close all;
clear;
clc;

%%
load('thelen2003_hilltype_muscle_models.mat'); % load models
load('ChickenFits.mat'); % load chicken models from experiments,
active and passive

%%
L_M = linspace(0, 2, 100)';
P_T1 = linspace(2, 6, 100)';
P_I1 = linspace(0, 1, 100)';
P_I2 = flip(linspace(0, 1, 100)');
P_T2 = linspace(0, 0.5, 100)';
del_tri = linspace(-2, 2, 100)';
D_K0 = linspace(0, 600, 100)';
D_K1 = linspace(0, 600, 100)';
D_K2 = linspace(0, 12000, 100)';
MTPang = strsplit(num2str(linspace(-30, 60, 100)));

% init_FLR_CURVE = FL_CE(L_M);
init_FLR_CURVE = actFit(L_M) .* 1.2;

F_T1 = zeros(length(L_M), 1);
F_T2 = zeros(length(L_M), 1);

THETA = zeros(length(L_M), 6);
THETA_p = zeros(length(L_M), 6);

P1 = zeros(length(L_M), 2);
P1_p = zeros(length(L_M), 2);
P2 = zeros(length(L_M), 2);
P2_p = zeros(length(L_M), 2);
Pa = zeros(length(L_M), 2);
Pa_p = zeros(length(L_M), 2);
Pb = zeros(length(L_M), 2);
Pb_p = zeros(length(L_M), 2);
P3 = zeros(length(L_M), 2);
P3_p = zeros(length(L_M), 2);
P4 = zeros(length(L_M), 2);
P4_p = zeros(length(L_M), 2);

p4_pose = [2, 2.25, 4];
t2_stiff = [-100, -75, 100];

F_IMPLANT1 = zeros(length(L_M), length(p4_pose));
F_IMPLANT2 = zeros(length(L_M), length(p4_pose));
```

```
implant_h = 0.5;
implant_stiff = 5000;
tendon_tri_stiff = 900;
tendon_stiff = 300;

for pp = 1:length(p4_pose)
    for n = 1:length(L_M)
        p1 = [0, (-5 - L_M(n))];
        p2 = [0, (0 + P_T2(n))];
        pa = [-0.5, (implant_h + P_I1(n))];
    %     pa = [-0.5, (implant_h + del_tri(n))];
        pb = [0.5, (implant_h + P_I2(n))];
        p3 = [-0.5, P_T1(n)];
        p4 = [0.5, p4_pose(pp)];

        pmid = [0, implant_h];

        e0 = norm(p2 - p1);
        ea = norm(pa - p2);
        eb = norm(pb - p2);
        ec = norm(pb - pa);
        e1 = norm(p3 - pa);
        e2 = norm(p4 - pb);
        e_tri_h = norm(pmid - p2);

        mc = (pb(2) - pa(2)) / (pb(1) - pa(1));
        mc_per = 1 / mc;

    %     p2(2) =
    %     p2(1) =

        th0 = atan2d(p2(2)-p1(2), p2(1)-p1(1)); % 1
        tha = atan2d(pa(2)-p2(2), pa(1)-p2(1)); % 2
        thb = atan2d(pb(2)-p2(2), pb(1)-p2(1)); % 3
        thc = atan2d(pb(2)-pa(2), pb(1)-pa(1)); % 4
        th1 = atan2d(p3(2)-pa(2), p3(1)-pa(1)); % 5
        th2 = atan2d(p4(2)-pb(2), p4(1)-pb(1)); % 6

        k0 = tendon_stiff + D_K0(n); % 1
        ka = tendon_tri_stiff; % 2
        kb = tendon_tri_stiff; % 3
        kc = implant_stiff; % 4
        k1 = tendon_stiff + D_K1(n); % 5
        k2 = tendon_stiff + t2_stiff(pp); % 6

        x1 = 0;
        y1 = 0;
        x2 = 0;
        y2 = 0;
        xa = 0;
        ya = 0;
        xb = 0;
        yb = 0;
```

```
        x3 = 0;
        y3 = 0;
        x4 = 0;
        y4 = 0;

        f1x = 0;
        f1y = -init_FLR_CURVE(n);
        f2x = 0;
        f2y = 0;
        fax = 0;
        fay = 0;
        fbx = 0;
        fby = 0;
        f3x = 0;
        f3y = 0;
        f4x = 0;
        f4y = 0;

        theta = [th0, tha, thb, thc, th1, th2];
        k = [k0, ka, kb, kc, k1, k2];

        K = cell(6, 1);

        for i = 1:length(theta)
            c = cosd(theta(i));
            s = sind(theta(i));

            m = [c^2 c*s;
                 c*s s^2];

            M =  repmat(m, [2, 2]);

            neg = [ones(2, 2), -ones(2, 2);
                   -ones(2, 2), ones(2, 2)];

            M = M .* neg;

            K{i} = k(i) .* M;
        end

        zero = zeros(2, 2);
        row1 = 1:2;
        row2 = 3:4;
        col1 = 1:2;
        col2 = 3:4;

        glo_stiffmat = [K{1}(row1, col1) K{1}(row1, col2) zero zero
zero zero;
                        K{1}(row2, col1) (K{1}(row2,
col2)+K{2}(row1, col1)+K{3}(row1, col1)) K{2}(row1, col2) K{3}(row1,
col2) zero zero;
```

```
                        zero K{2}(row2, col1) (K{2}(row2,
col2)+K{4}(row1, col1)+K{5}(row1, col1)) K{4}(row1, col2) K{5}(row1,
col2) zero;
                        zero K{3}(row2, col1) K{4}(row2, col1)
(K{3}(row2, col2)+K{4}(row2, col2)+K{6}(row1, col1)) zero K{6}(row1,
col2);
                        zero zero K{5}(row2, col1) zero K{5}(row2,
col2) zero;
                        zero zero zero K{6}(row2, col1) zero
K{6}(row2, col2)];

        F = [f1x; f1y; f2x; f2y; fax; fay; fbx; fby; f3x; f3y; f4x;
f4y];
        X = [x1; y1; x2; y2; xa; ya; xb; yb; x3; y3; x4; y4];

        X12ab = pinv(glo_stiffmat(1:8, 1:8)) * F(1:8, :);

        X(1:8, :) = X12ab(1:8);

        p1_p = p1 + X(1:2, :)';
        p2_p = p2 + X(3:4, :)';
        pa_p = pa + X(5:6, :)';
        pb_p = pb + X(7:8, :)';
        p3_p = p3 + X(9:10, :)';
        p4_p = p4 + X(11:12, :)';

        th0_p = atan2d(p2_p(2)-p1_p(2), p2_p(1)-p1_p(1));
        tha_p = atan2d(pa_p(2)-p2_p(2), pa_p(1)-p2_p(1));
        thb_p = atan2d(pb_p(2)-p2_p(2), pb_p(1)-p2_p(1));
        thc_p = atan2d(pb_p(2)-pa_p(2), pb_p(1)-pa_p(1));
        th1_p = atan2d(p3_p(2)-pa_p(2), p3_p(1)-pa_p(1));
        th2_p = atan2d(p4_p(2)-pb_p(2), p4_p(1)-pb_p(1));

        theta_p = [th0_p, tha_p, thb_p, thc_p, th1_p, th2_p];

        K_p = cell(6, 1);

        for ii = 1:length(theta_p)
            c_p = cosd(theta_p(ii));
            s_p = sind(theta_p(ii));

            m_p = [c_p^2 c_p*s_p;
                 c_p*s_p s_p^2];

            M_p =  repmat(m_p, [2, 2]);

            neg = [ones(2, 2), -ones(2, 2);
                   -ones(2, 2), ones(2, 2)];

            M_p = M_p .* neg;

            K_p{ii} = k(ii) .* M_p;
```

```
        end

        glo_stiffmat_p = [K_p{1}(row1, col1) K_p{1}(row1, col2) zero
zero zero zero;
                          K_p{1}(row2, col1) (K_p{1}(row2,
col2)+K_p{2}(row1, col1)+K_p{3}(row1, col1)) K_p{2}(row1, col2)
K_p{3}(row1, col2) zero zero;
                          zero K_p{2}(row2, col1) (K_p{2}(row2,
col2)+K_p{4}(row1, col1)+K_p{5}(row1, col1)) K_p{4}(row1, col2)
K_p{5}(row1, col2) zero;
                          zero K_p{3}(row2, col1) K_p{4}(row2, col1)
(K_p{3}(row2, col2)+K_p{4}(row2, col2)+K_p{6}(row1, col1)) zero
K_p{6}(row1, col2);
                          zero zero K_p{5}(row2, col1) zero K_p{5}(row2,
col2) zero;
                          zero zero zero K_p{6}(row2, col1) zero
K_p{6}(row2, col2)];

        F34 = glo_stiffmat_p(9:12, 1:8) * X12ab;

        F(9:12, :) = F34;

        F_T1(n) = sqrt(F34(1)^2 + F34(2)^2);
        F_T2(n) = sqrt(F34(3)^2 + F34(4)^2);
        THETA(n, :) = [th0, tha, thb, thc, th1, th2];
        THETA_p(n, :) = [th0_p, tha_p, thb_p, thc_p, th1_p, th2_p];
        P1(n, :) = p1;
        P1_p(n, :) = p1_p;
        P2(n, :) = p2;
        P2_p(n, 1) = p2_p(1, 1);
        P2_p(n, 2) = p2_p(1, 2);
        Pa(n, :) = pa;
        Pa_p(n, :) = pa_p;
        Pb(n, :) = pb;
        Pb_p(n, :) = pb_p;
        P3(n, :) = p3;
        P3_p(n, :) = p3_p;
        P4(n, :) = p4;
        P4_p(n, :) = p4_p;
    end

    F_IMPLANT1(:, pp) = F_T1;
    F_IMPLANT2(:, pp) = F_T2;
end

save('F_IMPLANTS.mat', 'F_IMPLANT1', 'F_IMPLANT2');

%%
figure();
hold on;
plot(L_M, init_FLR_CURVE, 'd');
plot(L_M, F_T1, 'o');
plot(L_M, F_T2, 'o');
```

```
xticks(linspace(0, 2, 7));
xticklabels([-30, -15, 0, 15, 30, 45, 60]);
xlabel('MTP Angle (deg)');
ylabel('MTP Moments (mNm) [+ tension]');
legend('Muscle', 'Tendon 1', 'Tendon 2');
hold off;

%%
figure();
hold on;
for pp = 1:length(p4_pose)
    plot(L_M, F_IMPLANT1(:, pp), 'o');
end
xticks(linspace(0, 2, 7));
xticklabels([-30, -15, 0, 15, 30, 45, 60]);
xlabel('MTP Angle (deg)');
ylabel('MTP Moments (mNm) [+ tension]');
legend('Muscle', 'Tendon 1', 'Tendon 2');
title('Toe 1');
hold off;

figure();
hold on;
for pp = 1:length(p4_pose)
    plot(L_M, F_IMPLANT2(:, pp), 'o');
end
xticks(linspace(0, 2, 7));
xticklabels([-30, -15, 0, 15, 30, 45, 60]);
xlabel('MTP Angle (deg)');
ylabel('MTP Moments (mNm) [+ tension]');
legend('Muscle', 'Tendon 1', 'Tendon 2');
title('Toe 2');
hold off;



%%
for nn = 1:20:length(L_M)
    figure();
    hold on;
    plot([P1(nn, 1); P2(nn, 1)], [P1(nn, 2); P2(nn, 2)], '--o');
    plot([P2(nn, 1); Pa(nn, 1)], [P2(nn, 2); Pa(nn, 2)], '--o');
    plot([P2(nn, 1); Pb(nn, 1)], [P2(nn, 2); Pb(nn, 2)], '--o');
    plot([Pa(nn, 1); Pb(nn, 1)], [Pa(nn, 2); Pb(nn, 2)], '--o');
    plot([Pa(nn, 1); P3(nn, 1)], [Pa(nn, 2); P3(nn, 2)], '--o');
    plot([Pb(nn, 1); P4(nn, 1)], [Pb(nn, 2); P4(nn, 2)], '--o');
    plot([P1_p(nn, 1); P2_p(nn, 1)], [P1_p(nn, 2); P2_p(nn, 2)], '-
o', 'Color', [0, 0.4470, 0.7410], 'MarkerEdgeColor', [0, 0.4470,
0.7410]);
    plot([P2_p(nn, 1); Pa_p(nn, 1)], [P2_p(nn, 2); Pa_p(nn, 2)], '-
o', 'Color', [0.8500, 0.3250, 0.0980], 'MarkerEdgeColor', [0.8500,
0.3250, 0.0980]);
```

```
    plot([P2_p(nn, 1); Pb_p(nn, 1)], [P2_p(nn, 2); Pb_p(nn, 2)], '-
o', 'Color', [0.9290, 0.6940, 0.1250], 'MarkerEdgeColor', [0.9290,
0.6940, 0.1250]);
    plot([Pa_p(nn, 1); Pb_p(nn, 1)], [Pa_p(nn, 2); Pb_p(nn, 2)], '-
o', 'Color', [0.4940, 0.1840, 0.5560], 'MarkerEdgeColor', [0.4940,
0.1840, 0.5560]);
    plot([Pa_p(nn, 1); P3_p(nn, 1)], [Pa_p(nn, 2); P3_p(nn, 2)], '-
o', 'Color', [0.4660, 0.6740, 0.1880], 'MarkerEdgeColor', [0.4660,
0.6740, 0.1880]);
    plot([Pb_p(nn, 1); P4_p(nn, 1)], [Pb_p(nn, 2); P4_p(nn, 2)], '-
o', 'Color', [0.3010, 0.7450, 0.9330], 'MarkerEdgeColor', [0.3010,
0.7450, 0.9330]);
    text(P1_p(nn, 1), P1_p(nn, 2), 'Node_0');
    text(P2_p(nn, 1), P2_p(nn, 2), 'Node_1');
    text(Pa_p(nn, 1), Pa_p(nn, 2), 'Node_a');
    text(Pb_p(nn, 1), Pb_p(nn, 2), 'Node_b');
    text(P3_p(nn, 1), P3_p(nn, 2), 'Node_2');
    text(P4_p(nn, 1), P4_p(nn, 2), 'Node_3');
    legend('Tendon_0', 'Tendon_{1a}', 'Tendon_{2a}', 'Implant',
'Tendon_{1b}', 'Tendon_{2b}', 'Location', 'northeast');
    xlim([-1 1]);
    ylim([-8 8]);
    set(gcf, 'position', [250 100 250 750]);
    hold off;
end

%%
for nn = 1
    figure();
    hold on;
    plot([0; 0], [-5; 0], '-o');
    plot([0; -0.5], [0; 0.5], '-o');
    plot([0; 0.5], [0; 0.5], '-o');
    plot([-0.5; 0.5], [0.5; 0.5], '-o');
    plot([-0.5; -0.5], [0.5; 4], '-o');
    plot([0.5; 0.5], [0.5; 4], '-o');
    text(0, -5, 'Node_0');
    text(0, 0, 'Node_1');
    text(-0.5, 0.5, 'Node_a');
    text(0.5, 0.5, 'Node_b');
    text(-0.5, 4, 'Node_2');
    text(0.5, 4, 'Node_3');
    legend('Tendon_0', 'Tendon_{1a}', 'Tendon_{2a}', 'Implant',
'Tendon_{1b}', 'Tendon_{2b}', 'Location', 'northeast');
    xlim([-1 1]);
    ylim([-8 8]);
    set(gcf, 'position', [250 100 250 750]);
    hold off;
end
```

Bibliography

[1] D. M. Sammer and K. C. Chung, "Tendon transfers: part I. Principles of transfer and transfers for radial nerve palsy," *Plast. Reconstr. Surg.,* vol. 123, no. 5, pp. 169e-177e, May 2009, doi: 10.1097/PRS.0b013e3181a20526.

[2] S. W. Wolfe, W. C. Pederson, S. H. Kozin, and M. S. Cohen, *Green's Operative Hand Surgery E-Book*. Elsevier Health Sciences, 2016.

[3] P. Brand, "Tendon transfers for median and ulnar nerve paralysis," *The Orthopedic Clinics of North America,* vol. 1, no. 2, pp. 447-454, 1970.

[4] W. P. Cooney, R. L. Linscheid, and K.-N. An, "Opposition of the thumb: an anatomic and biomechanical study of tendon transfers," *J. Hand Surg. Am.,* vol. 9, no. 6, pp. 777-786, 1984.

[5] R. L. Lieber, "Biology and mechanics of skeletal muscle: what hand surgeons need to know when tensioning a tendon transfer," *J. Hand Surg. Am.,* vol. 33, no. 9, pp. 1655-6, Nov 2008, doi: 10.1016/j.jhsa.2008.08.010.

[6] D. G. Thelen, "Adjustment of muscle mechanics model parameters to simulate dynamic contractions in older adults," *J. Biomech. Eng.,* vol. 125, no. 1, pp. 70-77, 2003.

[7] R. L. Lieber, B. O. Ljung, and J. Fridén, "Intraoperative sarcomere length measurements reveal differential design of human wrist extensor muscles," *J. Exp. Biol.,* vol. 200, no. 1, pp. 19-25, 1997.

[8] R. L. Lieber, *Skeletal muscle structure, function, and plasticity*. Lippincott Williams & Wilkins, 2002.

[9] F. E. Zajac, "Muscle and tendon Properties models scaling and application to biomechanics and motor," *Crit. Rev. Biomed. Eng.,* vol. 17, no. 4, pp. 359-411, 1989.

[10] R. Lieber, B. Fazeli, and M. Botte, "Architecture of Selected Wrist Flexor and Extensor Muscles," *J. Hand Surg. Am.,* vol. 15, no. 2, pp. 244-50, 1990.

[11] R. L. Lieber, "Skeletal Muscle Architecture," *J. Hand Ther.,* vol. 6, no. 2, pp. 105-113, 1993, doi: 10.1016/s0894-1130(12)80291-2.

[12] T. Fukunaga *et al.*, "Physiological cross-sectional area of human leg muscles based on magnetic resonance imaging," *Journal of orthopaedic research,* vol. 10, no. 6, pp. 926-934, 1992.

[13] K.-N. An, Y. Ueba, E. Chao, W. Cooney, and R. Linscheid, "Tendon excursion and moment arm of index finger muscles," *Journal of biomechanics,* vol. 16, no. 6, pp. 419-425, 1983.

[14] R. R. Richards, "Tendon transfers for failed nerve reconstruction," *Clin. Plast. Surg.,* vol. 30, no. 2, pp. 223-245, 2003.

[15] P. W. Brand and A. Hollister, *Clinical mechanics of the hand*. Mosby Incorporated, 1999.

[16] J. Boyes, "Tendon transfers for radial palsy," *Bull. Hosp. Joint Dis.,* vol. 21, pp. 97-105, 1961.

[17] C. L. STARR, "Army experiences with tendon transference," *JBJS,* vol. 4, no. 1, pp. 3-21, 1922.

[18] R. J. Smith, *Tendon transfers of the hand and forearm*. Little Brown & Company, 1987.

[19] S. Bunnell, "Surgery of the Hand, Preface," 1944.

[20] R. Curtis, "Fundamental principles of tendon transfer," *Orthop. Clin. North Am.,* vol. 5, no. 2, pp. 231-242, 1974.

[21] C. A. Makarewich and D. T. Hutchinson, "Tendon transfers for combined peripheral nerve injuries," *Hand Clin.,* vol. 32, no. 3, pp. 377-387, 2016.

[22] J. A. Ratner, A. Peljovich, and S. H. Kozin, "Update on tendon transfers for peripheral nerve injuries," *The journal of hand surgery,* vol. 35, no. 8, pp. 1371-1381, 2010.

[23] F. J. Valero-Cuevas, F. E. Zajac, and C. G. Burgar, "Large index-fingertip forces are produced by subject-independent patterns of muscle excitation," *Journal of biomechanics,* vol. 31, no. 8, pp. 693-703, 1998.

[24] J. Fridén and R. L. Lieber, "Tendon transfer surgery: clinical implications of experimental studies," *Clinical Orthopaedics and Related Research (1976-2007),* vol. 403, pp. S163-S170, 2002.

[25] M. Kreulen and M. J. Smeulders, "Assessment of Flexor carpi ulnaris function for tendon transfer surgery," *Journal of Biomechanics,* vol. 41, no. 10, pp. 2130-2135, 2008.

[26] C. A. Yucesoy, F. Ateş, U. Akgün, and M. Karahan, "Measurement of human Gracilis muscle isometric forces as a function of knee angle, intraoperatively," *Journal of Biomechanics,* vol. 43, no. 14, pp. 2665-2671, 2010.

[27] J. A. Friederich and R. A. Brand, "Muscle fiber architecture in the human lower limb," *Journal of biomechanics,* vol. 23, no. 1, pp. 91-95, 1990.

[28] G. Loren, S. Shoemaker, T. Burkholder, M. Jacobson, J. Friden, and R. L. Lieber, "Human wrist motors: biomechanical design and application to tendon transfers," *Journal of biomechanics,* vol. 29, no. 3, pp. 331-342, 1996.

[29] F. E. Zajac, "How musculotendon architecture and joint geometry affect the capacity of muscles to move and exert force on objects: a review with application to arm and forearm tendon transfer design," *J. Hand Surg. Am.,* vol. 17, no. 5, pp. 799-804, 1992.

[30] J. W. Strickland, "Development of flexor tendon surgery: twenty-five years of progress," *J. Hand Surg. Am.,* vol. 25, no. 2, pp. 214-235, 2000.

[31] H. Maas, G. C. Baan, and P. A. Huijing, "Dissection of a single rat muscle-tendon complex changes joint moments exerted by neighboring muscles: implications for invasive surgical interventions," *PLoS One,* vol. 8, no. 8, p. e73510, 2013, doi: 10.1371/journal.pone.0073510.

[32] H. Maas and P. A. Huijing, "Mechanical effect of rat flexor carpi ulnaris muscle after tendon transfer: does it generate a wrist extension moment?," *Journal of Applied Physiology,* vol. 112, no. 4, pp. 607-614, 2011.

[33] H. Maas and P. A. Huijing, "Effects of tendon and muscle belly dissection on muscular force transmission following tendon transfer in the rat," *J. Biomech.,* vol. 45, no. 2, pp. 289-96, Jan 10 2012, doi: 10.1016/j.jbiomech.2011.10.026.

[34] H. Maas and P. A. Huijing, "Myofascial force transmission between transferred rat flexor carpi ulnaris muscle and former synergistic palmaris longus muscle," *Muscles, ligaments and tendons journal,* vol. 1, no. 4, p. 127, 2011.

[35] S. L. Delp and J. P. Loan, "A computational framework for simulating and analyzing human and animal movement," *Computing in Science & Engineering,* vol. 2, no. 5, pp. 46-55, 2000.

[36] M. Millard, T. Uchida, A. Seth, and S. L. Delp, "Flexing computational muscle: modeling and simulation of musculotendon dynamics," *J. Biomech. Eng.,* vol. 135, no. 2, p. 021005, Feb 2013, doi: 10.1115/1.4023390.

[37] L. Birglen, T. Laliberté, and C. M. Gosselin, *Underactuated robotic hands*. Springer, 2007.

[38] M. Baril, T. Laliberté, F. Guay, and C. Gosselin, "Static analysis of single-input/multiple-output tendon-driven underactuated mechanisms for robotic hands," in *ASME 2010 International Design Engineering Technical Conferences and Computers and Information in Engineering Conference*, 2010: American Society of Mechanical Engineers, pp. 155-164.

[39] L. Birglen and C. M. Gosselin, "Force analysis of connected differential mechanisms: Application to grasping," *The International Journal of Robotics Research,* vol. 25, no. 10, pp. 1033-1046, 2006.

[40] H. Antoni, A. Chilbert, D. Sweeney, and J. Reilly, "Applied bioelectricity: From electrical stimulation to electrophathology," *JP Reilly,* pp. 12-72, 1998.

[41] J. T. Mortimer and N. Bhadra, "Peripheral nerve and muscle stimulation," in *Neuroprosthetics: theory and practice*: World Scientific, 2004, pp. 638-682.

[42] P. H. Peckham and J. S. Knutson, "Functional electrical stimulation for neuromuscular applications," *Annu. Rev. Biomed. Eng.,* vol. 7, pp. 327-360, 2005.

[43] J. B. Peter, R. J. Barnard, V. R. Edgerton, C. A. Gillespie, and K. E. Stempel, "Metabolic profiles of three fiber types of skeletal muscle in guinea pigs and rabbits," *Biochemistry,* vol. 11, no. 14, pp. 2627-2633, 1972.

[44] R. Burke, D. Levine, P. Tsairis, and F. Zajac Iii, "Physiological types and histochemical profiles in motor units of the cat gastrocnemius," *The Journal of physiology,* vol. 234, no. 3, pp. 723-748, 1973.

[45] R. Burke, "Firing patterns of gastrocnemius motor units in the decerebrate cat," *The Journal of physiology,* vol. 196, no. 3, pp. 631-654, 1968.

[46] R. Burke, "The control of muscle force: motor unit recruitment and firing patterns," *Human muscle power,* vol. 97, p. 106, 1986.

[47] D. R. McNeal, "Analysis of a model for excitation of myelinated nerve," *IEEE Transactions on Biomedical Engineering,* no. 4, pp. 329-337, 1976.

[48] C. M. Gregory and C. S. Bickel, "Recruitment patterns in human skeletal muscle during electrical stimulation," *Phys. Ther.,* vol. 85, no. 4, pp. 358-364, 2005.

[49] B. Bigland-Ritchie, F. Bellemare, and J. Woods, "Excitation frequencies and sites of fatigue," *Human muscle power,* pp. 197-213, 1986.

[50] R. H. Edwards, "Human muscle function and fatigue," in *Ciba Found Symp*, 1981, vol. 82: Wiley Online Library, pp. 1-18.

[51] E. Henneman, "Relation between size of neurons and their susceptibility to discharge," *Science,* vol. 126, no. 3287, pp. 1345-1347, 1957.

[52] C. S. Bickel, C. M. Gregory, and J. C. Dean, "Motor unit recruitment during neuromuscular electrical stimulation: a critical appraisal," *Eur. J. Appl. Physiol.,* vol. 111, no. 10, p. 2399, 2011.

[53] B. M. Doucet and L. Griffin, "Maximal versus submaximal intensity stimulation with variable patterns," *Muscle & Nerve: Official Journal of the American Association of Electrodiagnostic Medicine,* vol. 37, no. 6, pp. 770-777, 2008.

[54] B. I. Binder-Markey and W. M. Murray, "Incorporating the length-dependent passive-force generating muscle properties of the extrinsic finger muscles into a wrist and finger biomechanical musculoskeletal model," *Journal of biomechanics,* vol. 61, pp. 250-257, 2017.

[55] J. S. Knutson, G. G. Naples, P. H. Peckham, and M. W. Keith, "Electrode fracture rates and occurrences of infection and granuloma associated with percutaneous intramuscular electrodes in upper-limb functional electrical

stimulation applications," *Journal of rehabilitation research and development,* vol. 39, no. 6, pp. 671-684, 2002.

[56] S. Agarwal, R. Kobetic, S. Nandurkar, and E. Marsolais, "Functional electrical stimulation for walking in paraplegia: 17-year follow-up of 2 cases," *The journal of spinal cord medicine,* vol. 26, no. 1, pp. 86-91, 2003.

[57] P. Peckham, J. Mortimer, and E. Marsolais, "Controlled prehension and release in the C5 quadriplegic elicited by functional electrical stimulation of the paralyzed forearm musculature," *Ann. Biomed. Eng.,* vol. 8, no. 4-6, pp. 369-388, 1980.

[58] C. Caldwell and J. Reswick, "A percutaneous wire electrode for chronic research use," *IEEE Transactions on Biomedical Engineering,* no. 5, pp. 429-432, 1975.

[59] L. Vámhidy, M. Ferder, V. Biro, A. Salamon, and B. Strauch, "Anatomy of the chicken foot for the experimental investigation in flexor tendon surgery," *Acta Chir. Hung.,* vol. 35, no. 1-2, pp. 21-33, 1995.

[60] A. F. Huxley, "Muscle structure and theories of contraction," *Prog. Biophys. Biophys. Chem,* vol. 7, pp. 255-318, 1957.

[61] H. Hatze, "A theory of contraction and a mathematical model of striated muscle," *Journal of theoretical biology,* vol. 40, no. 2, pp. 219-246, 1973.

[62] A. Gordon, A. F. Huxley, and F. Julian, "The variation in isometric tension with sarcomere length in vertebrate muscle fibres," *The Journal of physiology,* vol. 184, no. 1, pp. 170-192, 1966.

[63] B. Katz, "The relation between force and speed in muscular contraction," *The Journal of Physiology,* vol. 96, no. 1, pp. 45-64, 1939.

[64] D. Morgan, "Separation of active and passive components of short-range stiffness of muscle," *American Journal of Physiology-Cell Physiology,* vol. 232, no. 1, pp. 45-49, 1977.

[65] P. Rack and D. Westbury, "Elastic properties of the cat soleus tendon and their functional importance," *The Journal of Physiology,* vol. 347, no. 1, pp. 479-495, 1984.

[66] B. Walmsley and U. Proske, "Comparison of stiffness of soleus and medial gastrocnemius muscles in cats," *J. Neurophysiol.,* vol. 46, no. 2, pp. 250-259, 1981.

[67] J. Hoffer, A. Caputi, I. Pose, and R. Griffiths, "Roles of muscle activity and load on the relationship between muscle spindle length and whole muscle length in the freely walking cat," in *Progress in brain research*, vol. 80: Elsevier, 1989, pp. 75-85.

[68] K. Schmidt-Nielsen and S.-N. Knut, *Scaling: why is animal size so important?* Cambridge university press, 1984.

[69] R. L. Lieber, C. G. Brown, and C. L. Trestik, "Model of muscle-tendon interaction during frog semitendinosis fixed-end contractions," *Journal of biomechanics,* vol. 25, no. 4, pp. 421-428, 1992.

[70] T. Homayouni, K. N. Underwood, K. C. Beyer, E. R. Martin, C. H. Allan, and R. Balasubramanian, "Modeling Implantable Passive Mechanisms for Modifying the Transmission of Forces and Movements Between Muscle and Tendons," *IEEE Trans. Biomed. Eng.,* vol. 62, no. 9, pp. 2208-14, Sep 2015, doi: 10.1109/TBME.2015.2419223.

[71] K. L. Mardula, R. Balasubramanian, and C. H. Allan, "Implanted passive engineering mechanism improves hand function after tendon transfer surgery: a cadaver-based study," *Hand (N Y),* vol. 10, no. 1, pp. 116-22, Mar 2015, doi: 10.1007/s11552-014-9676-0.

[72] J. Montgomery, "Embedding Adapative Engineering Mechanisms into a Coupled Tendon Transfer Surgery for High Median-Ulnar Nerve Palsy: A Simulation Study with OpenSim," BS, Mechanical Engineering, Oregon State University, 2013.